Studies of Image Processing for Phase Restoration in Electron Holography

Li Wei

Studies of Image Processing for Phase Restoration in Electron Holography

December, 2014

Nagoya University

Graduate School of Engineering

Department of Electrical Engineering and Computer Science

Li Wei

Preface

At present, new products and even new industries rely on radical advances in materials. However, it is also important to make incremental improvements using currently available materials.

In situ observations of phenomena are important in material science, where materials are observed and photographed in situations where they are used or produced in practice. In many cases, chemical intermediates are synthesized *in situ* during various processes.

In situ transmission electron microscope in dynamic conditions with real-time event monitoring can provide useful information during material processing.

In situ off-axis electron holography allows us to study accurate phase changes in a material in various active conditions with different experimental parameters. However, phase images often contain imperfections after they are reconstructed from holograms. With the development of computational techniques, the digital image processing can be used to improve the images obtained by electron microscopy. Thus, the present study aimed to apply digital image processing to eliminate the imperfections that occur during the digital reconstruction of electron hologram images. A novel method of image processing for phase imperfections in electron holography has been established and applied to the hologram of some specimens.

CONTENTS

Chapter one

1. Introduction

1.1 Preamble

At present, new products and even new industries rely on radical advances in materials. However, it is also important to make incremental improvements using currently available materials. Materials science includes materials design, cost-benefit tradeoffs, processing techniques, welding, ion implantation, crystal growth, thin-film deposition, sintering, and analytical techniques, where the most important areas are related to the structure of materials.

Since the development of nanomaterials, many new materials and devices have emerged with numerous applications based on nanotechnology, such as in medicine, electronics, biomaterials, and energy production[1,2,3].

Nanotechnology is defined as the manipulation of matter where at least one dimension is in the range of 1–100 nm according to the US National Nanotechnology Initiative. The direct control of matter at an atomic scale and new approaches based on molecular self-assembly are required for nanotechnology research and applications [4,5,6].

The ability of microscopes to resolve the details of an object is limited by the wavelength of the light used for imaging, as stated originally by Abbe [7]. Thus, the resolution of an optical microscope is limited to a few hundred nanometers. The ultraviolet microscopes produced by Köhler and Rohr increased the resolving power by about two times [8]. Thus, obtaining an image with sub-micrometer information is impossible using an optical microscope because of the wavelength constraint [9].

The deflection of "cathode rays" (electrons) using magnetic fields was first recognized

by Plücker in 1858 [10-12]. In 1931, the German physicist Ruska in the Knoll group successfully constructed a prototype electron microscope with a magnification of four hundred times. The device used two magnetic lenses to obtain higher magnifications and it was the first electron microscope [13]. The wave nature of electrons was predicted by de Broglie in 1927 [14]. The magnification achievable using light microscope was exceeded successfully in September 1933 [9].

Transmission electron microscope (TEM) is the original form of electron microscope, which has the capability of imaging at a significantly higher resolution than light microscopes because of the smaller de Broglie wavelength of electrons[15]. TEMs have applications in cancer research, virology, materials science, pollution, nanotechnology, semiconductor research, and so on.

In the 1970s, Crewe developed the field emission (FE) gun at the University of Chicago [16,17], which he installed in a scanning transmission electron microscope (STEM) that was used to image single atoms of thorium. Many TEMs use FE guns as the source of electrons. FE sources produce two to three orders of magnitude more brightness than conventional thermionic emission sources. Thus, FE electron sources produce much brighter and higher resolution images with highly coherent interference characteristics when used by TEMs [18,19].

The FE electron source with high stability and illumination characteristics in an FE-TEM was developed for electron holography by Tonomura in 1978 [20-22].

Electron holography was invented by Gabor in 1948 who tried to improve the resolution of electron microscopes [23,24]. Two schemes are used for electron

holography, i.e., off-axis and in-line, and Gabor proposed in-line electron holography. However, it is difficult to eliminate twin image effects with this scheme. Thus, Leith and Upatnieks proposed optical off-axis holography, which allows the reconstruction of separate image and complex conjugate images [25]. In off-axis electron holography, an electron wave is split into two parts by applying potential to a very thin filament. The deflection of the electron waves by a positive voltage leads to overlapping and an interference pattern with equidistantly spaced fringes [26-28].

In situ observations of phenomena are important in material science, where materials are observed and photographed in situations where they are used or produced in practice. In many cases, chemical intermediates are synthesized *in situ* during various processes. For example, aged catalysts in industrial reactors may be regenerated *in situ* without being removed from the reactors. *In situ* regeneration may be necessary because the specimen is unstable and cannot be isolated, or it may simply be more convenient.

In situ TEM in dynamic conditions with real-time event monitoring can provide useful information during material processing. Indeed, studies of how materials behave in their true state during actual conditions can be valuable [29].

The recent development of computational techniques means that digital image processing is a versatile and cheap method for enhancing images [30], and it can also be used to improve the images obtained by electron microscopy.

However, phase images often contain imperfections after they are reconstructed from holograms. Thus, the present study aimed to apply digital image processing to

eliminate the imperfections that occur during the digital reconstruction of electron hologram images. This study comprises eight main chapters.

In chapter one, the background and aims of the study are introduced, including *in situ* off-axis electron holography, phase reconstruction, some digital image processing methods for *in situ* off-axis electron holography and including aberration correction for high resolution electron microscopy.

In chapter two, a new method of digital image processing is proposed and applied to the restoration of the phase imperfections in reconstructed phase images own to the low contrast of the electron amplitude, which has not be solved at present.

In chapter there, the new digital image processing methods are applied to a crystal structure image, including aberration correction and the restoration of singularities.

Chapter four considers undulation noise and its elimination.

Chapter five addresses the simulation of holograms with noise, including Poisson noise and Gaussian noise. Image processing methods are also used for noise elimination and the restoration of singularities.

The last chapter summarizes the main achievements of this study.

1.2 Off-axis electron holography

1.2.1 Off-axis electron holography concept

In general, the phase shift information related to electrons is lost during electron microscopy.

However, the use of electron holography based on the wave properties of electrons overcomes this limitation and it allows the electron phase shift to be recovered.

In particular, off-axis electron holography, which uses an image hologram, has the advantage of separating a reconstructed image from its complex conjugate image. This facilitates the restoration of microscopic aberrations of phase objects such as electromagnetic fields.

This chapter begins with a description of the experimental and theoretical basis of the off-axis electron holography technique. The transmission and interference of electron waves are described. Next, electron wave phase shifts are explained based on the off-axis electron holography measurement technique. The analysis of aberration correction is introduced after describing how to obtain the phase shift information. Finally, the applications of *in situ* off-axis electron holography to nanostructured materials are reviewed briefly.

The wavelength of the photons used to probe the sample and the numerical aperture of the system has limited the maximum theoretical resolution that can be obtained with a light microscope [31]. All matter has both wave and particle properties, as theorized by de Broglie, so electrons exhibit wave-like properties. The wavelength of electrons is related to their kinetic energy according to the de Broglie equation. In a TEM, the

velocity of electrons approaches the speed of light. Thus, additional corrections must be performed to account for relativistic effects [32].

In a TEM, the electrons are accelerated by an electric potential and focused by electrostatic and electromagnetic lenses onto the specimen. Thus, information about the electron density and phase is contained in the transmitted electron beam.

1.2.2 Electron wave interference

Electrons can behave as waves, which means that phenomena exhibited by light waves may also apply to electron waves, including interference [33].

In physics, interference is a phenomenon where two waves superimpose to form a resultant wave of greater or lower amplitude. The interaction between waves that are correlated or coherent with each other generates interference. These waves either always come from the same source or they have exactly the same wavelength. Interference effects can be observed with all types of waves, thus interference from uniform waves is needed.

In practice, it is often difficult to obtain interference patterns from two individual waves that come from different sources, although the two waves are a uniform type. In order to obtain interference, therefore, it is better if both waves have the same source point.

1.2.3 Introduction to off-axis electron holography

Over 20 variants of electron holography have been identified [34,35], but off-axis electron holography is the most useful, which is illustrated schematically in Fig.1-1[36].

The highly coherent electron illumination that is incident onto the specimen is provided by a FE gun (FEG), which is a high-brightness electron source. The region of interest is then positioned to cover approximately half of the field of view.

A positive voltage, typically between 10 V and 250 V, is applied to the electrostatic biprism, which overlaps a wave that has passed through the specimen (object wave) with a wave that has passed through the vacuum (reference wave).

The spacing of the interference fringes produced has an inverse relationship to the biprism voltage and the total number of fringes is approximately proportional to the square of the biprism voltage.

The modulations of hologram interference fringes recorded by a charge-coupled device (CCD) camera can be interpreted in terms of the phase and amplitude changes caused by the specimen.

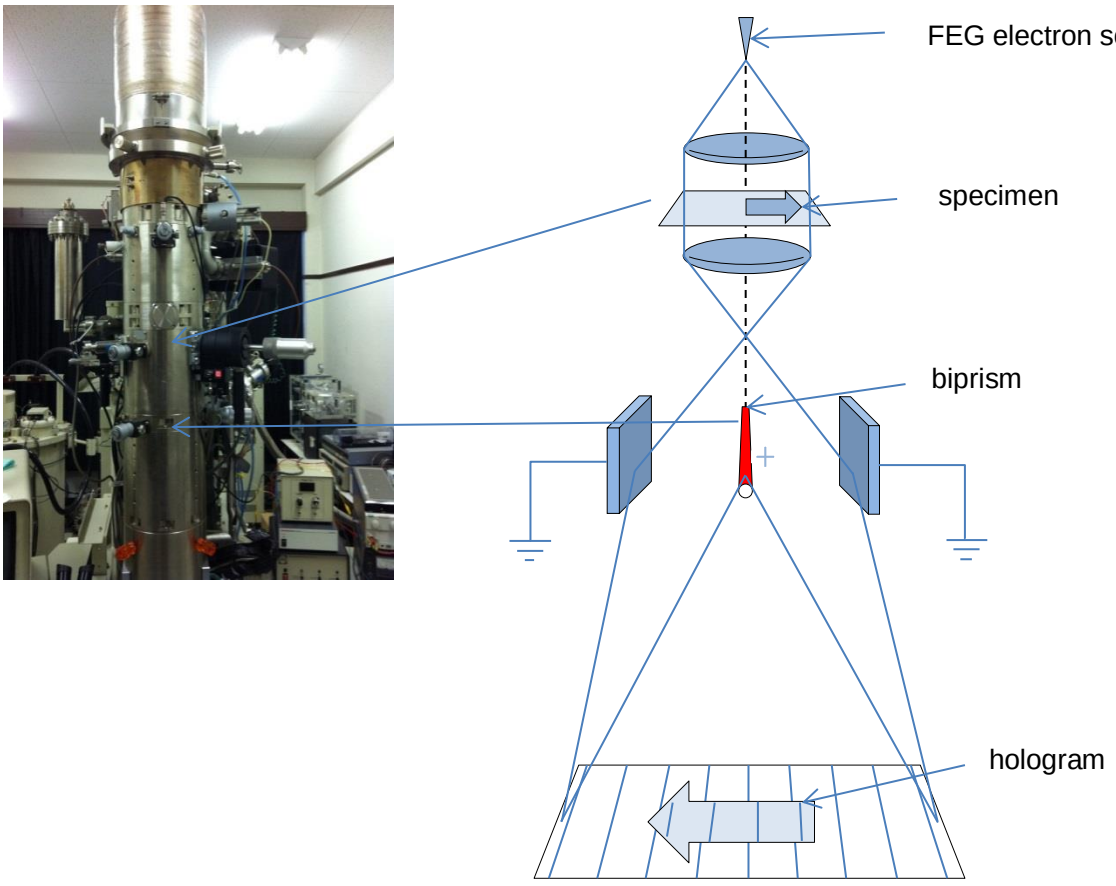

Fig. 1-1. Schematic illustration of microscope configuration for off-axis electron holography.

An off-axis electron hologram of a carbon nanofiber is shown in Fig.1-1, where the field of view is covered by two sets of fringes. The coarser fringes at the edges of the pattern are Fresnel fringes, which originate from the edges of the biprism wire, whereas the finer fringes visible across almost the entire field of view are the holographic interference fringes. The relative changes in the positions of these holographic fringes can be interpreted to obtain details of the phase shift.

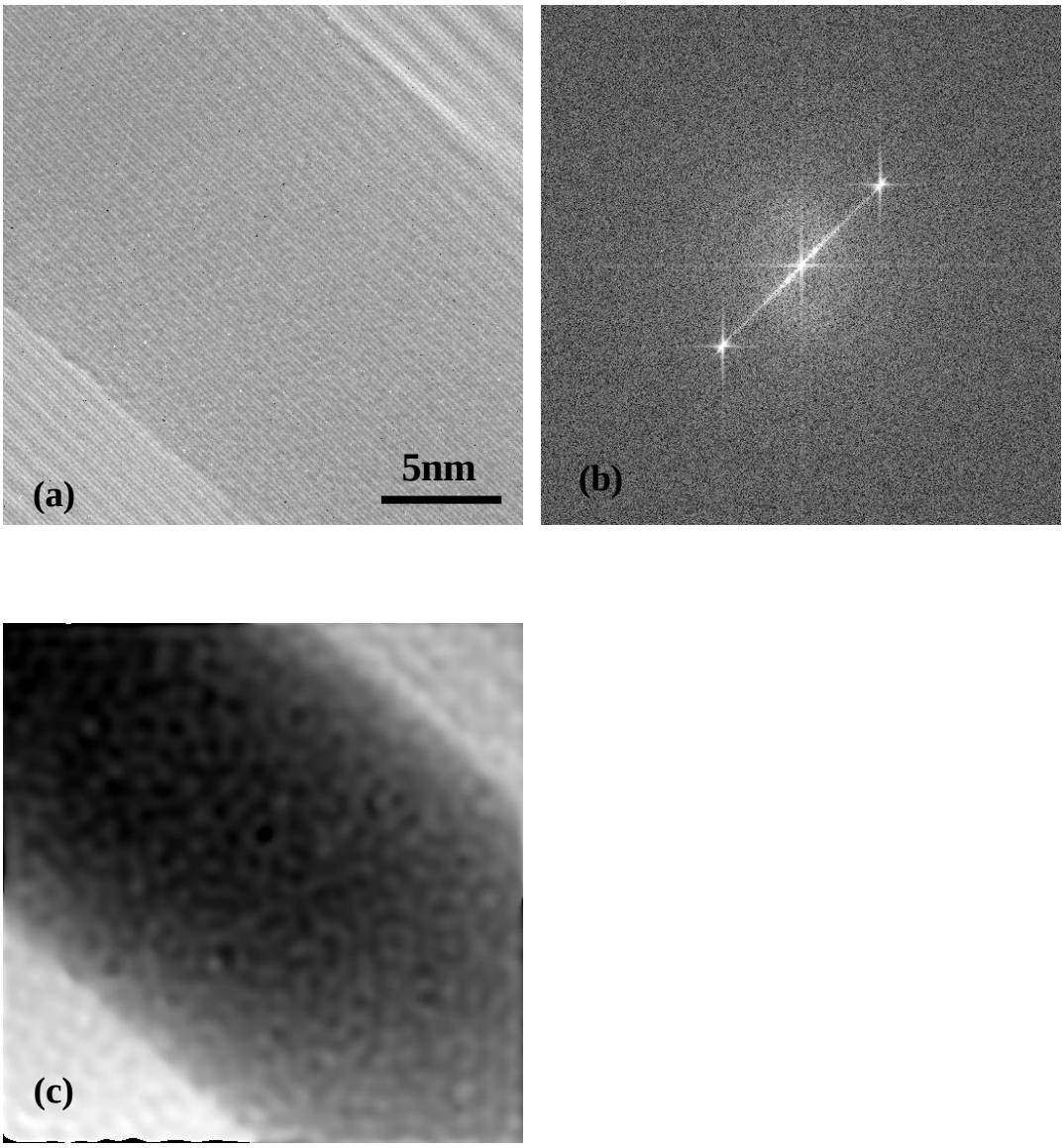

Fig. 1-2. (a) Off-axis electron hologram showing a nanofiber; (b) The fast Fourier transform (FFT) of the hologram; (c) Reconstructed phase image.

The center-band and side-band obtained by a fast Fourier transform (FFT) of the hologram are shown in Fig.1-2(b) and the phase shift information is shown in Fig. 1-2(c).

1.2.4 Principle of off-axis electron holography

In TEM, imaging can be considered in terms of modifications of the incident electron wave function [37].

The complex amplitude of the object wave in the image plane is expressed as:

$$\psi_1(x,y,z) = A(x,y)\exp\{i(\alpha kx + \varphi(x,y))\} \quad (1\text{-}1)$$

The beam tilting terms are expressed as αkx.

The complex amplitude of the reference wave in the image plane is expressed as:

$$\psi_2(x,y,z) = A(x,y)\exp\{i(-\alpha kx)\} \quad (1\text{-}2)$$

An expression for the intensity in hologram can be obtained by adding a reference wave to an object wave:

$$I(x,y) = |\psi_1 + \psi_2|^2$$

$$= 1 + A(x,y)^2 + 2A(x,y)\,cos\big(2\alpha kx + \varphi(x,y)\big)$$

$$= 1 + A(x,y)^2 + A\exp\{i(2\alpha kx + \varphi)\} + A\exp\{i(-2\alpha kx - \varphi)\} \quad (1\text{-}3)$$

The recorded hologram must be reconstructed to extract the required phase and amplitude information of the complex image wave.

First, the hologram is subjected to a FFT, which is described by the following equation:

$$FT[I(x,y)] = \delta(\boldsymbol{u}) + FT[A(x,y)^2] + FT[A(x,y)\exp\{i\varphi\}] * \delta(\boldsymbol{u} - \boldsymbol{u_c}) +$$

$$FT[A(x,y)\exp\{-i\varphi\}] * \delta(\boldsymbol{u} + \boldsymbol{u_c}) \quad (1\text{-}4)$$

where $*$ indicates a convolution operation.

There are two parts in the equation after the FFT process.

The first part is:

$$\delta(\boldsymbol{u}) + FT[A(x,y)^2] \qquad (1\text{-}5)$$

and this is related to the center-band. The central peak $\delta(\boldsymbol{u})$ at the origin corresponds to the Fourier transform (*FT*) of the uniform intensity of the reference image. A second peak $FT[A(x,y)^2]$ centered on the origin represents the FT of the conventional TEM micrograph of the specimen.

The second part is:

$$FT[A(x,y)\exp\{i\varphi\}] * \delta(u+u_c) + FT[A(x,y)\exp\{-i\varphi\}] * \delta(u-u_c) \qquad (1\text{-}6)$$

and this represents the side-bands. The remaining two peaks centered on $\boldsymbol{u_c}$ and $-\boldsymbol{u_c}$ comprise the desired image wave function and its complex conjugate, respectively.

The final part of the hologram reconstruction procedure involves filtering to select one of the side-bands, which is then inverse Fourier-transformed. The side-band region must be separated from the central peak by choosing sufficiently small fringe spacing and by selecting the size of the filter, which can be any shape.

The hologram reconstruction procedure can be expressed as follows:

$$FT^{-1}\left[FT[A\exp\{i(2\alpha kx+\varphi)\}]\right] \times \exp\{i(-2\alpha kx)\} = A(x,y)\exp\{i\big(\varphi(x,y)\big)\} \qquad (1\text{-}7)$$

where the reconstructed amplitude distribution

$$A(x,y) = Mod\{\varphi(x,y)\} \tag{1-8}$$

where the reconstructed phase distribution

$$\varphi(x,y) = Tan^{-1}\{\frac{Re\{\varphi(x,y)\}}{Im\{\varphi(x,y)\}}\}$$

$$IF\ Re\{\varphi(x,y)\} \geq 0,\ -\frac{\pi}{2} \leq \varphi(x,y) < \frac{\pi}{2}$$
$$Re\{\varphi(x,y)\} < 0,\ -\pi \leq \varphi(x,y) < -\frac{\pi}{2}\ \text{OR}\frac{\pi}{2} \leq \varphi(x,y) < \pi \tag{1-9}$$

1.2.5 Phase shift of an electron wave

Electrons that pass through a TEM specimen generate a phase shift, which is produced by the electrostatic potential and the in-plane component of the magnetic induction.

The phase shift of an electron relative to the electron passing through a vacuum can be expressed as follows [38]:

$$\psi(x) = C_E \int V(x,z)dz - [\frac{e}{\hbar} \iint B_{\perp}(x,z)t(x)dxdz] \quad (1\text{-}10)$$

where z is the incident electron beam direction, x is a direction in the plane of the specimen perpendicular to the electron biprism, V is the electrostatic potential, $B_{\perp}$ is a component of the magnetic induction, t is the specimen thickness, and C_E is an energy-dependent constant at an electron-accelerating voltage.

If neither V nor $B_{\perp}$ vary within the specimen along the beam direction, the equation can be simplified to:

$$\psi(x) = C_E V(x,z)t(x) - \frac{e}{h} \int B_{\perp}(x)t(x)dx \quad (1\text{-}11)$$

In the absence of magnetic and long-range electric fields, the dynamical diffraction can be neglected, such as that occurring in a depletion region in semiconductors, thus the equation can be re-written as [39]:

$$\psi(x) = C_E \int V_0(x,z)dz \quad (1\text{-}12)$$

where V_0 is the mean inner potential of the specimen, which depends on the local composition and density. This is usually the dominant contribution to the electrostatic potential.

If the specimen has a uniform structure and composition in the beam direction, then the expression reduces still further to:

$$\psi(x) = C_E V_0(x,z)t(x) \tag{1-13}$$

Electron holography is the most accurate technique that is currently available for measuring the mean inner potential of a specimen, as shown in Fig. 1-34[40].

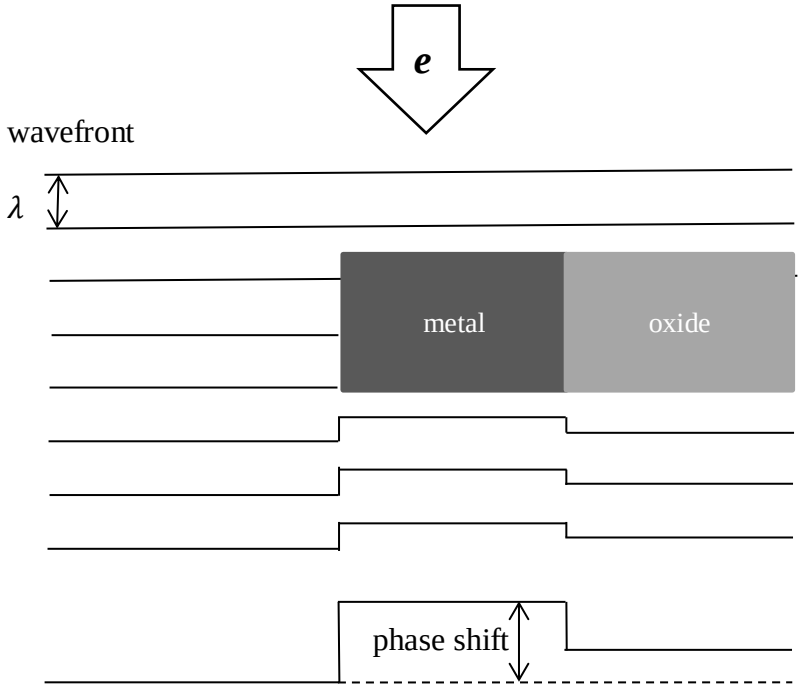

Fig. 1-3. Phase shift in off-axis electron holography. The phase shift is directly relevant to the mean inner potential distribution of a specimen in the matter with the constant thickness.

1.2.6 Phase shift of an electron wave

As stated previously, *in situ* TEM allows the study of materials in dynamic conditions. The behavior of materials in their true state may differ in various active conditions, according to the experimental parameters.

In situ off-axis electron holography allows us to study accurate phase changes in a material in various active conditions with different experimental parameters [41,42].

The holograms acquired in different active conditions may vary considerably, where Figs 1-4 (a) and (b) provide an example.

These two holograms were acquired in a vacuum and in an oxygen atmosphere, respectively, with the same illumination conditions, including adjustment for probe astigmatism, condenser lens power, condenser aperture, resolution, acquisition time, the current emission value of the cold FEG, and the voltage applied to the filament of the electron biprism.

The random noise present in the holograms differs greatly. Considerably more noise is present in the hologram acquired in an oxygen atmosphere compared with the hologram acquired in a vacuum.

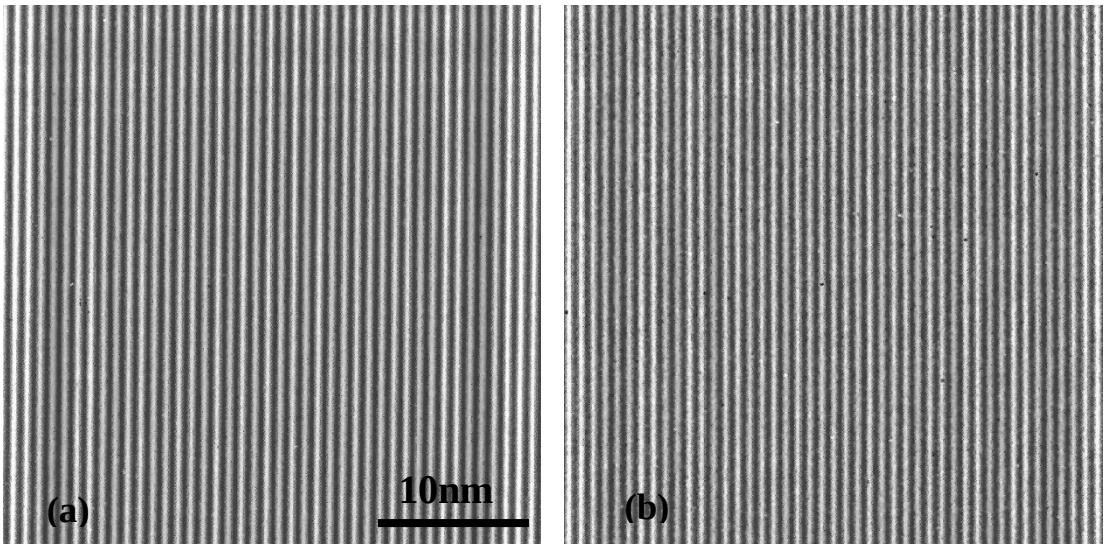

Fig. 1-4. (a) Electron wave interference pattern in a vacuum; (b) Electron wave interference pattern in an oxygen atmosphere.

The FT images shown in Figs 1-5(a) and 1-5(b) are based on the image frequency spectra in a vacuum and in an oxygen atmosphere, respectively.

The center-band and side-bands are fairly obvious compared with the surrounding regions of the frequency spectra for the image obtained in a vacuum, which means that there is a high signal to noise ratio (SNR). By contrast, the center-band and side-bands are less obvious compared with the surrounding regions of the frequency spectra for the image obtained in an oxygen atmosphere, i.e., low SNR performance.

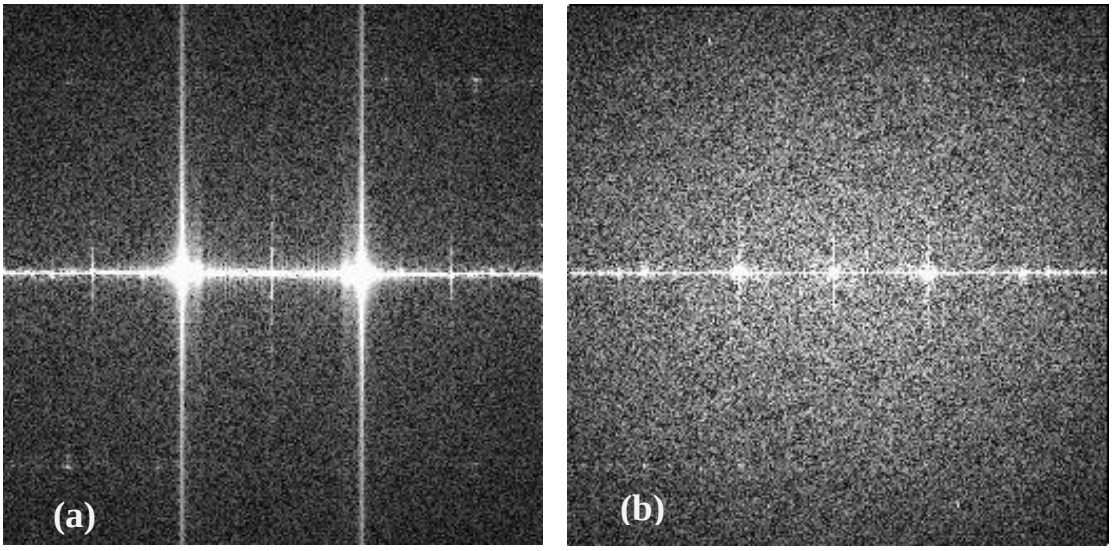

Fig. 1-5. (a) Diffractograms of the electron wave interference pattern in a vacuum; (b) Diffractograms of the electron wave interference pattern in an oxygen atmosphere.

The phase image reconstructed from the hologram in a vacuum is shown in Fig. 1-6(a), while that for the oxygen atmosphere phase image is shown in Fig. 1-6(b).

As shown in the reconstructed phase image, the noise level was higher with oxygen. Thus, the SNR is lower, which increases the difficulty of separating the signal from the noise. Therefore, image processing is required to overcome this issue.

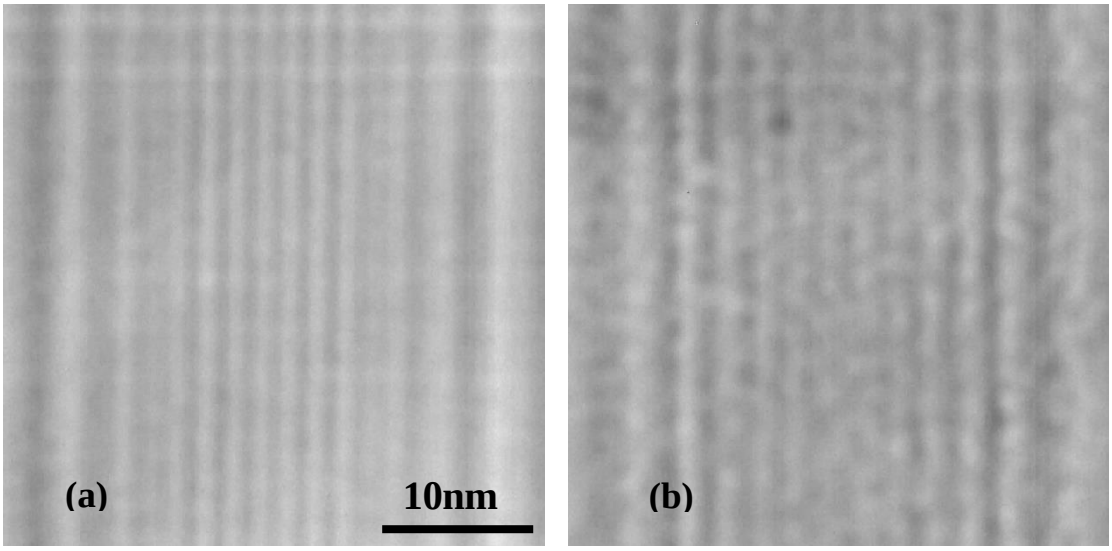

Fig. 1-6. (a) The phase image reconstructed from the hologram in a vacuum; (b) The phase image reconstructed from the hologram in an oxygen atmosphere.

1.3 Digital image processing

1.3.1 Electron microscope image

The availability of fast computers and signal processors in the 21st century means that digital image processing has become the most common form of image processing. It is used widely because it is the most versatile method and the cheapest.

Electron microscope images are a type of digital image, which are obtained using a form of electron beam as the energy source.

Thus, digital image processing has been applied to electron microscope images.

This section introduces the digital image processing techniques used for processing electron microscope images.

1.3.2 Spatial domain processing

Image enhancement approaches belong to two broad categories: spatial domain methods and frequency domain methods. The term spatial domain refers to the image itself and the approaches that belong to this category are based on the direct manipulation of pixels in an image in the real space.

There is no general theory of image enhancement. Thus, when an image is processed, the user is the ultimate judge of how well a particular method works[43].

Spatial domain processes are denoted by the following expression, which operates directly on the pixels:

$$g(x,y) = T[f(x,y)] \qquad (1\text{-}14)$$

where $f(x,y)$ is the input image, $g(x,y)$ is the processed image, and T is an operator applied to an image.

In general, spatial domain methods include basic grayscale level transformation, histogram processing, image arithmetic/logic operations, smoothing spatial filters, sharpening spatial filters, and spatial combining methods.

All of these spatial domain methods can be used to process electron microscope images, depending on the user's requirements. However, smoothing spatial filters and histogram processing are used more frequently than other methods for processing electron microscope images.

Histograms are the basis of numerous spatial domain processing techniques. Histogram manipulations can be effective for image enhancement and the applications

of these manipulation techniques are described in a later chapter.

Histogram manipulations include histogram equalization, histogram matching, local enhancement, and image enhancement using histogram statistics.

The process of spatial filtering can be expressed as follows, which is performed directly on the pixels in an image:

$$g(r) = \frac{1}{N}\sum I(r+q)W(q) \qquad (1\text{-}15)$$

where I is the input image, g is the processed image, W is the filter, and q is the size of the filter window.

Smoothing spatial filters are generally used for blurring and noise reduction. Blurring is always used in preprocessing steps, such as the removal of small details from an image prior to object extraction, and for bridging small gaps in lines or curves.

Noise reduction can also be achieved by blurring with a linear filter and by nonlinear filtering.

The output of a smoothing linear spatial filter is simply the average of the pixels present in the neighborhood of the filter mask, thus they are sometimes known as averaging filters. The process of smoothing spatial filtering can be expressed as follows:

$$g(r) = \frac{1}{N}\sum_{i=1}^{N} I_i(r) \qquad (1\text{-}16)$$

where $\boldsymbol{I}$ is the input image, $\boldsymbol{g}$ is the processed image, and N is the sum of the pixels in the filter mask.

Figure 1-7 shows two smoothing filters and the sum of the pixels, i.e., $N = 9$, and

$N = 16$, respectively.

1	1	1
1	1	1
1	1	1

1	2	1
2	4	2
1	2	1

Fig. 1-7. Two smoothing filters with different values of *N*.

Smoothing spatial filtering is often used to reduce various types of noise in electron microscope images. These types of noise are derived mainly from recording noise, contamination of the sample, and quantum noise caused by the weakness of the incoming electron wave.

1.3.3 Frequency domain processing

Frequency domain processing techniques are based on modifying the Fourier transform of an image.

The Fourier transform may be viewed as a "mathematical prism," which separates a function into various components based on the frequency content. The frequency contents of a function (signal) can be characterized using the Fourier transform.

Digital images can be viewed as a two-dimensional discrete function, which is applicable to the two-dimensional discrete Fourier transform.

Filtering is straightforward in the frequency domain, which can be expressed as follows:

$$G(u,v) = H(u,v)F(u,v) \qquad (1\text{-}17)$$

where $H(u,v)$ is the frequency filter, $G(u,v)$ is the Fourier transform of the processed image, and $F(u,v)$ is the Fourier transform of the original image.

Sharp transitions such as noise in the grayscale level of an image contribute significantly to the high-frequency content of its Fourier transform in the frequency domain.

Smoothing is achieved by attenuating a specified range of high-frequency components in the frequency domain of a given image.

In general, the noise is not periodic in electron microscope images [44,45]. Thus, performing an inverse Fourier transformation using only the areas surrounding the diffraction point in the Fourier transform image can eliminate most of the nonperiodic

noise.

However, great care must be taken not to eliminate useful information in the Fourier transform image.

Figure 1-8 shows an example of the elimination of nonperiodic noise.

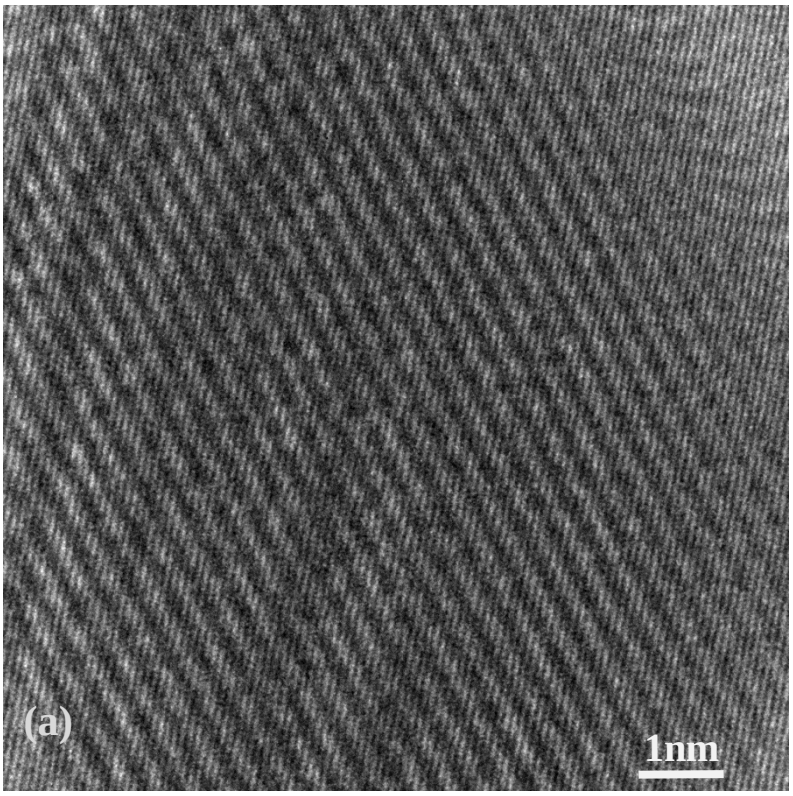

Fig. 1-8. The elimination of nonperiodic noise. (a) High resolution hologram.

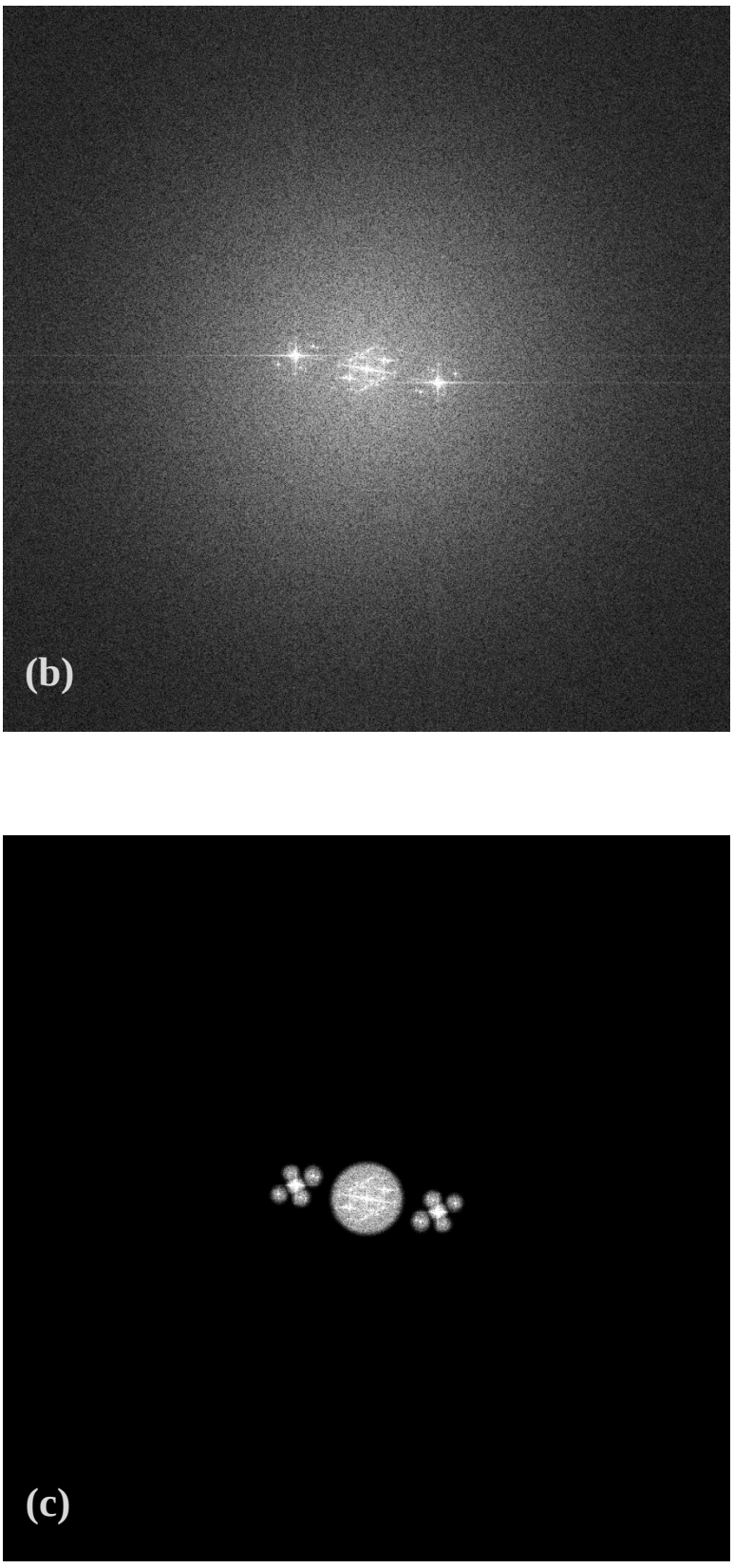

Fig. 1-8 (b) The FFT of the hologram; (c) The areas surrounding the diffraction point in the Fourier transform image.

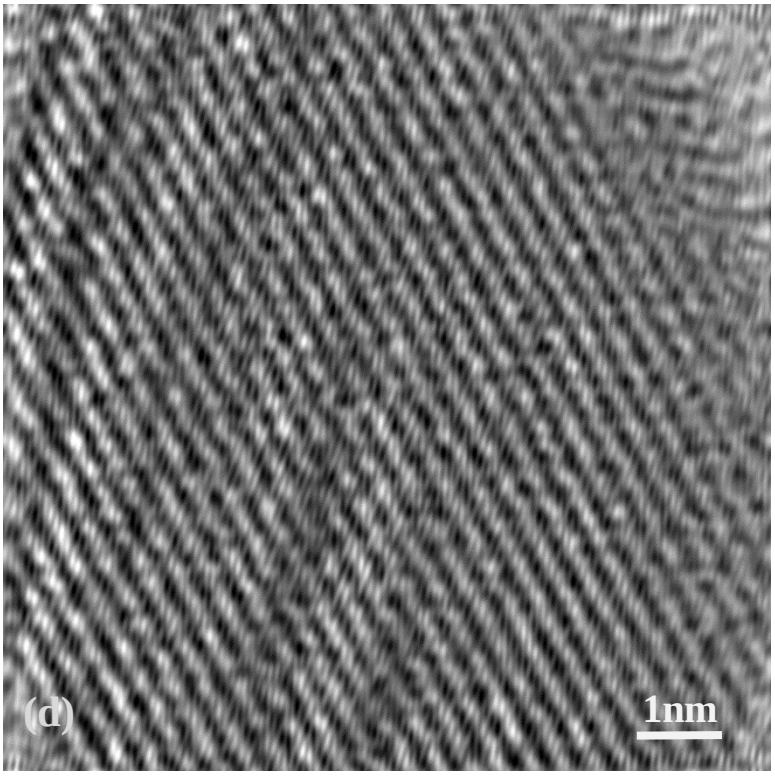

Fig. 1-8(d) The reconstructed image from (c).

In addition, there are other frequency domain processing techniques, such as sharpening frequency domain filters. All of these frequency domain processing techniques can be applied to electron microscope images, if necessary.

1.3.4 Morphological image processing

Mathematical morphology, which was developed by Matheron and Serra [46], is an effective tool for extracting image components. Some components are useful for the representation and description of region shapes. Boundaries, skeletons, and the convex hull are used regularly as region shapes during processing. Morphology is a unified and powerful approach for addressing numerous image processing problems [47].

In mathematical morphology, sets represent the objects in an image. The set of all black pixels in a binary image is a complete morphological description of the image. This concept will be applied to processing in a later chapter.

The fundamental operations of morphological processing are dilation and erosion, and many morphological algorithms are based on these two primitive operations.

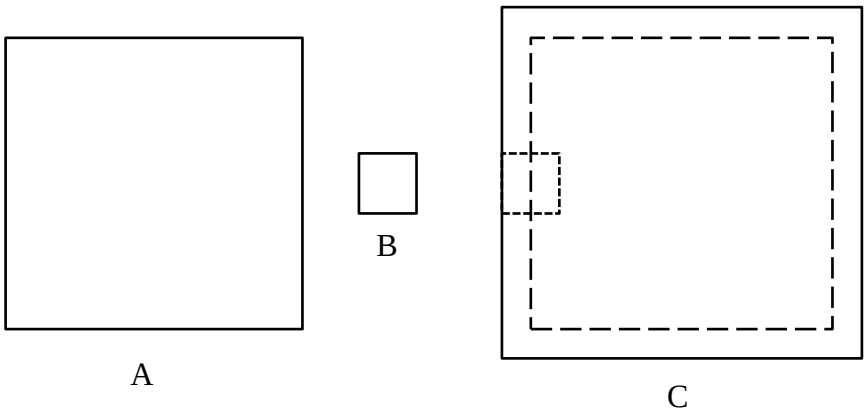

Fig. 1-9. The operational principle of dilation.

Figure 1-9 illustrates the operational principle of dilation, where C is the dilation of A using element B.

Dilation refers to “expanding” or “thickening” in a binary image, where the dilation

operation can bridge gaps.

Erosion refers to “shrinking” or “thinning” in a binary image. Thus, the erosion operation can be used to eliminate irrelevant details. Dilation and erosion complement each other.

Figure 1-10 shows the operational principle of erosion, where C is the erosion of A using element B.

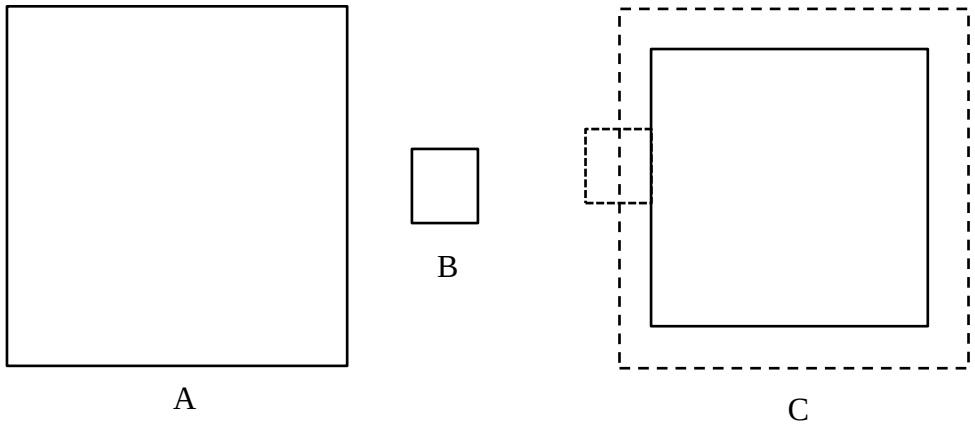

Fig. 1-10. The operational principle of erosion.

Opening and closing are two other important morphological operations.

In general, opening can be used to smooth the contours of an object, break narrow connections, and eliminate thin protrusions. Closing also tends to smooth section of

contours, but it is generally used to fuse narrow breaks and long thin gulfs, to eliminate small holes, and to fill gaps in the contour.

Several methods have been developed for frequent use, such as skeletons, thinning, thickening, boundary extraction, and region filling.

Skeletons will be discussed in a later chapter.

A skeleton can be expressed in terms of several erosions and openings, which can be described as removing the boundary pixels continuously.

Some programs can perform skeleton processing using specific functions in their tool boxes. We describe this type of processing using software in a later experiment.

1.3.5 Reconstructed phase image and unwrapping method

In general, reconstructed phase images use the grayscale level to indicate the phase value.

However, the Fourier transform method is normally used in the digital reconstruction process, although this method always causes a phenomenon where the phase contrast reverses abruptly from white to black in reconstructed phase images.

One cause of these contrast reverses is the well-known 2π phase jump attributable to the digital reconstruction process. Arctangent functions can be used to reconstruct the phase, but the region of the inverse of the arctangent functions is restricted within the range $[-\pi/2, \pi/2]$. Thus, even if we expand the region shown in equation (1-9), the maximum is in the range $[-\pi, \pi]$.

Phase contrast reverses occur when the phase is outside the domains.

Phase unwrapping has an important role in phase measurement. The depth information for the object being measured is defined implicitly by certain equations derived from data.

In this type of 2π reverse, the phase can be unwrapped and connected smoothly using the appropriate program [48]. The unwrapping program coded by Gatan Inc. was used in the present study.

First, we must unwrap the wrapped phase of the entire image to obtain the actual phase.

Figure 1-11 shows the effects of the unwrapping processing, where (a) is the original hologram, (b) is the reconstructed phase image from (a), and (c) is part of the phase

image after unwrapping processing.

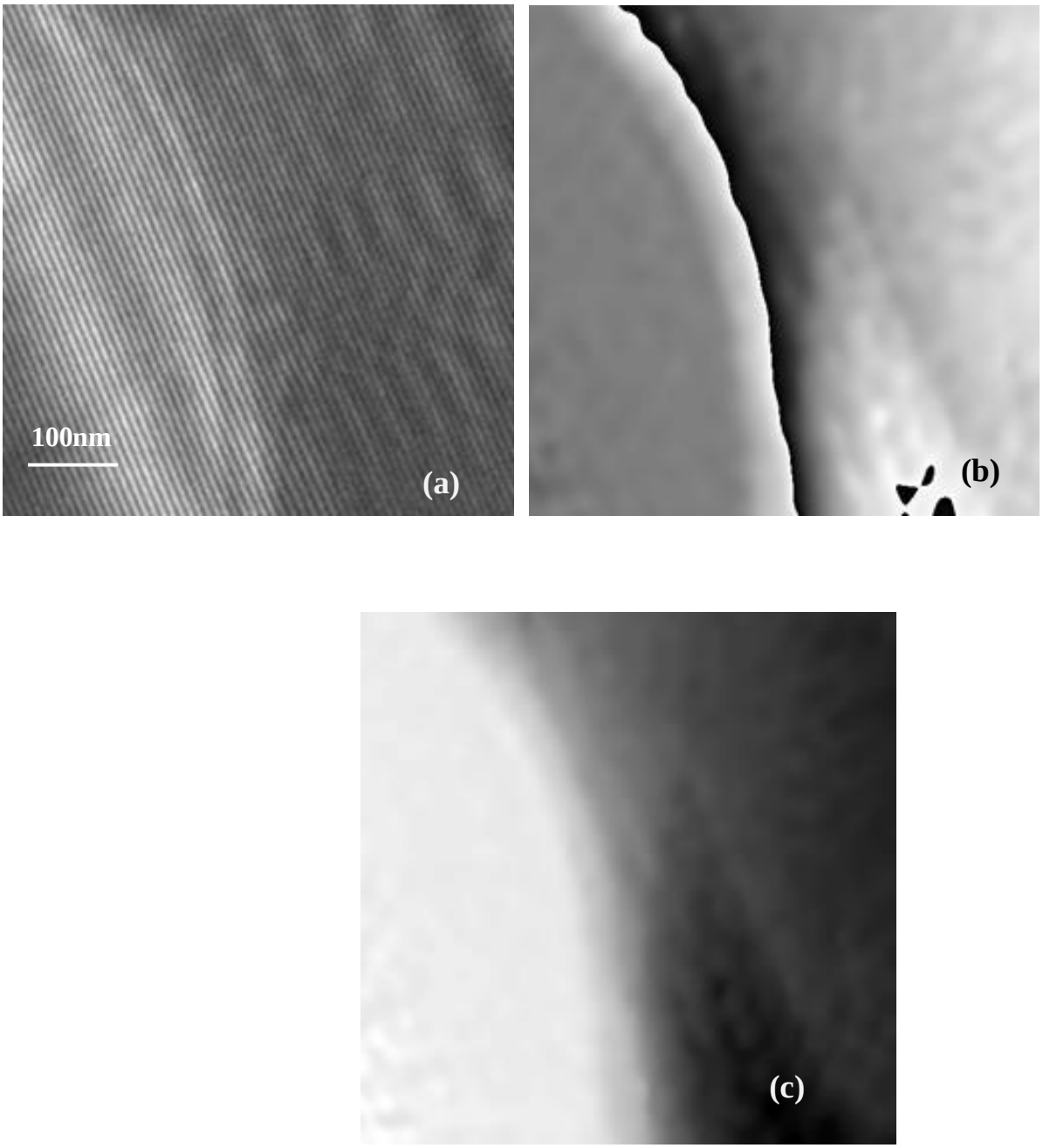

Fig. 1-11. The unwrapping processing. (a) the original hologram.(b) the reconstructed phase image from (a). (c) the phase image after unwrapping processing.

1.3.6 Aberration correction for high resolution electron microscopy

Aberrations have very complex effects at higher spatial frequencies and they cannot be corrected easily using image processing techniques based on linear light optics [49]. The only exceptions are weak phase objects with almost linear imaging. However, the samples suitable for weak phase object approximation are restricted to very special cases. Electron holography is one of the most powerful tools subjected to nonlinear image processing [50].

The wave function in the image plane of an electron microscope can be expressed by the following function, where o(r) is the penetration wave and p(r) is the point spread function,

$$\psi(\boldsymbol{r}) = o(\boldsymbol{r}) * p(\boldsymbol{r}). \quad (1\text{-}17)$$

Its Fourier transformation can be given as

$$\Psi(\boldsymbol{u}) = FT[\psi(\boldsymbol{r})] = O(\boldsymbol{u})P(\boldsymbol{u}) \quad (1\text{-}18)$$

where P($\boldsymbol{u}$) is a transfer function and $\chi(\boldsymbol{u})$ is an aberration function, which can be written as

$$\mathrm{P}(\boldsymbol{u}) = \exp[-\mathrm{i}\chi(\boldsymbol{u})], \quad (1\text{-}19)$$

where

$$\chi(k) = 0.5\pi Cs\lambda^3|\boldsymbol{u}|^4 + \pi df\lambda|\boldsymbol{u}|^2, \quad (1\text{-}20)$$

where Cs is the spherical-aberration constant of the objective lens, df is the defocusing distance, and λ is the electron wavelength.

Assuming that the correction function is

$$\mathrm{H}(\boldsymbol{u}) = 1/\mathrm{P}(\boldsymbol{u}), \quad (1\text{-}21)$$

we can represent

$$\mathrm{O}(\boldsymbol{u}) = \Psi(\boldsymbol{u})\mathrm{H}(\boldsymbol{u}) \qquad (1\text{-}22)$$

and we obtain

$$\mathrm{o}(\boldsymbol{r}) = \mathrm{FT}^{-1}[\mathrm{O}(\boldsymbol{u})]. \qquad (1\text{-}23)$$

1.3.7 Software used for processing

MATLAB

MATLAB (matrix laboratory) was developed by MathWorks and it provides a numerical computing environment with a fourth generation programming language. MATLAB allows matrix manipulations, the plotting of functions and data, implementation of algorithms, creation of user interfaces, and interfacing with programs written in other languages [51].

An optional toolbox using the Multi Processing Algebra Data Tool (MuPAD) symbolic engine also provides access to symbolic computing capacities, in addition to primarily numerical computing,

In the present study, we used MATLAB for digital image processing because it can readily handle an image as a matrix and it also has a toolbox for image processing, which is a set of functions. Thus, it was sometimes possible to use functions present in the toolbox without coding the functions ourselves.

In the following processes, MATLAB was used as the primary tool.

Thus, the phase correction methods and some smooth filters were based on MATLAB.

Digital micrograph

Digital micrograph (DM) is leading industrial software, which was developed by Gatan Inc, and it provides TEM users with a complete package for the acquisition, processing, analysis, and presentation of image and spectrum data. DM provides powerful functions and useful features, which make it the preferred choice for digital imaging in TEM.

In the present study, we used several plug-in modules to increase our productivity while performing microscopy. On occasions, we also used a scripting language to code the functions we needed.

In this study, the unwrapping methods and some smooth filters were based on DM.

1.4 Phase imperfection

At present, the other type of abrupt phase contrast reverses usually occurs in the areas with low contrast of the electron wave amplitude, which is evidently different with the well-known 2π phase jump attributable to the digital reconstruction process.

This type of phase reverses will result in phase imperfections in the reconstructed phase image as the phase information is erroneous, and it has not been studied and solved effectively.

The disconnection and wrong connection of interference fringes due to low contrast of the electron wave amplitude in specific areas of the sample could cause this type of abrupt phase reverses by analysis of the interference fringe in our studies.

Computers may confuse the connection between fringes because of the low contrast of the electron-wave amplitudes when the reconstruction of the phase is executed.

The presence of the phase imperfections by low contrast of electron-wave amplitudes will be shown in the next chapter, and the detail of the study and solutions will be described also.

1.5 Conclusion

In situ off-axis electron holography has evolved over the years and it is now considered to be a routine and reliable technique for characterizing nanostructured materials.

In situ off-axis electron holography may be a valuable approach for solving industrial problems. However, there is a problem with this method because noise is introduced during different active conditions, but the development of computational image processing techniques may overcome this limitation.

In summary, digital image processing plays an important role in modern imaging techniques, which have been facilitated by the development of high-speed computers. Digital image processing can also be applied to electron microscope images due to the development of the CCD camera.

In the next chapters, digital image processing techniques are introduced to handle the phase information from electron holograms, which may eliminate phase imperfections to a great extent.

Many digital image processing methods are available for electron microscope image processing, depending on the user's needs. Combinations of these processing methods may allow a microscopist to improve the quality of their microscope images. The use of combinations of methods is described in a later chapter.

References

[1] A. Dowling, et al. (2004)"Nanoscience and nanotechnologies: opportunities and uncertainties". Royal Society and Royal Academy of Engineering. July 2004. Retrieved 13 May 2011

[2] S. Rajiv, S. Santosh, S. Sugandha (2010). "Nanotechnology: The Future Medicine". Journal of Cutaneous and Aesthetic Surgery 3 (1): 32–33.

[3] C. Buzea, I. Pacheco, and K. Robbie (2007). "Nanomaterials and Nanoparticles: Sources and Toxicity". Biointerphases 2 (4): MR17–71.

[4] Drexler, K. Eric (1986). Engines of Creation: The Coming Era of Nanotechnology. Doubleday.

[5] Drexler, K. Eric (1992). Nanosystems: Molecular Machinery, Manufacturing, and Computatin. New York: John Wiley & Sons.

[6] Apply nanotech to up industrial, agri output, The Daily Star (Bangladesh), 17 April 2012.

[7] A. Ernst (1874). "A Contribution to the Theory of the Microscope and the Nature of Microscopic Vision". Proceedings of the Bristol Naturalists' Society 1: 200–261

[8] Ultraviolet microscope. (2010). In Encyclopædia Britannica. Retrieved November 20, 2010, from Encyclopædia Britannica Online

[9] E. Ruska, translation by T. Mulvey. The Early Development of Electron Lenses and Electron Microscopy.

[10] J. Plücker (1858). "Über die Einwirkung des Magneten auf die elektrischen Entladungen in verdünnten Gasen" [On the effect of a magnet on the electric discharge

in rarified gases]. Poggendorffs Annalen der Physik und Chemie 103: 88–106.

[11] Ernst Ruska (1986)."The Nobel Prize in Physics 1986, Perspectives – Life through a Lens". nobelprize.org.

[12] F. Braun (1909). "The Nobel Prize in Physics 1909, Biography". nobelprize.org.

[13] R. Reinhold (May 30, 1931). "Configuration for the enlarged imaging of objects by electron beams".

[14] L. Broglie (1928). "La nouvelle dynamique des quanta". Électrons et Photons: Rapports et Discussions du Cinquième Conseil de Physique. Solvay.

[15] P. Hawkes,(1985). The beginnings of Electron Microscopy. Academic Press.

[16] A. V. Crewe, M. Isaacson and D. Johnson (1969). "A Simple Scanning Electron Microscope". Rev. Sci. Inst. 40 (2): 241–246

[17] Crewe Albert V, J. Wall and J. Langmore (1970). "Visibility of a single atom". Science 168 (3937): 1338–1340.

[18] R. Egerton (2005). Physical principles of electron microscopy. Springer.

[19] A. Hubbard, (1995). The Handbook of surface imaging and visualization. CRC Press.

[20] A. Tonomura (1978). "Development of a Field Emission Electron Microscope". J. Electron Microscopy .vol. 28,No.1,1-11.

[21] A. Tonomura (1984).Applications of electron holography using a field-emission electron microscope. J. Electron Microscopy .vol. 33,No.2,101-115.

[22] A. Tonomura, (1987). Applications of electron holography, Rev. Mod. Phys. 59, 639.

[23] D. Gabor (1948). A new microscopic principle, Nature 4098, 777.

[24] D. Gabor (1949) Microscopy by reconstructed wavefronts. Proc. Roy. Soc. London A197: 454-487.

[25] Leith and Upatnieks (1964). Wavefront Reconstruction with Diffused Illumination and Three-Dimensional Objects. Journal of the Optical Society of America. Vol.54,No.11.

[26] G. Möllenstedt and H. Düker (1956). Beobachtungen und Messungen an Biprisma-Interferenzen mit Elektronenwellen, Zeitschrift für Physik, 145, 377

[27] M. Lehmann, H. Lichte (2002). Tutorial on off-axis electron holography, Microsc. Microanal. 8(6), 447–466.

[28] R. E. Dunin-Borkowski et al. (2004),Micros. Res. and Tech. 64, 390.

[29] P.L.Gai, *In situ* microscopy in the materials research,(1997), Klumer Academic Publisheres.

[30] R.C. Gonzalez and R. E. Woods (2002) Digital Image Processing. Prentice Hall, Upper Saddle River, New Jersey.

[31] B. Fultz and J. Howe, (2007). Transmission Electron Microscopy and Diffractometry of Materials. Springer.

[32] P. E. Champness, (2001). Electron Diffraction in the Transmission Electron Microscope. Garland Science.

[33] L. Broglie, (1928). "La nouvelle dynamique des quanta". Électrons et Photons: Rapports et Discussions du Cinquième Conseil de Physique. Solvay.

[34] J.M. Cowley, (1992). Ultramicroscopy 41:335.

[35] P.A. Midgley,(2001). An introduction to off-axis electron holography. Micron 32, 167–184

[36] A . Tnomura, (1998) Electron Holography, 2nd Enlarged Edition, Springer Series in Optical Sciences vol.70.

[37] J.M. Cowley, (1995). Diffraction Physics, 3rd Edition North Holland, Amsterdam.

[38] L. Reimer,(1991). Transmission Electron Microscopy. Springer, Berlin.

[39] M.R.McCartney, R. E. Dunin-Borkowski, D.J.Smith, (2005). Off-Axis Electron Holography, Handbook of Microscopy of Nanotechnology, Kluwer Academic Publishers.

[40] M. Gajdarcziska-Josifovsk and A. Carim, (1998). Introduction to Electron Holography. Kluwer, New York.

[41] T. Tanji, K. Urata, k. Ishizuka, Q.Ru, A. Tonomura, (1993) Obervation of Atomic Surface Potential by Electron Holography. Ultramicroscopy, 49,259-264.

[42] T. Tanji, S. Mizuno, T. Kato, T. Hirayama, (2009) Electron Holography of Hetero-Interfaces in Solid Oxide Fuel Cells. Microscanal.15(2), 1424-1425.

[43] R. C. Gonzalez, and R. E. Woods Steven (2002). Digital Image Processing, 2nd, Prentice Hall,NJ.

[44] J.F. Walkup, J.W. Goodman, (1973). J. Opt. Soc. Am. 63, 399.

[45] H. Lichte, et al. (1987). Optik 77 (3).

[46] J. P. Serra (1984) Image analysis and mathematical morphology. Academic Press, New York.

[47] J. P. Serra, P. Soille, (1994). Mathematical morphology and its applications to image processing, Kluwer Academic Publishers.

[48] D. C. Ghiglia and M. D. Pritt, (1995). Two-Dimensional Phase Unwrapping: Theory Algorithms and Software. Wiley, New York.

[49] T. Tanji, T. Ohno, K. Ishizuka and A. Tonomura, (1994). Aberation-Free Image of an MgO Crystal Edge-An application of Image Restoration in Electron Holography, Joural of Electron Microscopy,43(5),318-321.

[50] A. Tonomura, L. F .Allard, G. Pozzi , D. C. Joy, and Y. A. Ono (1995) Electron Holography. Elsevier Science, New York. 45–54.

[51] A. Gilat, (2004). MATLAB: An Introduction with Applications, 2nd Edition, John Wiley & Sons.

Chapter two

2. Image processing to correct phase imperfections

2.1 Preamble

Recently, electron holography has been used widely for characterizing materials [1], even in severe conditions such as *in situ* observations in gas atmospheres, sharp or large phase changes such as crystal lattice images, and bulk specimen edges in low S/N ratio conditions. In these applications, it is necessary to obtain accurate phase information without changing the conditions in the actual applications. Thus, it is essential to develop a method for eliminating imperfections based on posterior image processing.

In electron holography, phase imperfections may occur in a digitally reconstructed phase image, potentially resulting in inaccurate phase information.

In this section, we apply a image processing method which is propose firstly to eliminate the imperfections owing to the low contrast of electron wave amplitude in the phase reconstruction images.

A relatively accurate phase information image is reconstructed using the proposed method.

2.2 Phase imperfections in reconstructed phase image

At present, most holograms are reconstructed using the Fourier transform method [2,3]. In some cases, however, a phenomenon occurs where the contrast reverses abruptly from white to black in phase images that are reconstructed directly using a digital Fourier transform.

In general, phase contrast images use the grayscale level to indicate the phase value. Two types of abrupt reversal mainly occur in phase contrast images.

The first type of abrupt reversal is the well-known 2π phase jump [4] during the digital reconstruction process, which occurs because the reconstructed phase falls within a range of $[-\pi, \pi]$ [5]. In this case, the phase can be unwrapped and connected in a smooth manner to allow such a jump using the appropriate software, as explained earlier.

The other type of abrupt reversal usually occurs in the areas with low contrast of the electron wave amplitude. However, at present this type of reversal has not been studied and solved effectively. Therefore, this is the key problem we need to address.

The other type of reversal is caused by the disconnection of interference fringes due to low contrast of the electron wave amplitude in specific areas of the sample by analysis of the interference fringe.

People may recognize the correct connection between fringes intuitively, but computers may confuse the connection between fringes because of the low contrast of the electron-wave amplitudes.

The presence of low contrast of the electron-wave amplitudes in specific areas of a

sample is shown in Fig. 2-1.

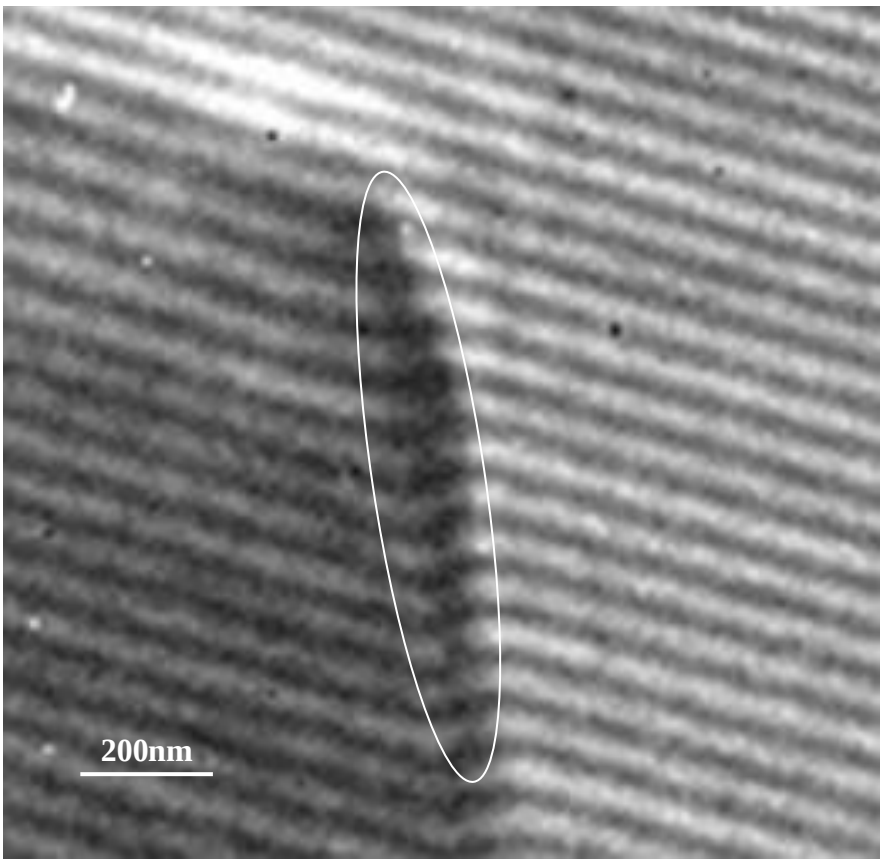

Fig. 2-1. Electron hologram with weak
electron-wave amplitudes in specific areas.

A phase imperfection in the reconstructed phase image of the CeO_2 particle is indicated by the gray oval in Fig. 2-2. In this case, the smooth change in the phase is normal on one side of the defect edge (A), whereas the abrupt reversal of phase is abnormal on the opposite side of the defect edge (B), which is indicated by the spiral arrow in Fig. 2-2.

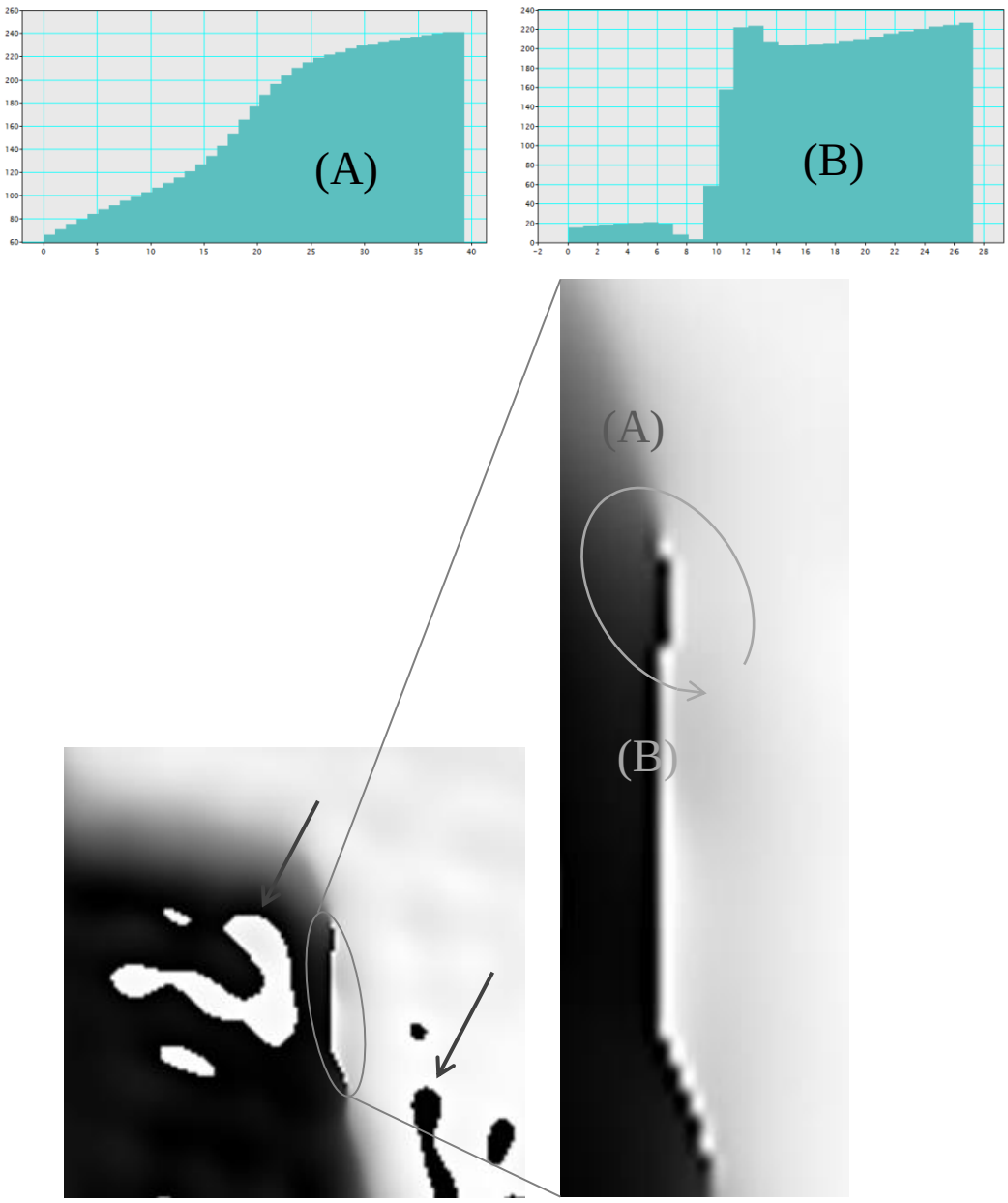

Fig. 2-2. Phase imperfection in the reconstructed phase image.

2.3 Off-axis electron holography

An example of an electron hologram of a CeO_2 particle captured by a CCD camera is shown in Fig. 2-3(a). The interference pattern in the electron hologram of the sample was captured using a slow-scan CCD camera (Gatan; Model 794), which was attached to the bottom of a Hitachi field-emission electron microscope (HF-2000) with an acceleration voltage of 200 kV. An electron biprism was positioned immediately above the image plane of an objective to produce the electron interferogram.

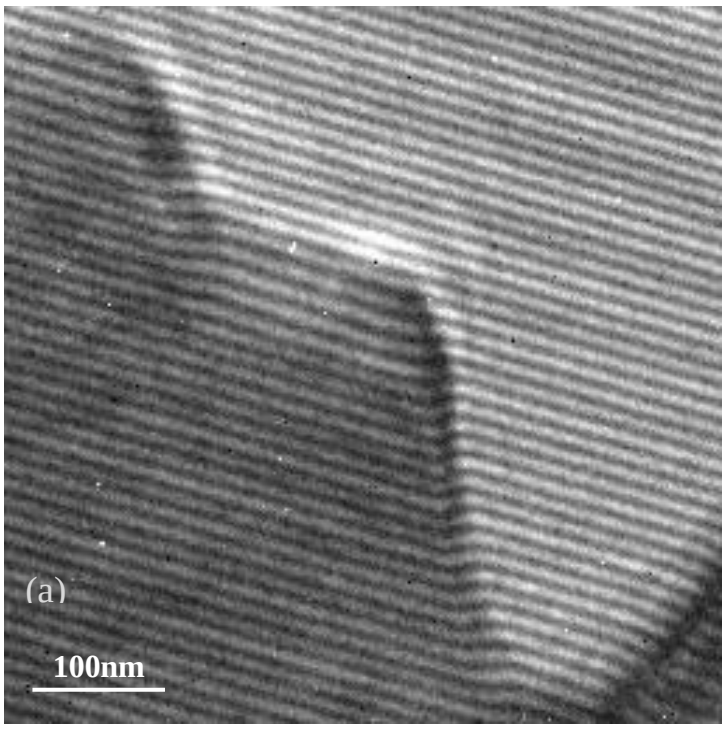

Fig. 2-3.(a) Electron hologram.

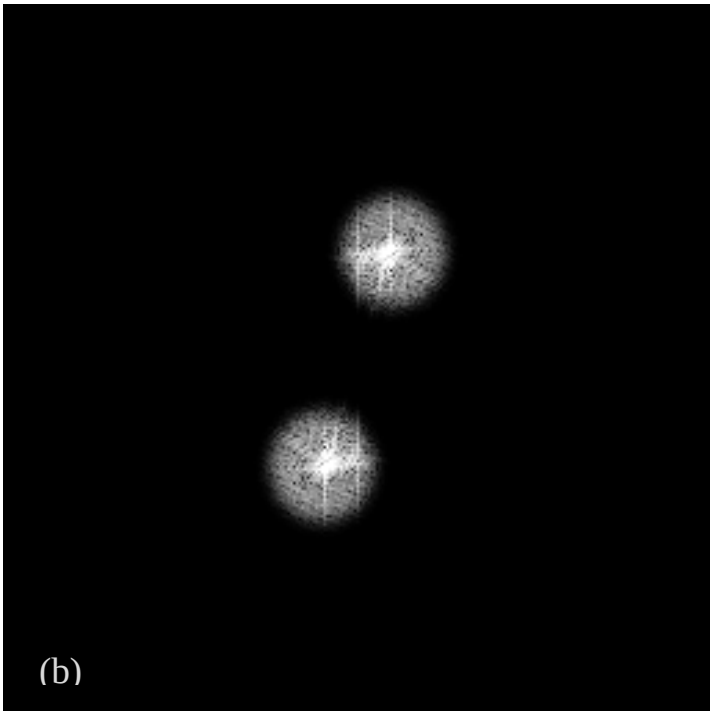

Fig. 2-3. (b) FFT with the aperture from Electron hologram.

The FFT aperture for reconstruction should be selected in the frequency domain shown in Fig. 2-3(b).

The reconstructed phase image obtained directly from the electron hologram is shown in Fig. 2-2, which includes some phase imperfections indicated by arrowheads.

2.4 Image processing procedure

The overall procedure is illustrated in Fig. 2-4.

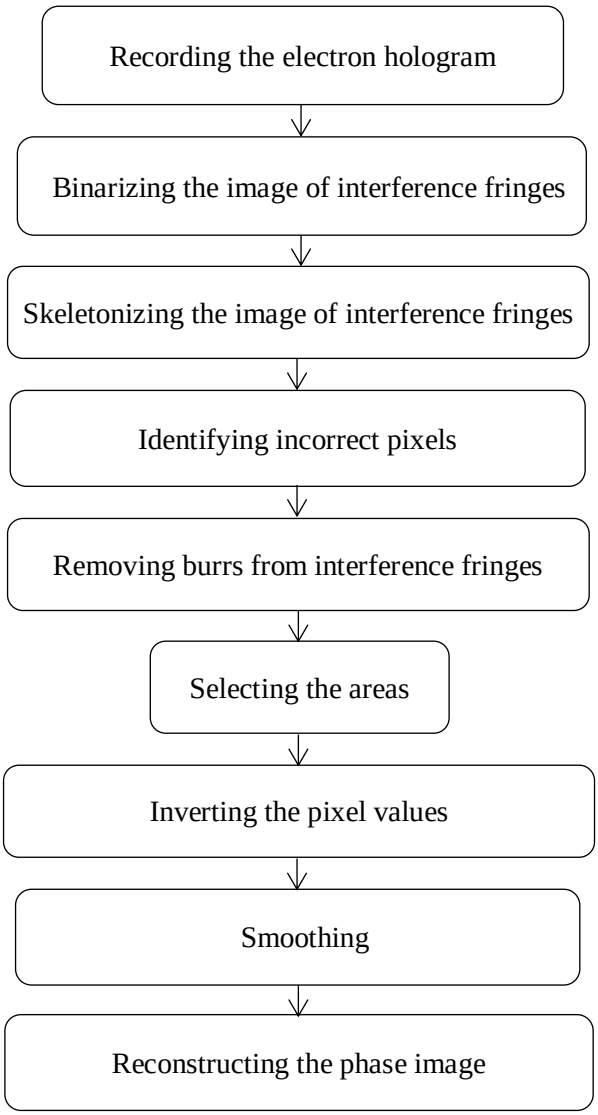

Fig. 2-4. Flowchart of the overall process.

The process can be described using nine steps.

2.5 Restoration of singularities in the phase image

2.5.1 Binary image of interference fringes in an electron hologram

The original electron hologram was converted into a binary image, which made it possible to find the disconnected and incorrectly connected points based on mathematical morphology. This binary image can be processed relatively easily by a computer because there are only two different values in the image [6]. We cut the center band leaving only the sideband. Then, binarization was performed to obtain binary interference fringes

A binary image of the interference fringes can be used to reconstruct the phase images. However, imperfections in the interference fringes, i.e., disconnected and incorrectly connected fringes, occur in the binary image, as shown in Fig. 2-5.

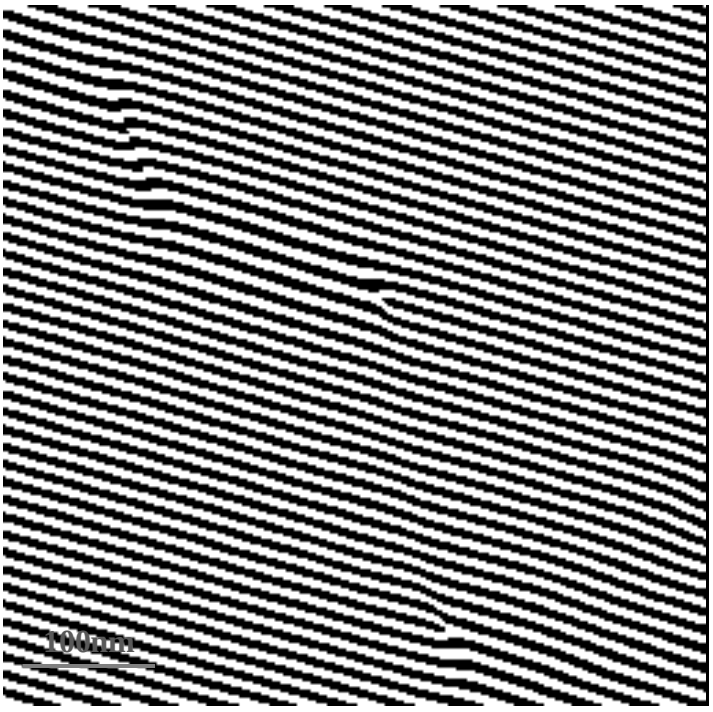

Fig. 2-5. Binary image of interference fringes.

During the cutting of the center-band, care must be taken when selecting the radius of the frequency filter to prevent the loss of useful information [7]. The radius of the filter is usually one-third the bandwidth, which is the distance from the center band to the center of the sideband. We could change the radius on basis of resolution. The reconstructed phase image shown in Fig. 2-6, which was obtained from the hologram in Fig. 2-5, includes some phase imperfections because the interference fringes were not corrected.

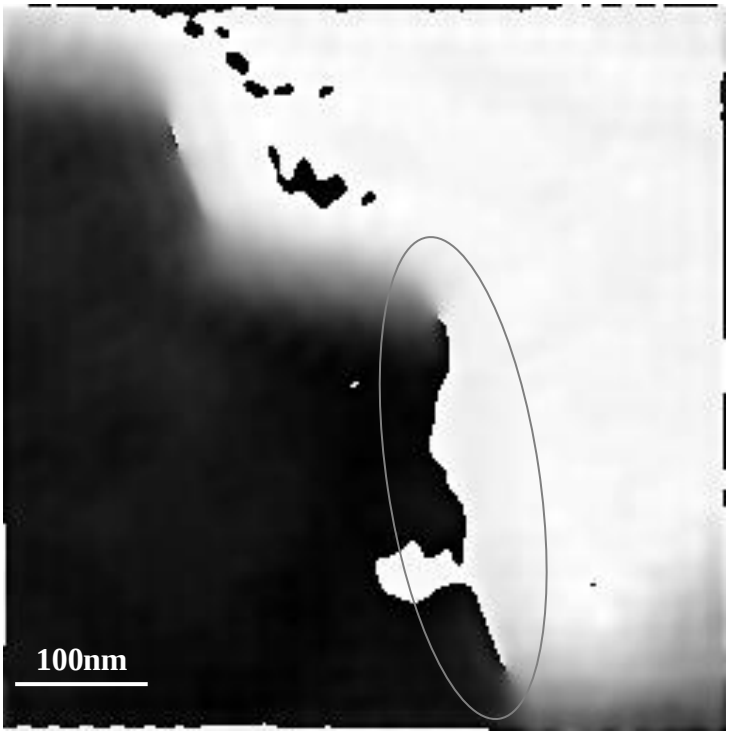

Fig. 2-6. Phase image reconstructed from Fig. 2-5.

2.5.2 Skeletonizing a binary image of interference fringes

The skeletonized binary image of interference fringes shown in Fig. 2-7 is used for burr removal, where the incorrectly connected fringes are circled in red. Here we can use the skeletonize function " bwmorph(image, 'skel' Inf) " to skeletonize the image in the toolbox of the MATLAB.

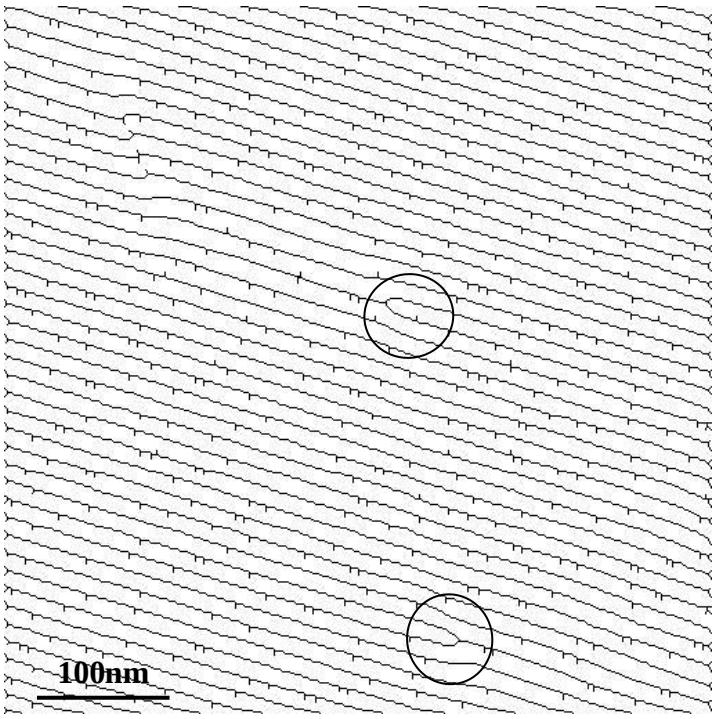

Fig. 2-7. Skeletonized binary image containing burrs.

The skeletonized binary image without burr pixels after burr removal using the function “bwmorph(image, ‘spur’ Inf)” in MATLAB is shown in Fig. 2-8, where the incorrectly connected fringes are circled in red.

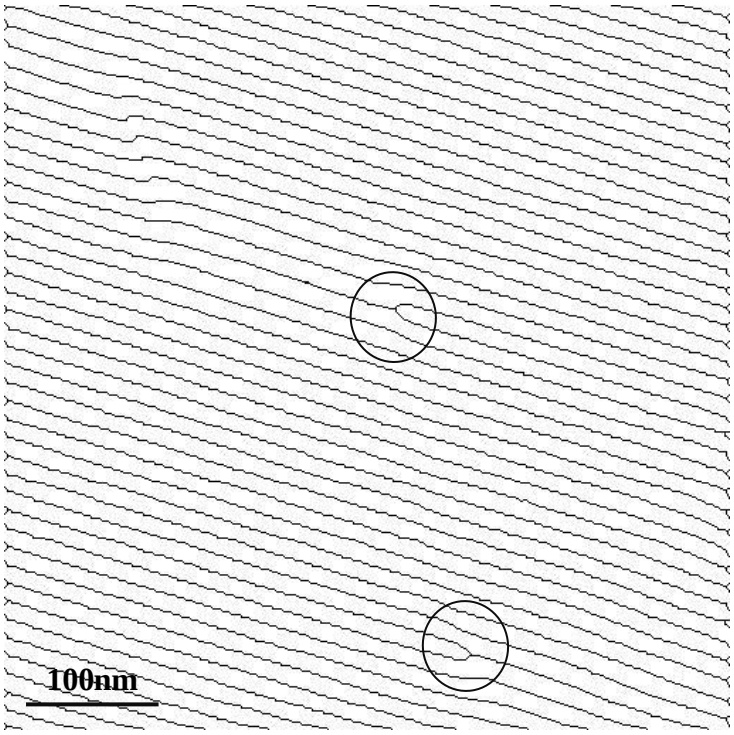

Fig. 2-8. Skeletonized binary image after burr removal.

2.5.3 Identifying incorrect points

To find the disconnected areas of the interference fringes caused by weak electron-wave amplitudes, an image containing the interference fringes only is reproduced using a low-pass filter to reduce the effects of Fresnel diffraction and noise . The radius of the low-pass filter is about 13 pixels (one-third of the carrier frequency), which is the distance from the center-band to the center of the side-band. We cut the center-band and leave only the side-band, and binarization is performed to obtain the binary interference fringes . We skeletonize the binary image to identify disconnected pixels in the fringes. Burrs sometimes remain at the sides of the skeletonized fringes, as shown later, but removing these burrs from the binary image allows us to obtain an image of the interference fringes with a width of only one pixel. The key point is to remove any burrs that remain in the interference fringes after skeletonization because these burrs can lead to errors in the pixel search results. Every pixel has eight neighboring pixels, except those at the edge of the image, and there must be an incoming line and an outgoing line for every pixel in a fringe line according to mathematical morphology, which is a tool used developed by Matheron and Serra for extracting image components that are useful for representation and description, as shown in Fig. 2-9. Thus, a correct pixel must share the same two pixels among its eight neighboring pixels, except for those at the edge of the image. Otherwise, the pixel is judged to be incorrect. The sets of pixels are indentified as disconnected and incorrectly connected pixels using the method described above.

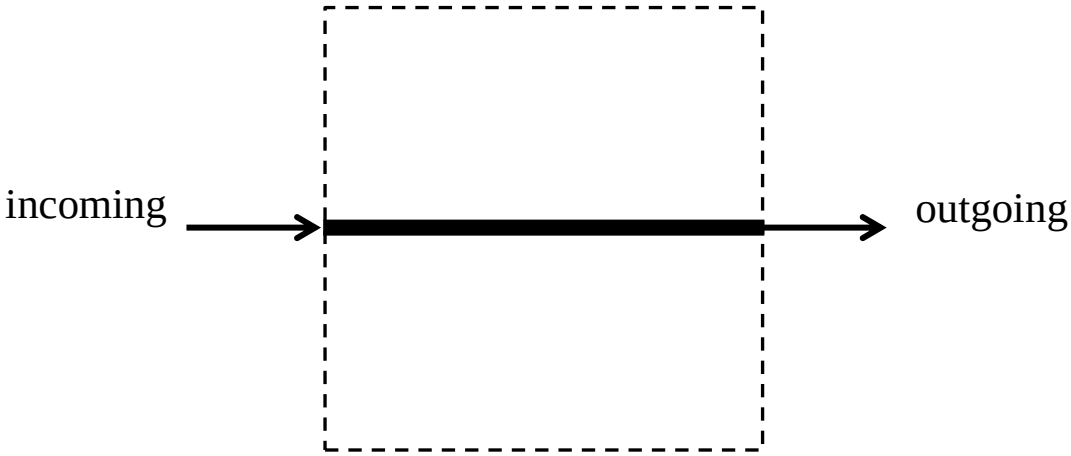

Fig. 2-9. Illustration showing incoming and outgoing lines.

In general, the disconnected and incorrectly connected points in the interference fringes occur in areas with abrupt intensity variation or rather low intensity, and these points always appear in pairs. If one point is connected incorrectly, there must be a corresponding point to form a pair. One pair cause one imperfection. Figure 2-10 shows the disconnected and incorrectly connected pixel positions identified using the skeletonized binary image.

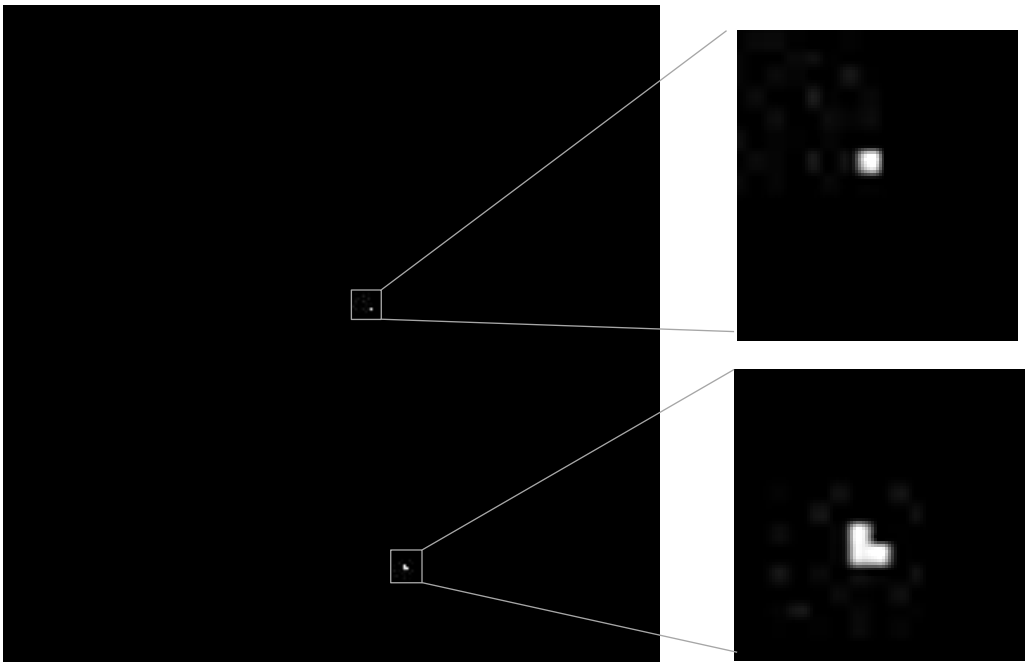

Fig. 2-10. Image showing the points identified.

2.5.4 Correction of interference fringes

To correct the interference fringes, the incorrectly connected fringes need to be cut and reconnected. The interference fringes are viewed as a binary image, so the binary pixels can be inverted to the opposite values in these areas, which depends on finding the incorrect pixels. The cut-and-reconnect process is illustrated in Fig. 2-11. The length of the area is determined by the distance between incorrect pixels. The width of the area is determined by the interval between the fringes. In this case, a width of six pixels was selected, which was equal to the interval between the fringes. Pixel-value reversal can be interpreted as changing zero to one and one to zero.

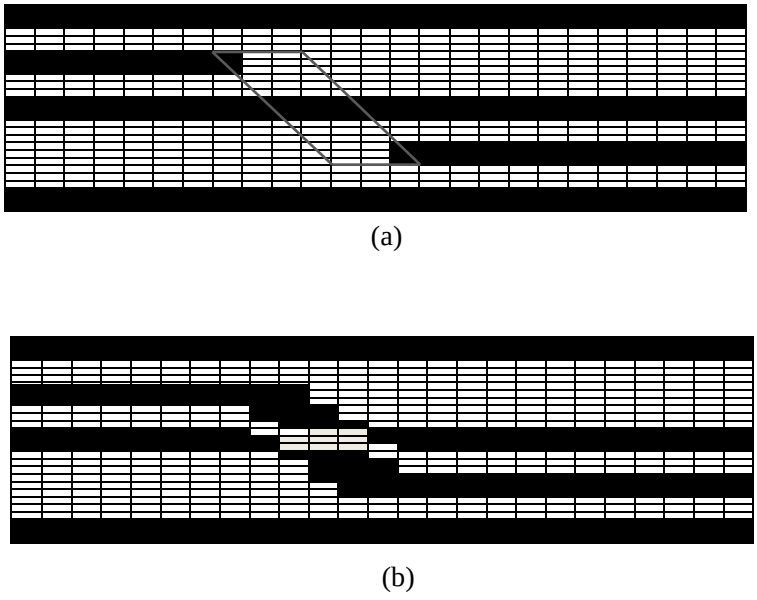

(a)

(b)

Fig. 2-11. Cut-and-reconnect process.

(a) Unconnected fringes; (b) Reconnected fringes.

The distorted interference fringes in Fig. 2-5 are corrected by cut-and-reconnect processing. When inverting the pixel values, the widths of the rectangle areas marked in Fig. 2-11 are determined by the interval between the fringes. In this case, a width of six pixels was selected, which was equal to the interval between the fringes. Another selection, such as approximately one pixel, could be made to improve the results, but six pixels worked well in this case. When the interval between the fringes is changed, we change the width of the area to obtain better results. The widths of the rectangle areas are selected twice of the interval between the fringes generally.

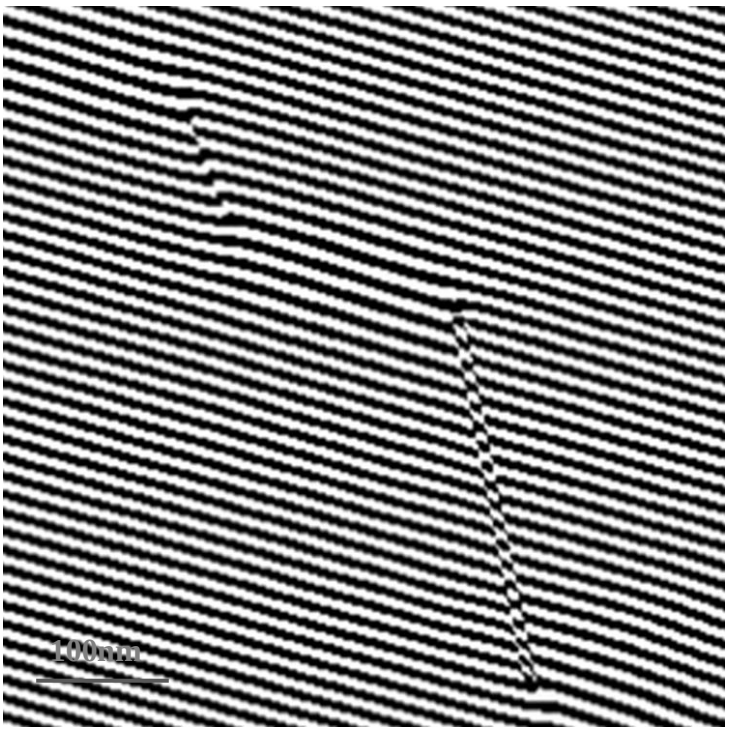

Fig. 2-12. Corrected fringes.

The corrected interference fringes shown in Fig. 2-12 were smoothed using a median filter, which can suppress isolated noise [8]. In this case, the median filter replaced a pixel with the median of all pixels in the neighborhood. The window size of the median filter was 5×5 pixels which is the better here and the results are shown in Fig. 2-13.

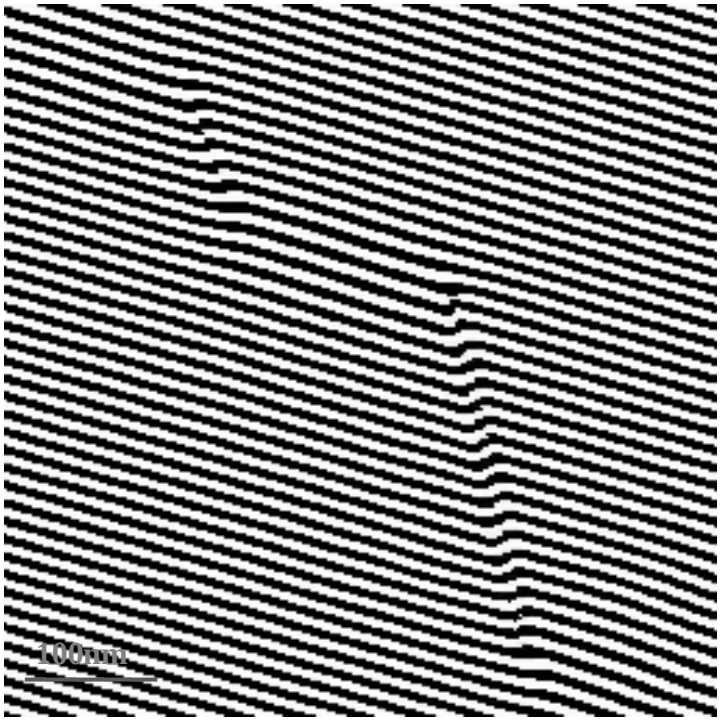

Fig. 2-13. Corrected fringes after smoothing.

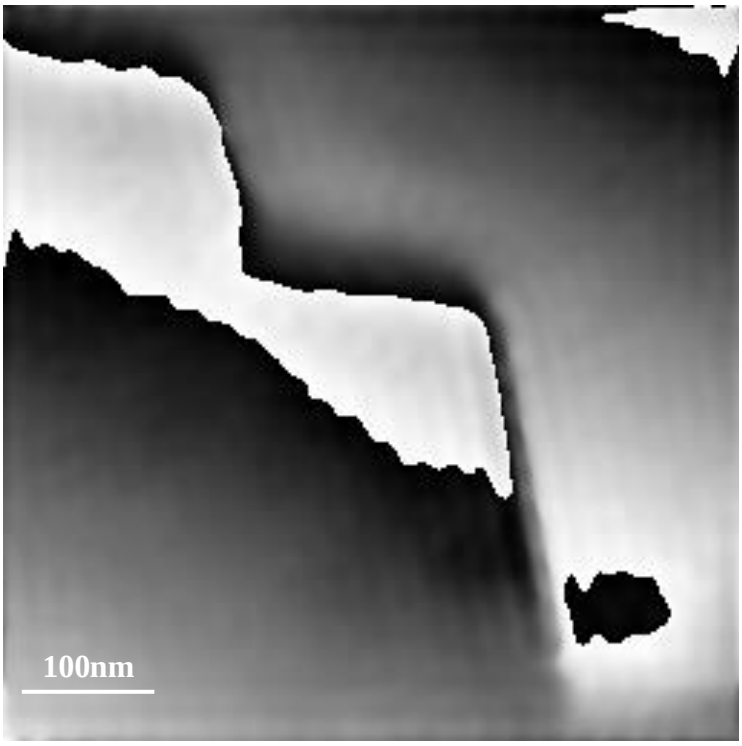

Fig. 2-14. Phase image reconstructed from corrected fringes.

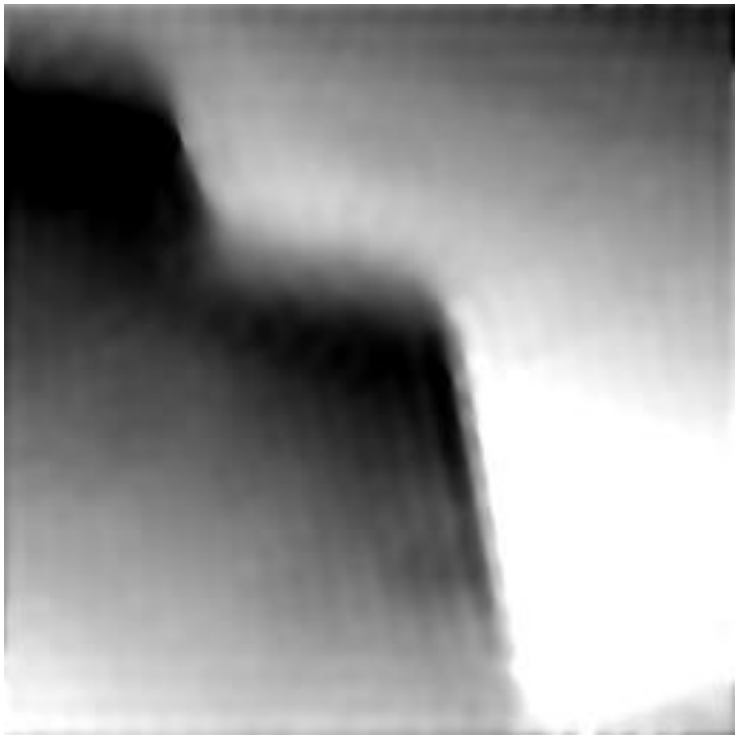

Fig. 2-15. Final phase image after unwrapping.

The reconstructed phase image (Fig. 2-14) obtained from the corrected interference fringes shows that the phase error due to the weak electron-wave amplitude has been reduced dramatically.

The unwrapping process is used to remove the phase jump caused by the digital reconstruction process to obtain a final image without phase jump, as shown in Fig. 2-15.

2.6 Evaluation

A new method of image processing for phase imperfections in electron holography has been proposed to remove the influence of imperfections on the reconstructed phase. We studied the phase imperfections and firstly classified the phase jumps in the reconstructed phase as two main types according to their cause.

The phase jumps owing to low contrast of electron-wave amplitude was eliminated by the proposed method in practice. The proposed method is unique, and the processing for phase imperfections in electron holography is unique also.

This method is applicable and efficacious for 2π jumps but fails to deal with 4π jumps in the hologram. Actually, the 4π jumps are rare in practice.

The present technique enables to obtain comparatively accurate phase information for studying the inner electrostatic potential without changing the conditions in actual applications. In particular, the method can be very useful and effective under severe conditions, such as in-situ holographic experiments. It is also enables the study of the inner electrostatic potential and the in-plane component of the magnetic induction at nanometer and subnanometer scales.

2.7 Conclusion

The phase image reconstructed from an electron hologram sometimes contains some imperfections because the interference fringes are not connected due to the weak electron-wave amplitudes. Thus, we propose a new image processing method for phase imperfections in electron holography, which removes the effects of imperfections on the reconstructed phase.

A binary image of the interference fringes that contains phase information can be used to reconstruct the phase images. The disconnected and incorrectly connected points in the interference fringes generally occur in the areas with abrupt intensity variations or a rather low intensity, and these points always appear in pairs.

We also propose a technique based on mathematical morphology for identifying the disconnected points and for correcting the interference fringes. Finally, a comparatively accurate phase information image is reconstructed from the corrected interference fringes after smoothing.

The reconstructed phase information image obtained from the corrected interference fringes showed that the phase error caused by the low contrast of the electron-wave amplitudes in the sample was reduced dramatically using the proposed method.

References

[1] T. Hirayama, Q. Ru, T. Tanji and A. Tonomura, (1993). Observation of magnetic-domain states of barium ferrite particles by electron holography. Appl. Phys. Lett. 63: 418.

[2] Q. Ru, G. Lai, K. Aoyama, J. Endo and A. Tonomura, (1994). Principle and application of phase-shifting electron holography. Ultramicroscopy. 55: 209-220.

[3] K. Ishizuka, (1993). Optimized sampling schemes for off-axis holography. Ultramicroscopy 52: 1.

[4] D. J. Smith, W. J. de Ruijiter, M. R. McCartney and J. K. Weiss. In: Völkl E, Allard L F and Joy D C eds ,(1998). Introduction to Electron Holography. Kluwer, New York.

[5] A. Tonomura (1999) Electron Holography. Springer-Verlag, Berlin.

[6] R.C. Gonzalez, R. E. Woods and S. L. Eddins, (2004). Digital Image Processing using MATLAB. Pearson Education.

[7] T. Tanji, H. Hashimoto, H. Endoh and H. J. Tomioka, (1982). Theory and application of noise filter for periodic objects. Electron Microscopy 31: 1.

[8] W. W. Boles, M. Kanefsky, M. Simaan, (1990). A reduced edge distortion median filtering algorithm for binary images.Signal Processing, Volume 21, 1, 37-47

Chapter three

3. Application to a high resolution image of a crystal

3.1 Preamble

The development of electron holography has played an important role in the production of many nanostructured materials and devices. In particular, high-resolution electron holography has facilitated the investigation of complex structures.

However, phase singularities often occur in the reconstructed phase image, which severely reduces the quality of the information obtained. Image processing is particularly effective for increasing the quality of the characterization of nanostructured materials during high-resolution electron holography.

This section considers the application of digital image processing to phase image restoration using a high resolution image of a thin crystal.

We obtain relatively accurate phase information for a thin crystal structure using the original electron hologram.

3.2 Model crystal structure of tungsten niobate

The thin crystal of tungsten niobate ($Nb_2O_5WO_3$) is a well-known, typical electrochromic oxide material. The crystal structure of tungsten niobate projected onto the (001) plane is shown in Fig. 3-1 [1]. It has a tetragonal structure where a = 2.36 nm and c = 0.38 nm. Moreover, its structure is characterized as 5 × 5 oxygen octahedrons, each of which contains one cation at the center and the dark dots represent tungsten atoms. Therefore, its image can be characterized as large 4 × 4 and small 3 × 1 tunnels.

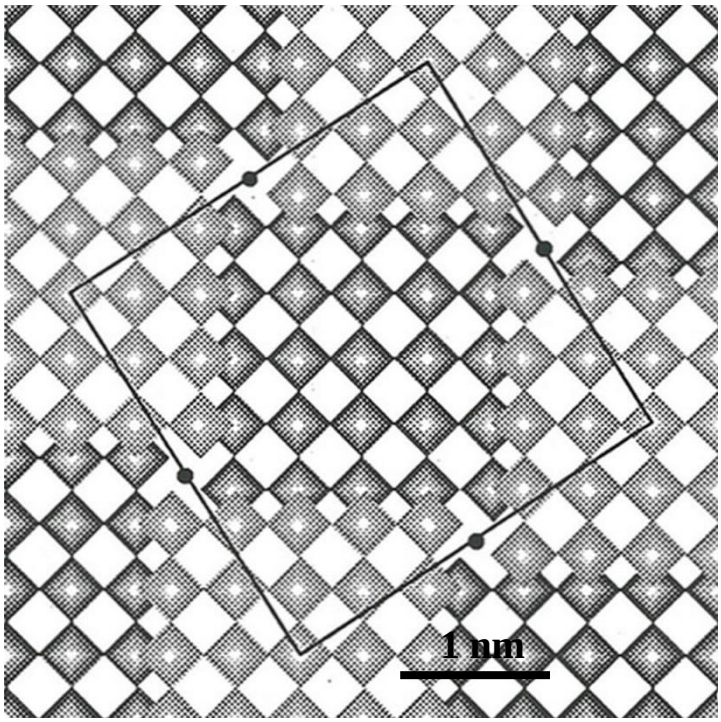

Fig. 3-1. Structure model of $Nb_2O_5WO_3$ containing 5 × 5 oxygen octahedra, each of which contains one cation at the center, sharing the different plane with others; dark dots represent tungsten atoms. Black square marks one unit.

3.3 Off-axis electron holography

The interference pattern of an electron hologram with sufficiently narrow fringes for high-resolution reconstruction was obtained using an electron-optical system, where the electron biprism was installed near the second image plane between the first and second intermediate lenses. The interference pattern of the electron hologram of a sample was recorded on photographic film using a Hitachi field-emission electron microscope (HF-2000) at an accelerating voltage of 200 kV and digitized with an optical camera, as shown in Fig. 3-2. The spherical aberration coefficient was 1.7 ± 0.1 mm. The interference pattern of an electron hologram with a carrier fringe spacing of 0.05 nm is narrow enough for high-resolution reconstruction up to 0.15 nm.

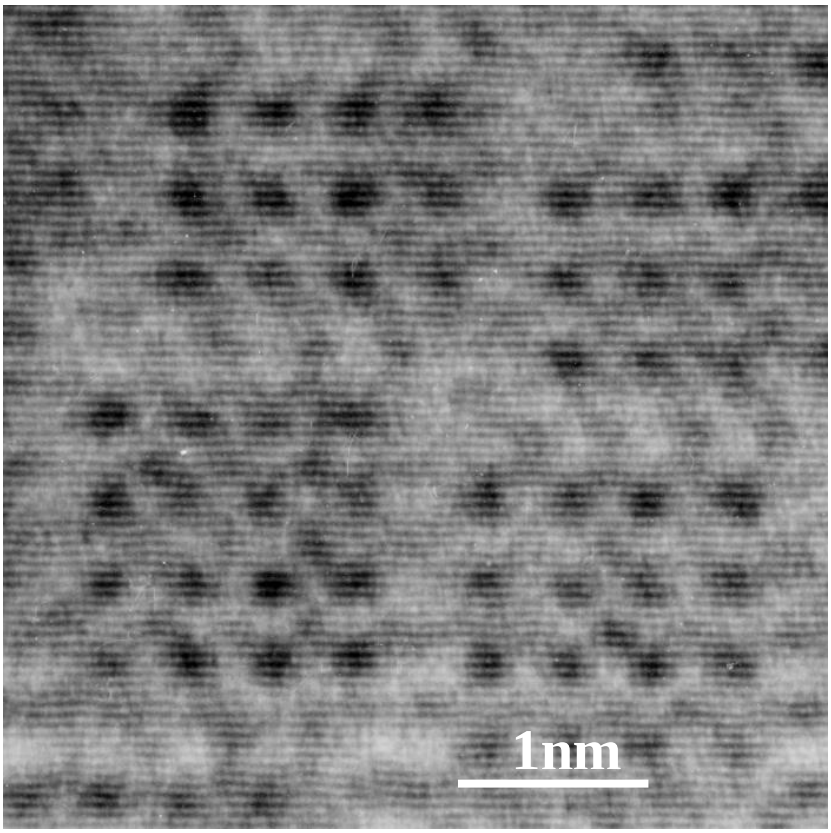

Fig. 3-2. Interference pattern in an electron hologram of a thin crystal of tungsten niobate.

3.4 Phase imperfection

The low contrast of an electron hologram in a specific area of the sample (tungsten niobate) is shown in Fig. 3-3.

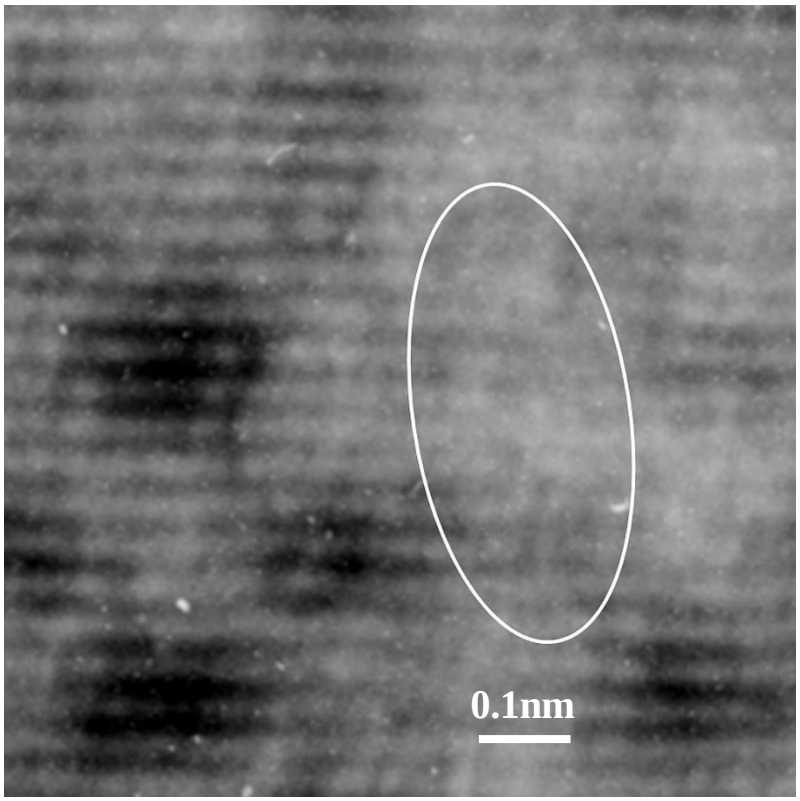

Fig. 3-3. Part of an electron hologram of a thin crystal of tungsten niobate with a low contrast fringe.

The phase imperfection in the directly reconstructed phase image that corresponds to the area marked with an oval in Fig. 3-3 is shown in Fig. 3-4. In this case, the phase changes smoothly on one side of the defect edge (A), whereas it reverses abruptly on the opposite side of the defect edge (B). At the other end, this reversal is abnormal because the phase should connect along a closed circle, which is the same type of imperfection described in the previous section. This type of reversal stems from an error in fringe connection by the computer owing to poor contrast in the hologram. On

the other hand strong phase objects tend to produce many phase the 2π jumps indicated by arrowheads in Fig. 3-4. Fortunately, we can easily find out the miss connection and wrong connection of the interference fringes in the interference fringes images. Therefore, we can easily distinguish the error 2π jumps in the reconstructed images.

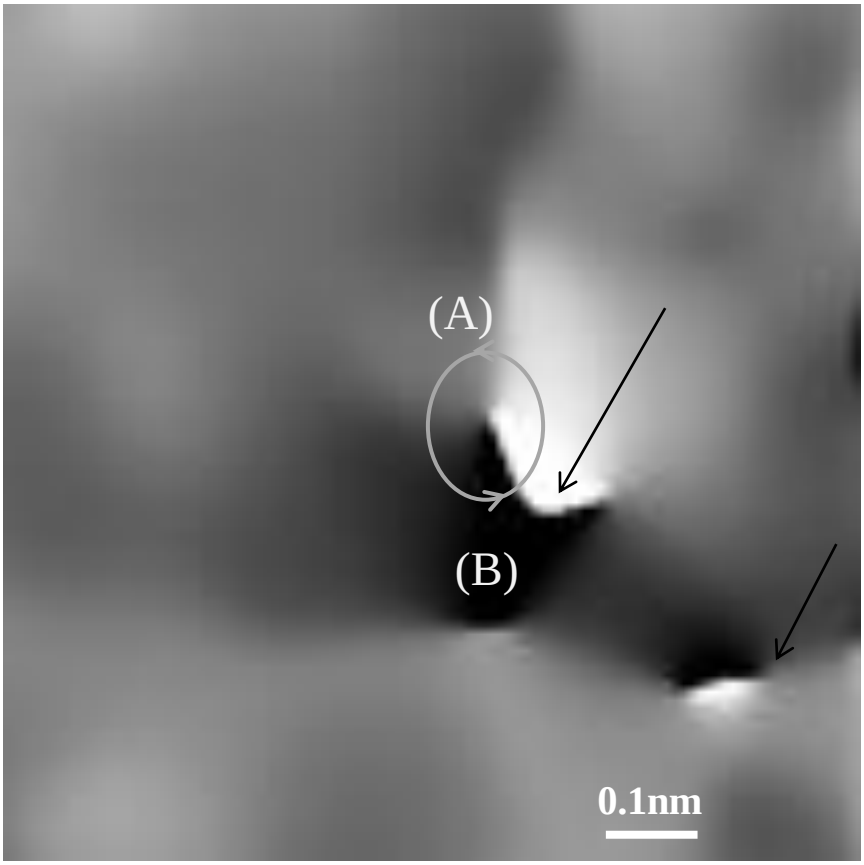

Fig. 3-4. Phase image reconstructed directly from Fig. 3-3.

3.5 Aberration correction for a hologram

Aberration has a very complicated effect at higher spatial frequencies and cannot be easily corrected by the image processing techniques used in linear light optics. The only exception is for weak phase objects with nearly linear imaging. However, the specimens suitable for weak phase object approximation are restricted to very special rare cases. Electron holography can help with the problem of nonlinear imaging [2,3].

Estimation the levels of aberration requires improvement of the resolution [4,5]. Several aberration estimation methods have been proposed [6]. In the present study, we use an algorithm that allows assessment based on only one hologram with imprecise information about the aberrations [7]. By minimizing the contrast of the reconstructed amplitude image with appropriate processing parameters (Cs and df), the optimum parameters can be obtained for image restoration during phase object approximation. However, we may obtain many contrast minima based on df when we reconstruct the crystal images, so an additional restriction is required. The contrast of the amplitude distribution is low, but accurate aberration correction provides us with clear patterns of the phase and the amplitude distribution. In this case, we adopted the optimum conditions, where the standard deviation of the amplitude distribution of the processed image is close to the minimum, whereas the correlation coefficient of the amplitude and phase distribution is close to the maximum.

The standard deviation can be defined by the following function.

$$\mathrm{STD} = \sigma = \frac{1}{N}\sqrt{\sum_{i=1}^{N}\sum_{j=1}^{N}[I(i,j) - M]^2}$$

Where $I(i,j)$ is image, N is the size of image, $M = \frac{1}{N}\sum_{i=1}^{N}\sum_{j=1}^{N} I(i,j)$ is the mean. The correlation coefficient can be defined by the following function.

$$\mathrm{r} = \frac{1}{N\sigma_1\sigma_2}\sum_{i=1}^{N}\sum_{j=1}^{N}[I_1(i,j) - M_1][I_2(i,j) - M_2]$$

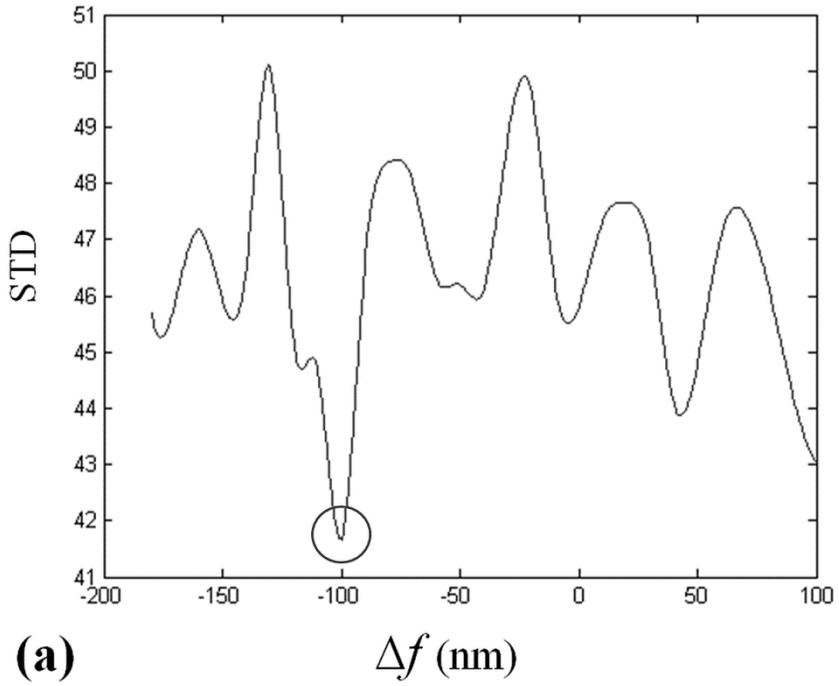

Fig. 3-5. (a) Standard deviation (STD) for the amplitude distribution of the processed image.

To estimate the optimum aberration correction parameter, the standard deviation of the amplitude distribution of the processed image, shown in Fig. 3-5(a), and the correlation coefficient of the amplitude and phase distribution of the processed image, shown in Fig. 3-5(b), are monitored for various Δf values in the restoration function.

The optimum condition is found around the point where the standard deviation is smallest and the correlation coefficient is largest with the constant value of Cs = 1.7 mm. Here the optimum condition was estimated as $\Delta f = -100$ nm. The wavelength of the electronic wave was about 2.5×10^{-12} m with an accelerating voltage of 200 kV.

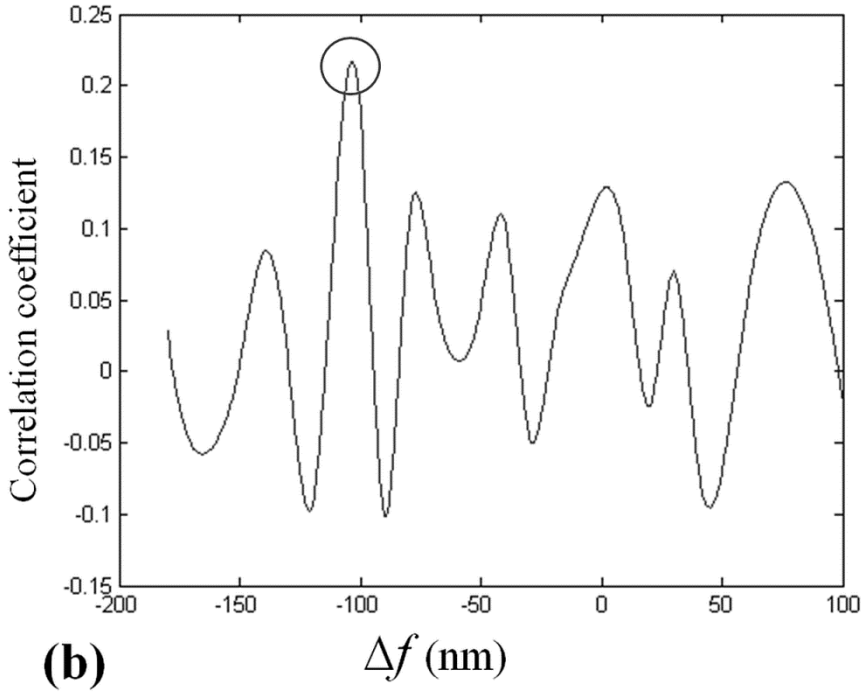

Fig. 3-5. (b) Correlation coefficient of the amplitude and phase distribution of the processed image. The optimum condition (encircled) appears around the point where the standard deviation is smallest and the correlation coefficient is largest.

3.6 Restoration of singularities

The phase imperfections owing to the poor contrast of the hologram need to be restored using image processing methods, which remove the imperfections in the reconstructed phase by repairing the fringes of the electron holograms using phase correction [8]. To restore the phase image correctly, any inappropriately connected fringes should be cut and reconnected. A hologram with corrected interference fringes can be reconstructed to eliminate the abrupt reversals owing to the poor contrast of the hologram in the phase contrast images. The unwrapping process is then executed to obtain a final image without any phase jump.

The FFT technique is used for phase reconstruction. Figure 3-6(b) shows the directly reconstructed phase image obtained from the electron hologram showed in Fig. 3-6(a), while Fig. 3-6(c) shows the reconstructed phase image in which the effects of spherical aberration and defocussing have been corrected using the methods described in the previous section. Numerous phase imperfections are indicated by arrows in Figs. 3-6(b) and 3-6(c).

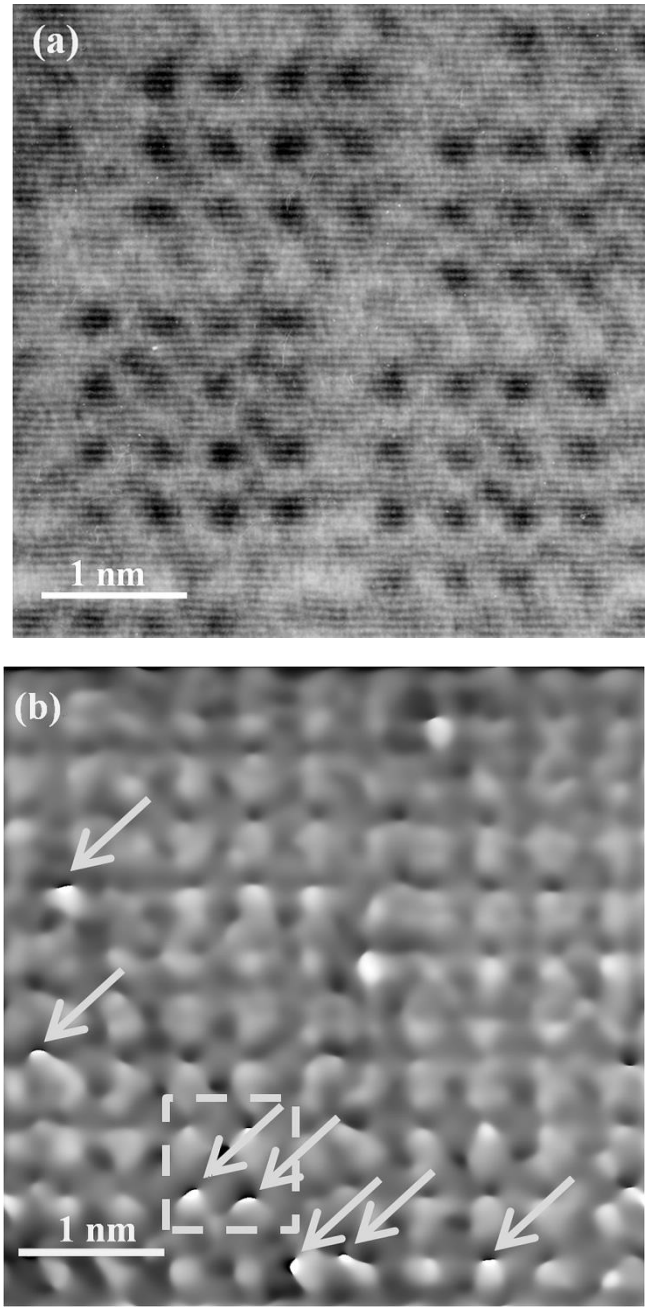

Fig. 3-6. (a) Interference pattern of electron hologram and (b) phase image directly reconstructed from (a).

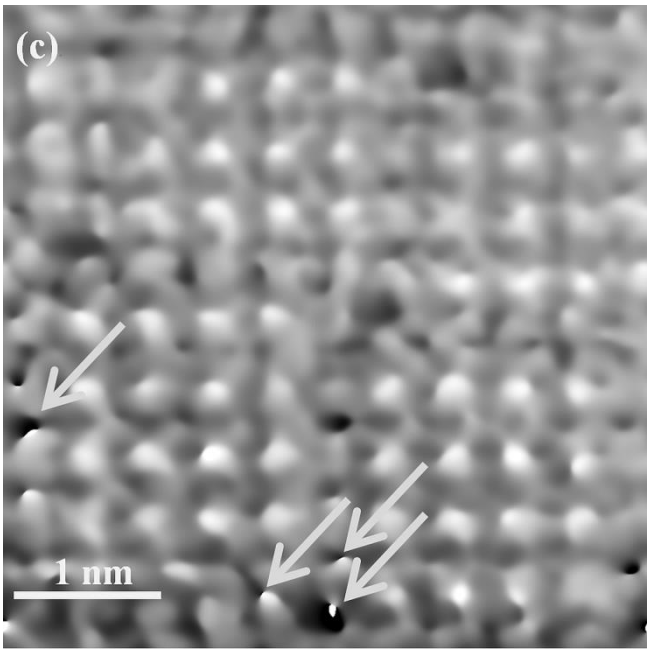

Fig. 3-6.(c) Phase image reconstructed from (a) with spherical aberration and defocussing corrected. Arrowheads indicate the phase imperfections.

A low-pass filter is used to remove most of the process noise. Great care must be taken to remove as much noise as possible, but without removing useful information. In the present case, most of the noise was cut before reconstruction and only some points remained because of the weak electron-wave amplitude.

The binary interference fringes that are used to reconstruct the phase images include imperfections indicated with circles in Fig. 3-7.The disconnected points (endpoints of fringes) or incorrectly connected points in the interference fringes usually occur in areas having abrupt intensity variations or rather low contrast, and such points always appear in pairs. If one disconnected or incorrectly connected point appears, there must be another coordinate point. We can mark disconnected pair as X type pair and incorrectly connected pair as Y type pair. No matter X type pair or Y type pair, one pair of points may generate one singularity in the reconstructed phase image.

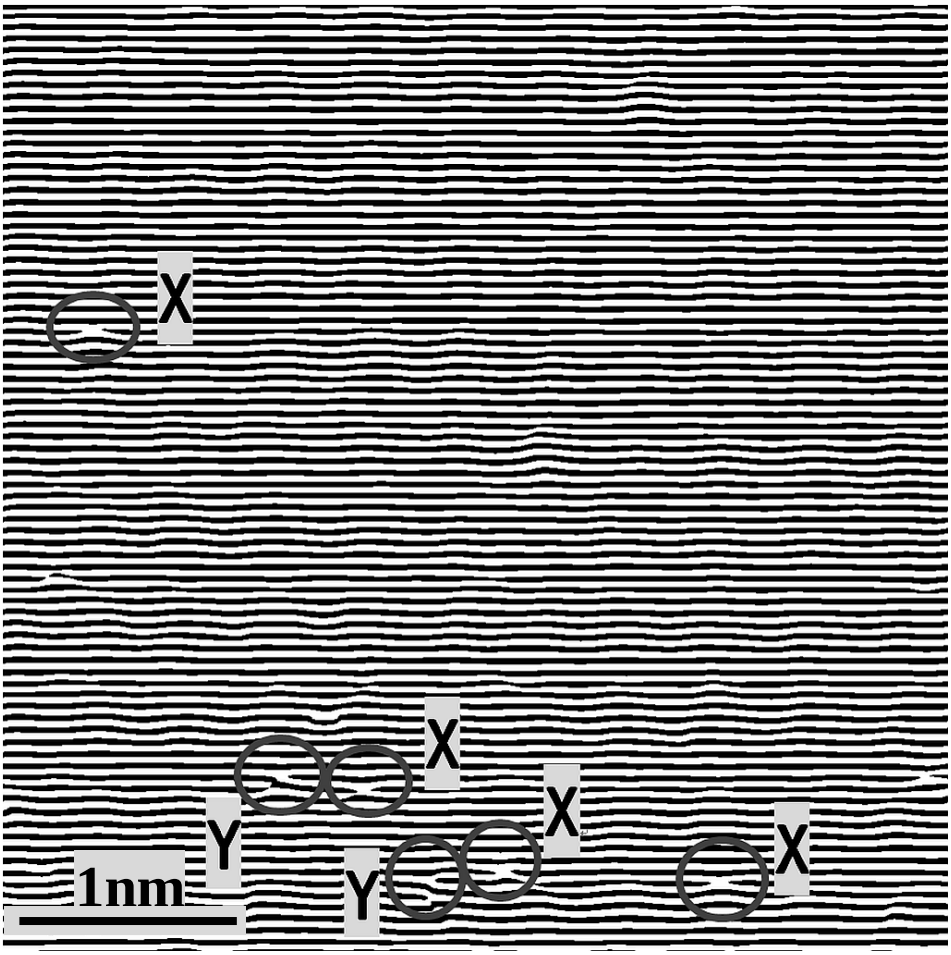

Fig. 3-7. Binary image of interference fringes. The imperfections occur in the encircled areas where the fringes are disconnected (X type pair) and incorrectly connected (Y type pair).

During the binarization process, the threshold of the binary may affect the interference fringes. In the present case, the optimum threshold was 0.48. However, the optimal threshold may vary depending on the interference fringes in the images.

The disconnected and incorrectly connected points always appear in pairs. Thus, we select the nearest points in the pairs.

The distorted interference fringes shown in Fig. 3-7 are corrected by cut-and-reconnect digital image processing, before the corrected interference fringes are smoothed out using a median filter to suppress isolated noise. The results are shown in Fig. 3-8.

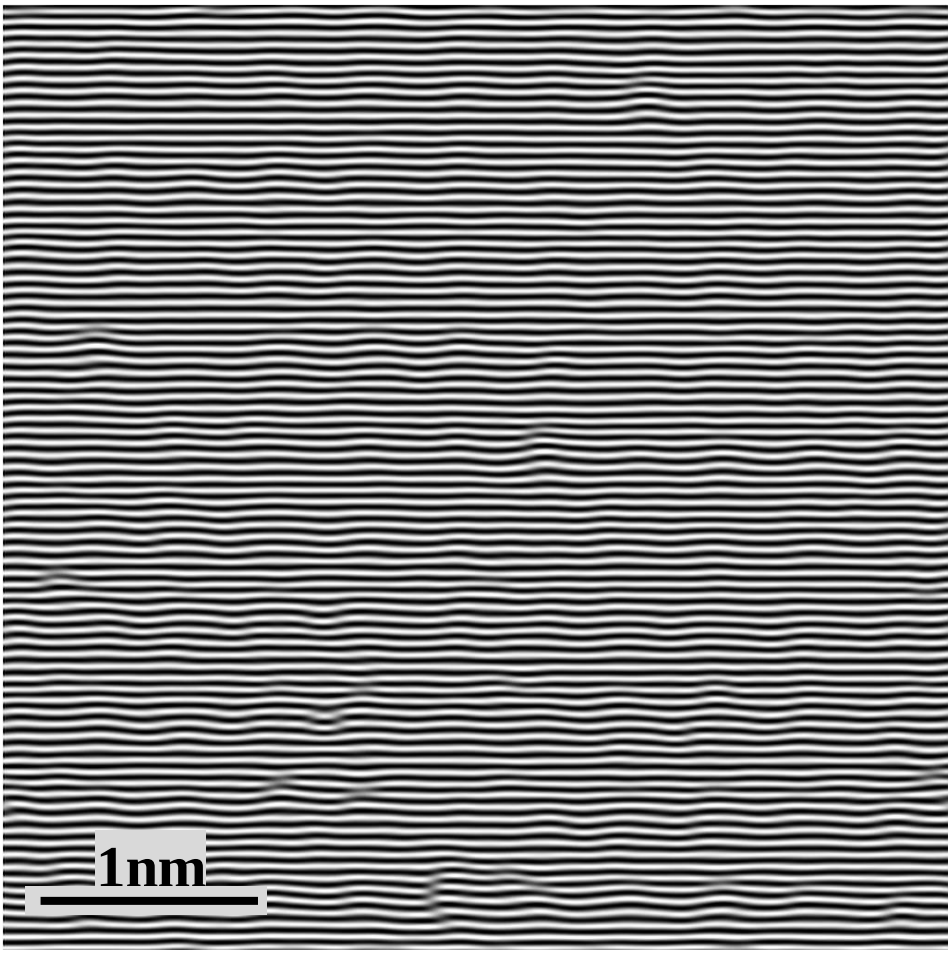

Fig. 3-8. Corrected fringes from binary image of interference fringes. The fringes are smoothly connected after restoration.

We use aberration correction when reconstructing the corrected interference fringes. Accurate aberration correction is used to reconstruct the phase-information image. This technique allows us to obtain a phase distribution image with a clearer structural resolution compared with no aberration correction.

The reconstructed phase image shown in Fig. 3-9 was obtained from the corrected interference fringes and the abrupt phase reversal caused by the weak electron-wave amplitude has been reduced dramatically. The structure of the crystal specimen is shown clearly in the final phase information image.

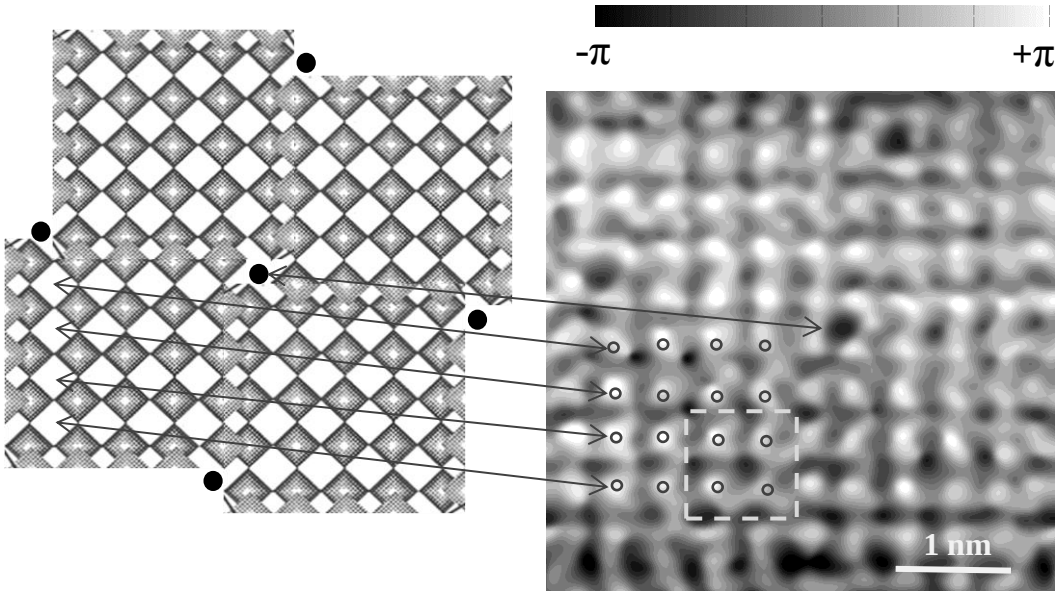

Fig. 3-9. Illustration showing the final phase.

In general, the unwrapping process is required to eliminate the abrupt reversal caused by the limited range of the digital reconstruction process. In the case of Fig. 3-9, however, abrupt reversal is not present in the final phase distribution image. In addition, all of the phases in the image area range between $-\pi$ and π. Finally, the unwrapping process is not executed.

A clear wire-frame image of part of the original phase image shown in Fig.3-6(b) is depicted in Fig. 3-10(a), where the abrupt reversals are clearly evident compared with the surroundings.

A wire-frame image of the corrected phase of the same area is shown in Fig. 3-10(b). No abrupt reversals are evident in the corrected phase.

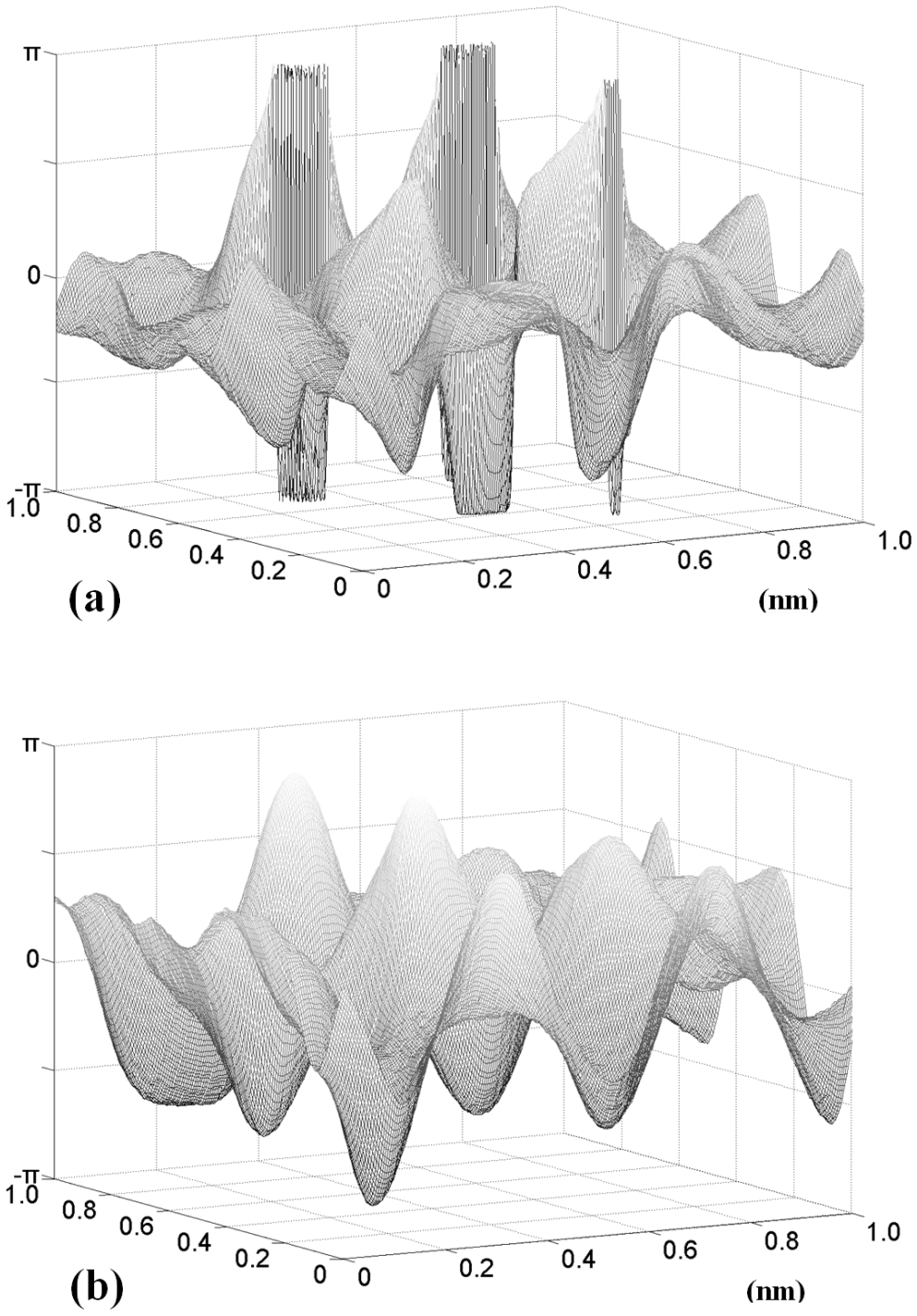

Fig. 3-10(a). Wire-frame image of the original phase. (b). Wire-frame image of the corrected phase.

3.7 Conclusion

In this section, digital image processing was used for phase restoration in a reconstructed phase image using high-resolution electron holograms of a well-known thin crystal.

The processing methods are similar to those described in the previous chapter, including binarization, phase reconnection, and smoothing. Aberration correction was also introduced for processing high-resolution electron holograms.

Furthermore, the quality of the reconstructed phase image was improved by removing singularities from the phase based on the crystal phase structure results.

More work is required to improve the resolution and to obtain sharper or larger phase change images, but this crystal phase image restoration method produces a clearer phase distribution image, which facilitates the study of the inner electrostatic potential and the in-plane component of magnetic induction in a sample.

References

[1] R. S. Roth and A. D. Wadsley. Acta Cryst.19(1965) 38-46

[2] H. Lichte (1991) Optimum focus for taking electron holograms. Ultramicroscopy 38: 13–22.

[3] T. Tanji and K. Ishizuka In: Tonomura A, Allard L F, Pozzi G, Joy D C, and Ono Y A (1995) Electron Holography. Elsevier Science, New York. 45–54.

[4] K. Ishizuka (1993) Optimized sampling schemes for off-axis holography. Ultramicroscopy 52: 1.

[5] Y. Wang, K. Du, H. Ye, and H Lichte (2002) Correction of aberration for a high-resolution electron hologram by means of the amplitude contrast criterion of image wave. Micron 33(1): 15–21.

[6] K. Ishizuka et al. (1994) Aberration correction using off-axis holography II. beyond the scherzer limit. Ultramicroscopy 55(2): 197–207.

[7] T. Tanji and K. Ishizuka (1994) Observation of Crystal Structures by Using Image Restoration in Electron Holography. Microscopy Society of America. vol. 24, no.2: 494–500.

[8] W. Li, J. Zhang, and T. Tanji (2013) Image Processing for Phase Imperfections in Electron Holography Microscopy. 62(6): 583–588.

Chapter four

4. Elimination of undulation noise

4.1 Preamble

During image processing or computing, the noise mainly comprises unwanted random additions to an image.

Noise refers to unwanted information or data that is not relevant to the analysis. Image noise is an undesirable by-product of image capture that adds spurious and extraneous information, which is usually related to electronic noise. This noise can be generated by the sensor and circuitry of a scanner or digital camera. Image noise can also originate from the film grain and the unavoidable shot noise of an ideal photon detector.

The reconstructed phase image obtained from the corrected interference fringes shows that phase errors can be reduced dramatically, but undulation noise may sometimes be present in the phase image.

The undulation noise that originates during digital image processing is unwanted additional information and it must be reduced.

This chapter addresses the causes of undulation noise and the efforts made to eliminate it.

4.2 Undulation noise

4.2.1 Electron hologram of a particle

Figure 1 shows the interference pattern of an electron hologram of a CeO_2 particle, which was captured using a slow-scan CCD camera (Gatan; Model 794) attached to the bottom of a Hitachi field-emission electron microscope (HF-2000) that operated at 200 kV.

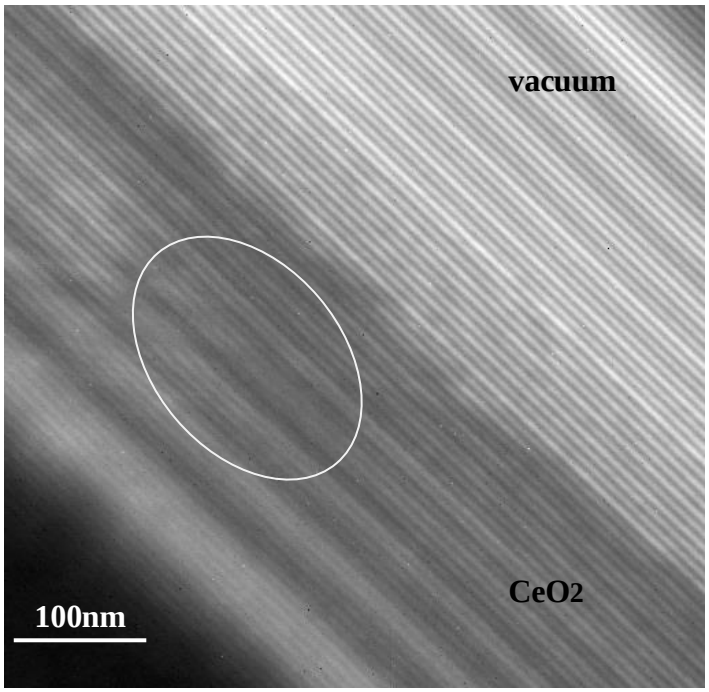

Fig. 4-1. Electron hologram with weak electron-wave amplitudes in specific areas.

The red oval in Fig. 4-1 shows the weak electron-wave amplitudes found in specific areas of the sample, which may cause problems during the connection of fringes. The fringes in the hologram are not clearly defined, which can lead to confusion when

computing connections in these areas.

The reconstructed phase image obtained directly from the electron hologram is shown in Fig. 4-2.

Some phase imperfections that jump 2π are indicated by the red arrowhead in an area with weak electron-wave amplitudes.

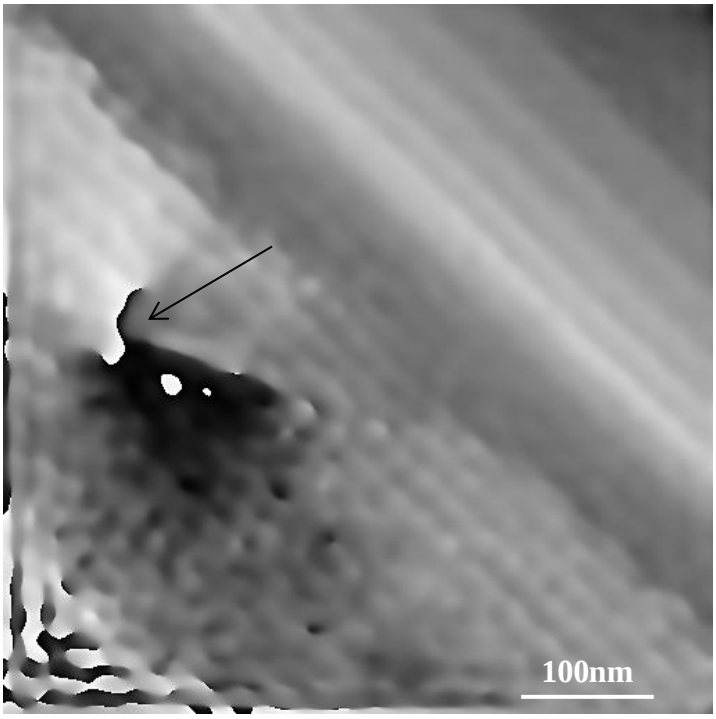

Fig. 4-2. Reconstructed phase image.

A binary image of the interference fringes obtained from the interference fringes of the electron hologram can be used to reconstruct the phase images. However, some imperfections in the interference fringes, i.e., the disconnected and incorrectly connected fringes indicated by red ovals, occur in the binary image, as shown in Fig.4-3.

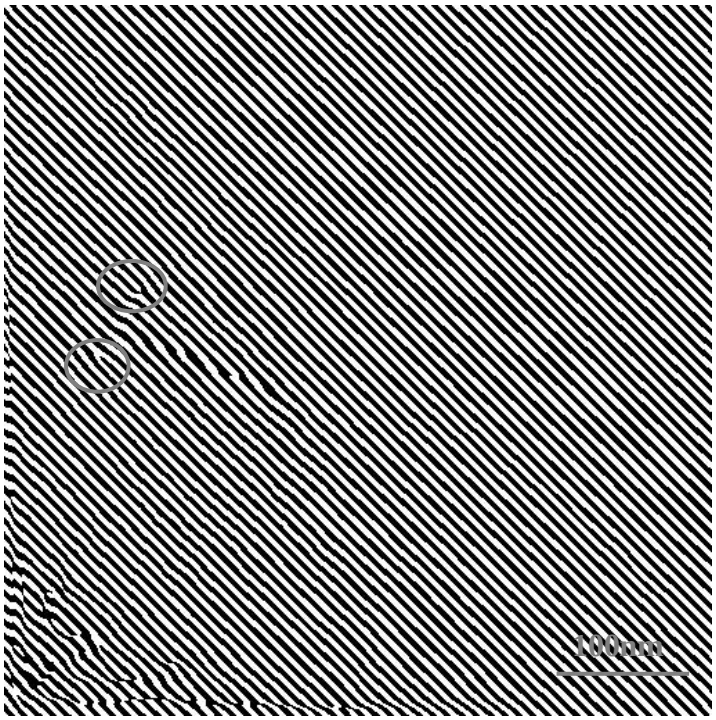

Fig. 4-3. Disconnected and incorrectly connected fringes.

Figure 4-4 shows the reconstructed phase image obtained from the hologram in Fig. 4-3, which also contains phase imperfections indicated by arrowhead.

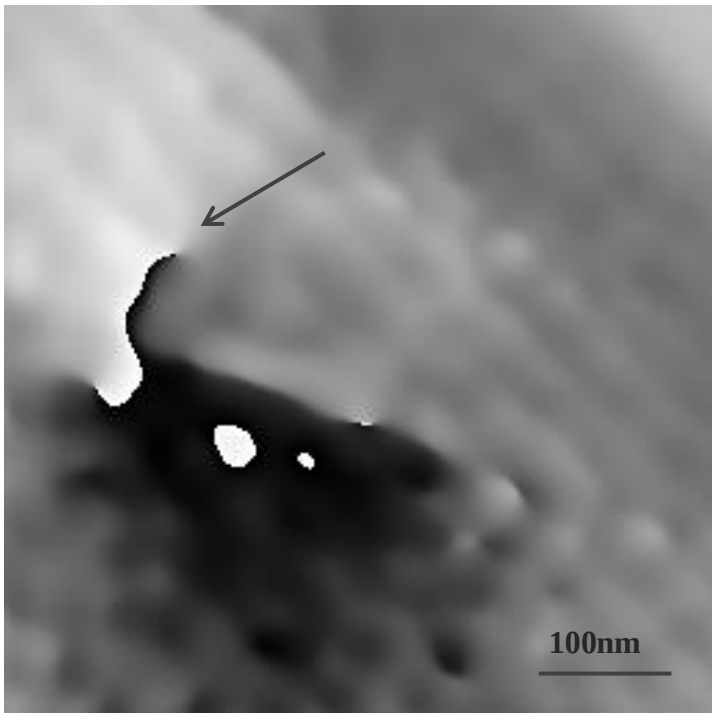

Fig. 4-4. Phase image reconstructed from the hologram in Fig. 4-3.

4.2.2 Undulation noise in the corrected phase image

To correct the phase imperfections, we must first identify the incorrect fringes. Based on the methods described in the previous chapter, the skeletonized binary image of the interference fringes shown in Fig. 4-5 is used for burr removal. An example of a burr in the interference fringes is indicated by the red oval.

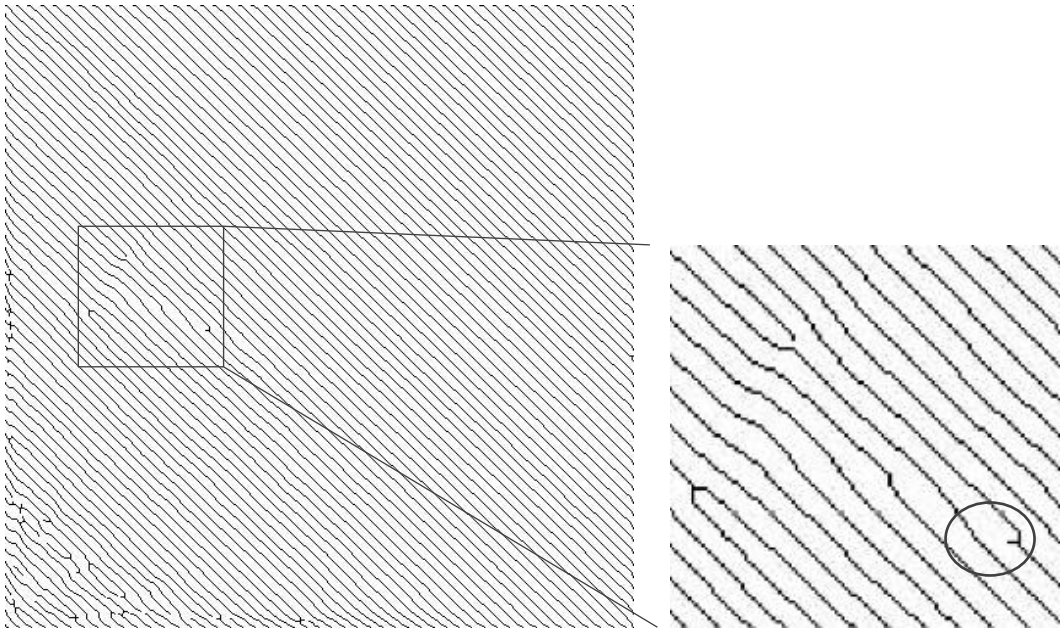

Fig. 4-5. Example showing a burr in the interference fringes.

Figure 4-6 shows a skeletonized binary image without the burr points indicated by the red oval mark after burr removal using MATLAB.

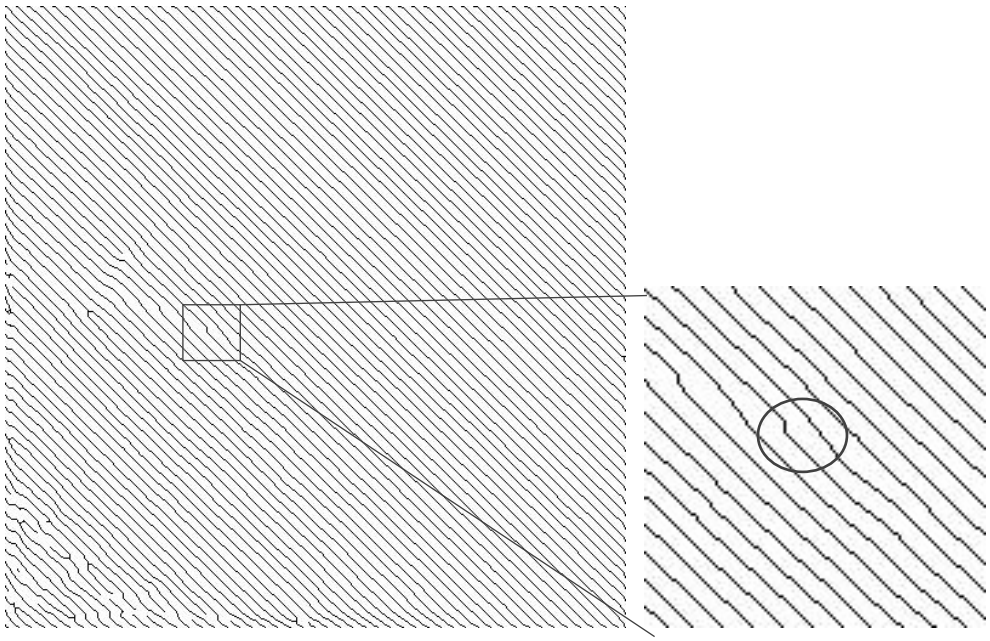

Fig. 4-6. Binary image without burr points.

The disconnected and incorrectly connected points are indicated in Fig. 4-7 based on the skeletonized binary image without burr points.

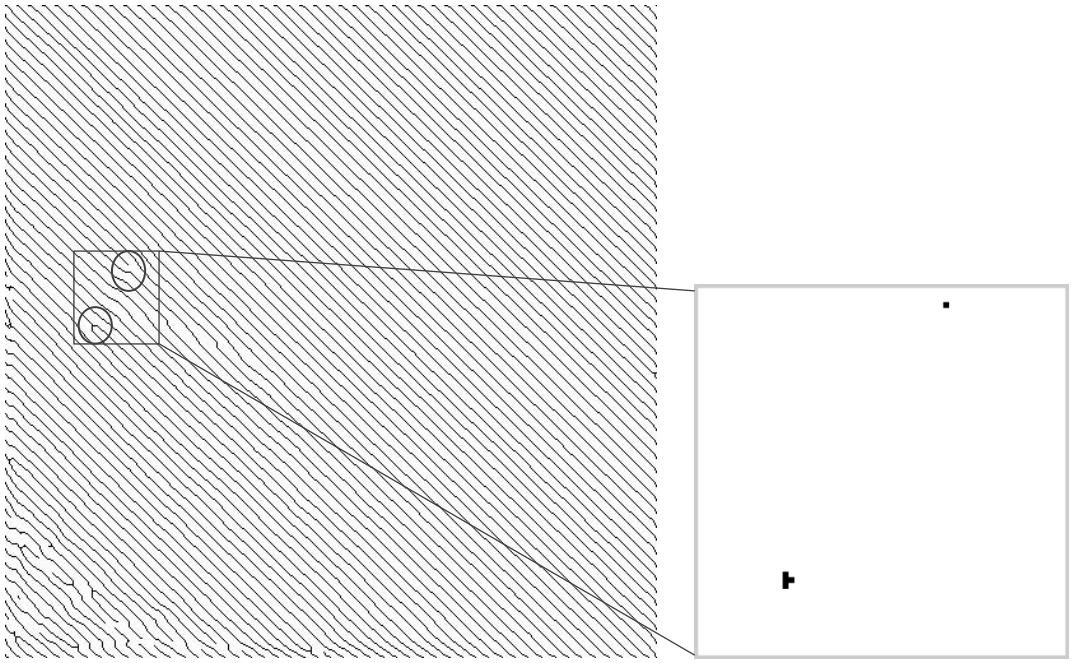

Fig. 4-7. Incorrectly connected points.

The distorted interference fringes are corrected by cut-and-reconnect processing, before smoothing using a median filter, as shown in Fig. 4-8.

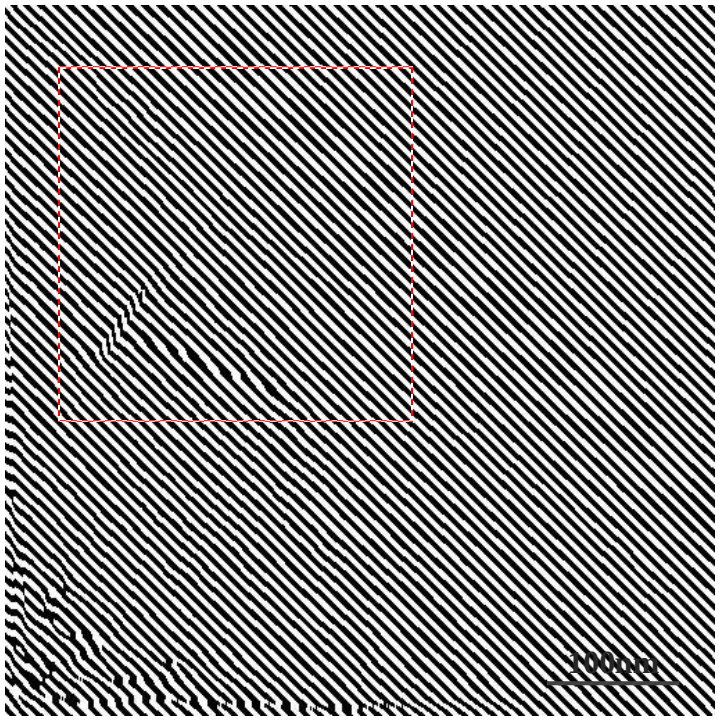

Fig. 4-8. Distorted interference fringes.

The reconstructed phase image shown in Fig. 4-9, which was obtained from the corrected interference fringes, demonstrates that the phase error caused by the weakness of the electron-wave amplitudes has been reduced.

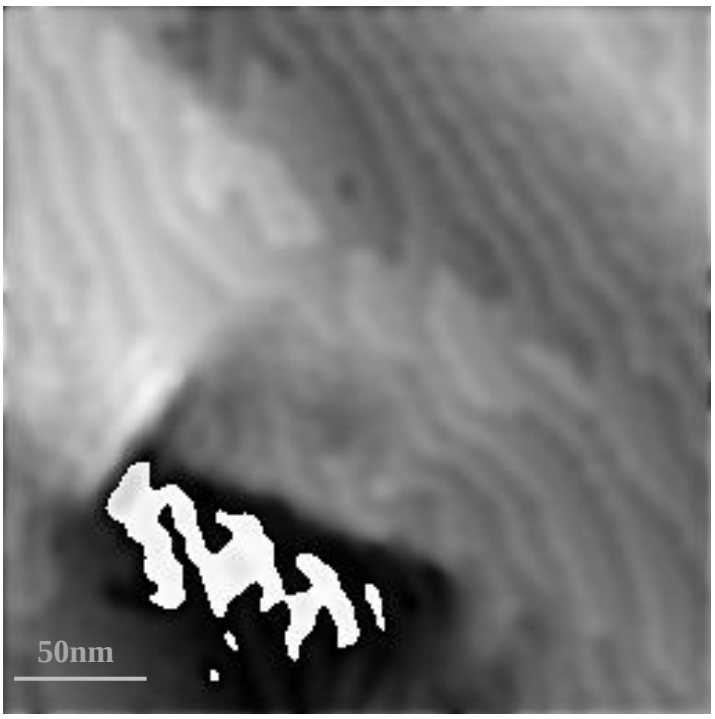

Fig. 4-9. Reconstructed phase image obtained from the corrected interference fringes.

The unwrapping process (designed by Gatan) is used to remove the phase jump caused by the digital reconstruction process to obtain the final image without any phase jump, as shown in Fig. 4-10.

The phase error in the reconstructed phase image was reduced dramatically, but a new type of noise is sometimes present in the phase image: undulation noise.

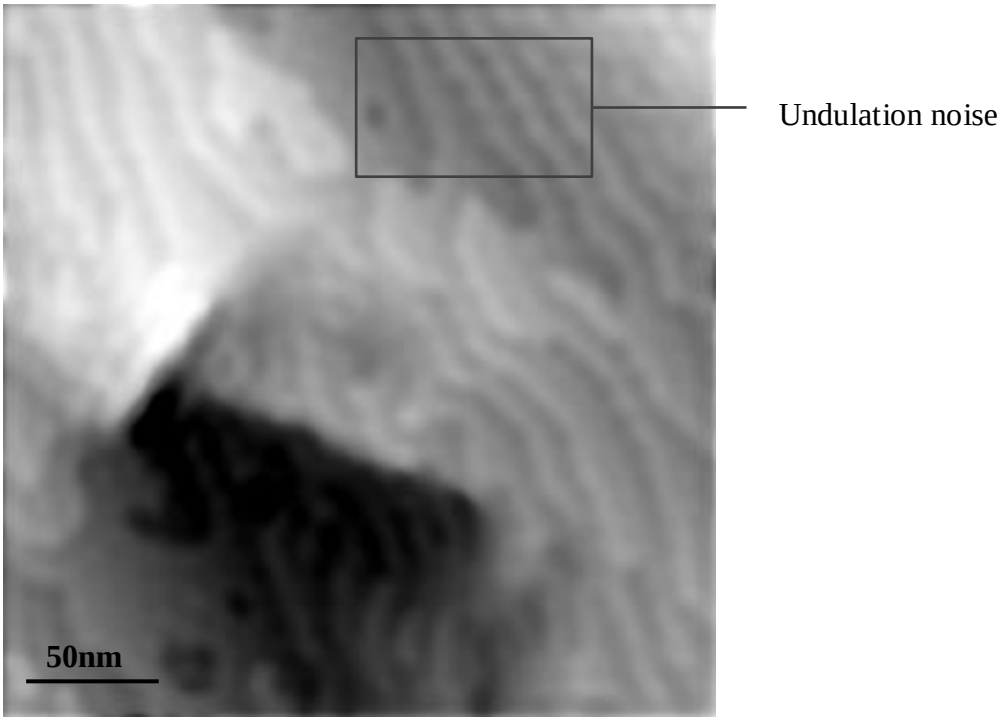

Fig. 4-10. Final reconstructed phase image with undulation noise.

4.3 Origin of undulation noise

Identifying the source of undulation noise is important for improving the restoration quality. The interference pattern of an electron hologram was captured using another sample with the same external conditions (same electron microscope, same illumination condition, same CCD camera in vacuum). The same image processing method was used to obtain the phase image, but undulation noise did not occur.

After comparing the images produced, the source of this noise was found to be the unevenness of the interference fringes in the binary image shown in Fig. 4-11. This unevenness originates from the incline in the fringes during computational binarization[1].

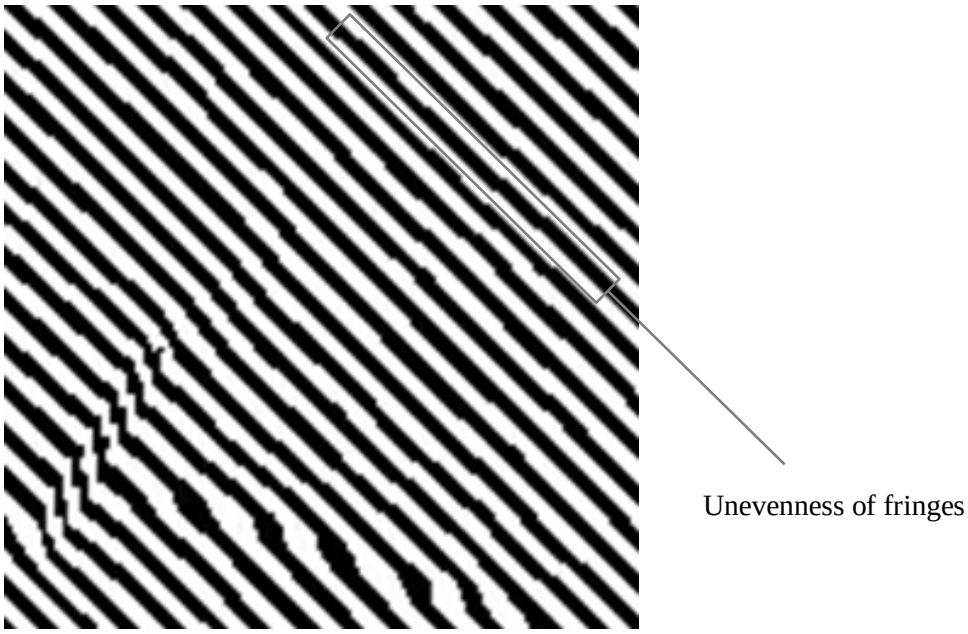

Fig. 4-11. Unevenness of the fringes.

Figure 4-12 shows a profile image of the phase image where this is unevenness in the fringes in the rectangular regions indicated the width of the fringes in fringes direction. The unevenness of the fringes can be characterized clearly. This unevenness originates from the binarization processing because the images processed by the computer are digital signals rather than analog signals. Thus, the pixels in the image are processed as rectangles by the computer and there is no smooth distinction between one pixel and its neighboring pixels. Thus, the binarization of fringes at some angles will cause unevenness because the computer mistakenly recognizes rectangles and separates the values of the pixels.

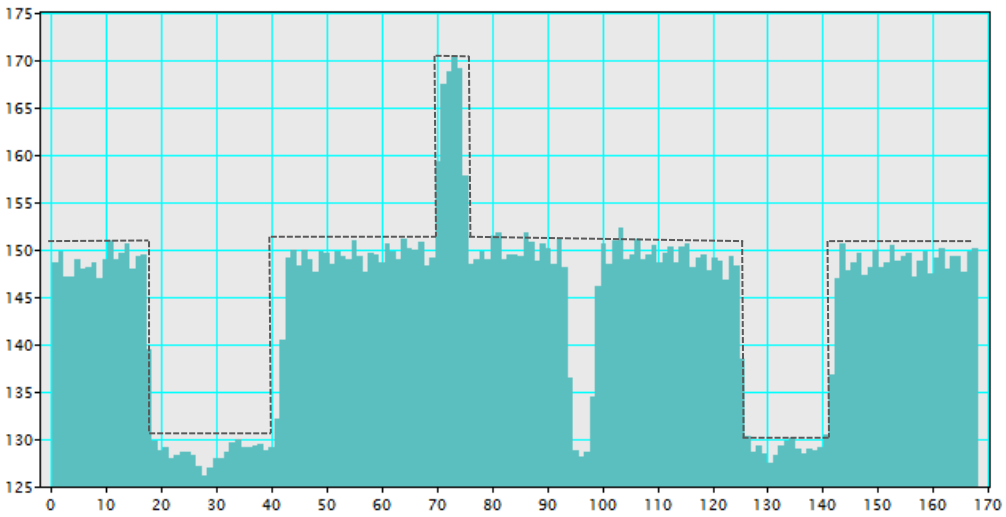

Fig. 4-12. Profile image of a phase image with unevenness in the fringes.

4.4 Elimination of undulation noise

4.4.1 Elimination method

This problem can be solved by rotating the electron hologram by several degrees before processing. In the present case, we rotated the electron hologram by 20° and the unevenness of the interference fringes was eliminated after rotating the binary image, as shown in Fig. 4-13.

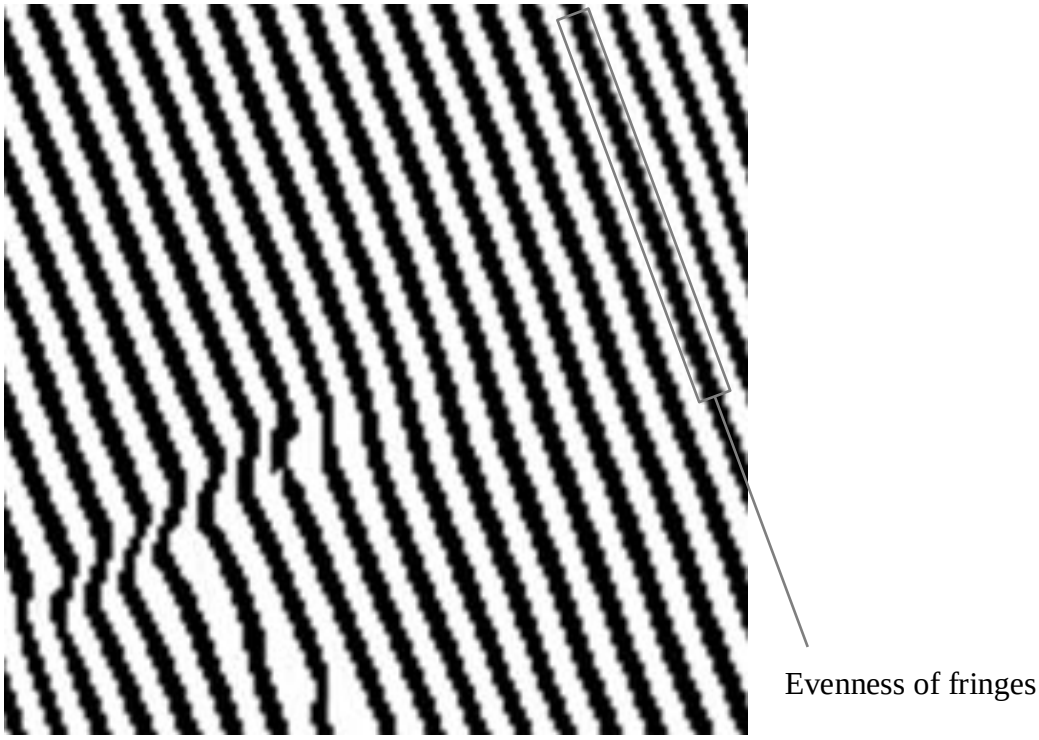

Fig. 4-13. Evenness of the fringes.

Figure 4-14 shows the line profile of a phase image with evenness in the fringes in the rectangular region. Thus, the unevenness of the fringes can be corrected well.

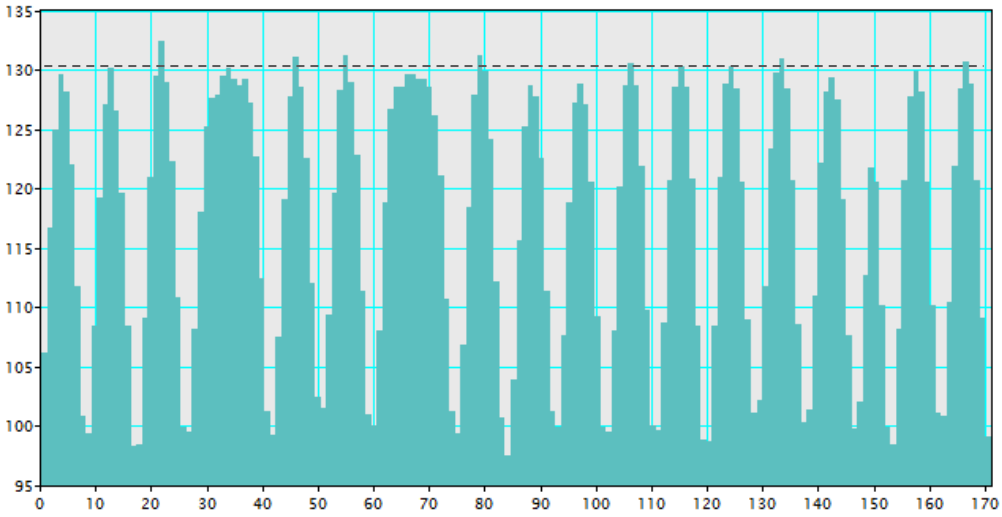

Fig. 4-14. Profile image of a phase image with evenness in the fringes.

The reconstructed phase image in Fig. 4-15, which was obtained from the even interference fringes, shows that the undulation noise caused by the unevenness of the fringes has been reduced dramatically.

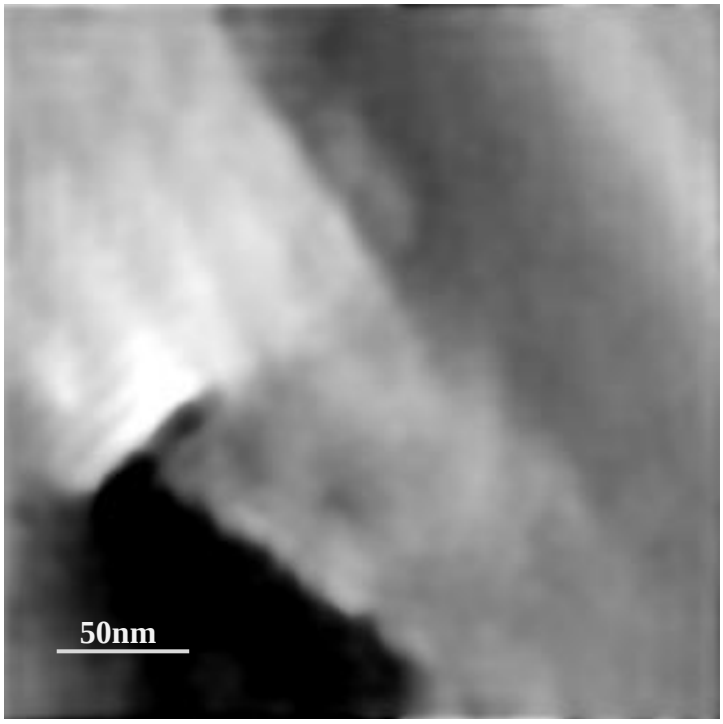

Fig. 4-15. Final image produced.

4.4.2 Evaluation of the elimination method

We compared the phase image generated after elimination with that containing undulation noise using the profile image of the same region.

The profile image of the phase image with undulation noise in the rectangular region is shown in Fig. 4-16.

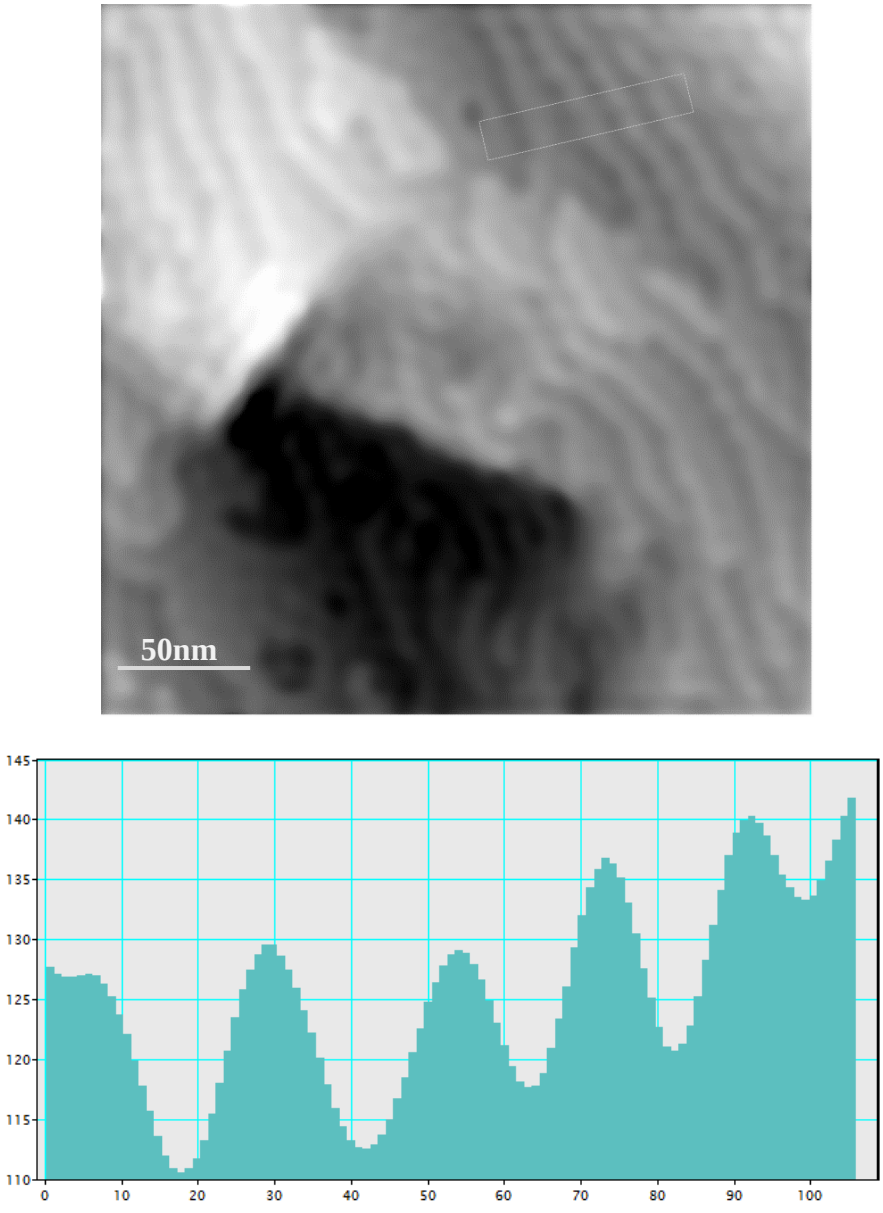

Fig. 4-16. The profile image of the phase image with undulation noise in the rectangular region.

The profile image of the phase image after applying the elimination process to the rectangular region is shown in Fig. 4-17.

The results show clearly that the undulation noise has been eliminated to a great extent based on a comparison of these two output images.

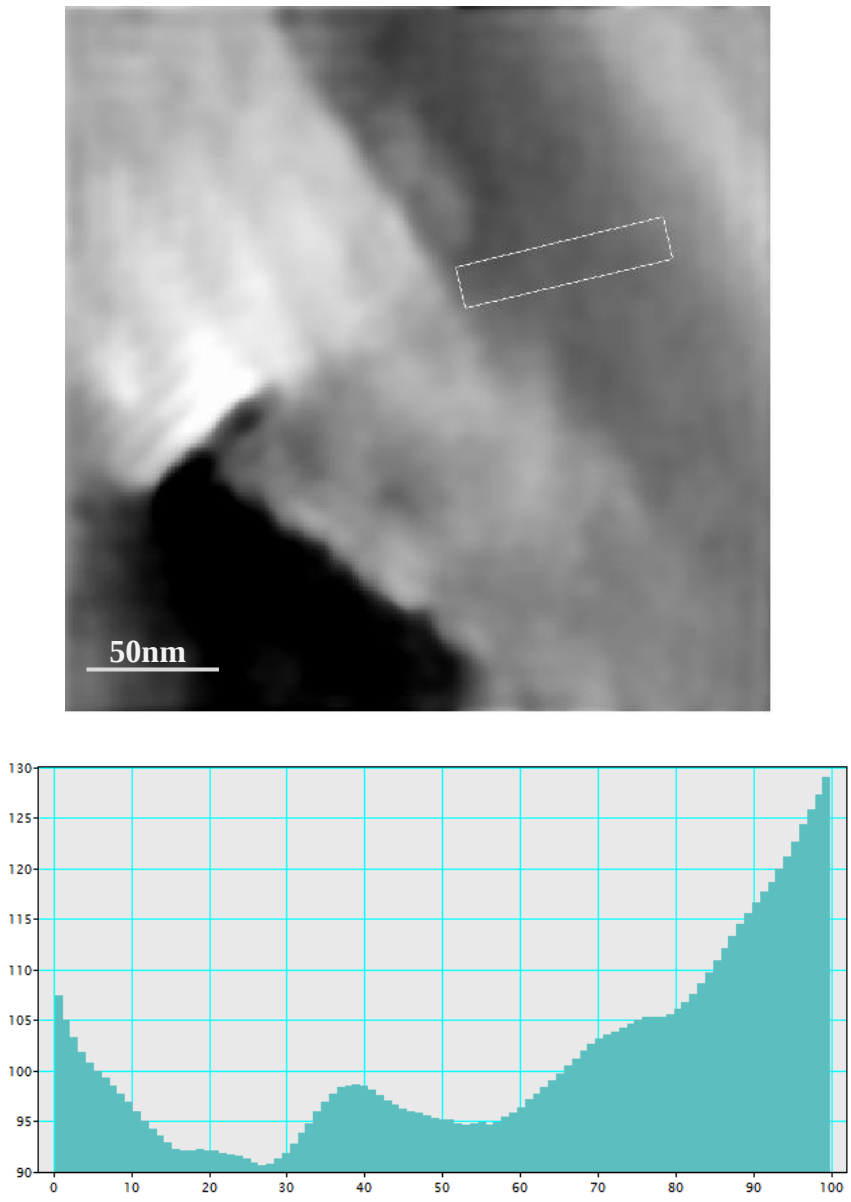

Fig. 4-17. The profile image of the phase image after applying the elimination process to the rectangular region.

4.5 Conclusion

The reconstructed phase image obtained from the corrected interference fringes showed that the phase error was reduced dramatically, but undulation noise was present in the phase image.

Thus, it was necessary to find the source of the undulation noise.

A comparison of the two phase image before and after processing showed that the unevenness of the interference fringes in the binary image was the source of the undulation noise.

This problem was solved by rotating the electron hologram by an appropriate angle before processing.

References

[1] J. C. Stoffel, (1982) Graphical and Binary Image Processing and Applications. Artech House, Dedham, MA.

Chapter five

5. Simulation of the processing of holograms with noise

5.1 Preamble

Noise refers to any unwanted and not necessarily random information. Noise is always a random fluctuation in the electrical signal in electronic systems, which is a characteristic of all electronic circuits. Various types of noise are generated by electronic devices, which can be produced by several different effects.

Thermal noise is a type of unavoidable noise that occurs at non-zero temperatures, while other types such as shot noise depend mostly on the device type [1, 2].

In practice, two main types of noises may occur when capturing holograms, i.e., Poisson noise and Gaussian noise. The interference fringes may not be distinguished for much noise in the hologram. In addition, low electron luminance can also make the interference fringes undistinguishable, as seldom electrons hardly form the fringes. We aimed to eliminate the imperfections in the hologram in these noise and low electron luminance situations

This chapter addresses the simulation of holograms with noise and low electron luminance, and these two main noises were added to the hologram in the simulation. Thus, we applied the phase reconstruction processing to a simulated hologram, which contained much more noise and lower electron luminance than that found in practice.

5.2 Poisson noise

In this case, Poisson noise is a type of shot noise.

In electronic devices, shot noise originates from unavoidable random statistical fluctuations in the electric current [3]. When the charge carriers traverse a gap, the number of traversable carriers is random, such as specific electrons. The current can be regarded as a flow of discrete charges and the shot noise originates from fluctuations when these charges arrive. Shot noise is similar to the noise created by snow falling on a flatbed. The flow of snow may be relatively constant, but the snowflakes arrive discretely on the flatbed.

Shot noise may be a major problem when the finite number of particles with energy, such as electrons in an electronic circuit or photons in an optical device, is sufficiently small. Thus, uncertainties related to the Poisson distribution that describes the occurrence of independent random events can describe these uncertainties. Shot noise is important in electronics.

Shot noise is temperature- and frequency-independent noise, which may be the dominant source of noise at high frequencies and low temperatures.

Shot noise is relatively insignificant in many cases of electrical conduction, but it can be significant with very small currents and short time scales.

If the intensity of the electron wave is extremely weak in a TEM, shot noise will be a significant problem. The emission of electrons from the FEG is random according to the quantum theory, so if the average number emitted is eight, the actual number may be 6 or 10.

A Poisson process is a random process that counts the number of events within a given time interval. The time between each pair of continuous events has an exponential distribution with parameter λ and each of these inter-arrival times is assumed to be independent of other inter-arrival times.

A Poisson distribution can be defined by the following probability mass function.

$$P(X = k) = \frac{\lambda^k e^{-\lambda}}{k!} \qquad (5\text{-}1)$$

where X is the discrete random variable, $k = 0,1,2, \ldots$.

This probability mass function can be used to formulate Poisson noise.

Figure 5-1 shows a plot of the probability mass function with different values of λ.

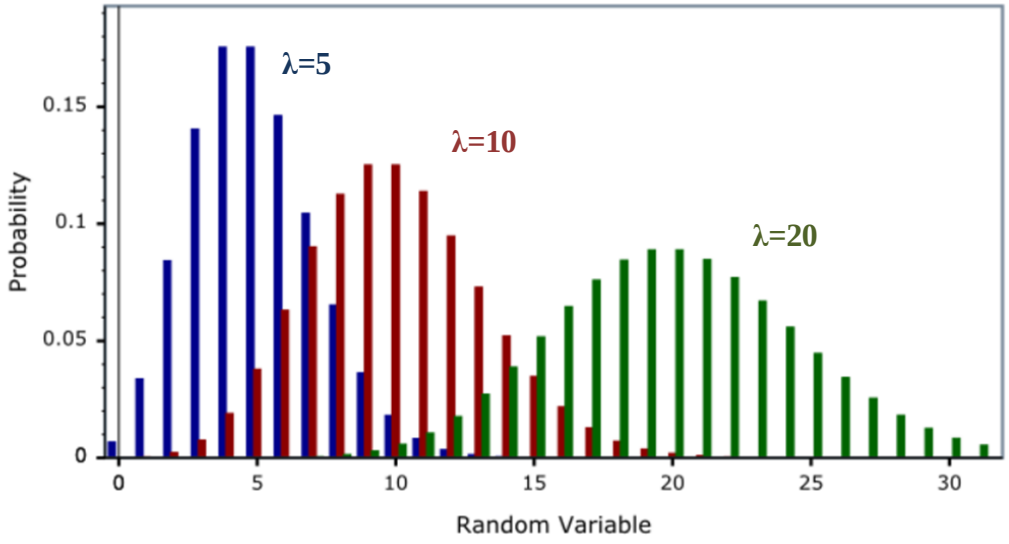

Fig. 5-1. A plot of the probability mass function with different values of λ.

5.3 Simulation of a hologram with Poisson noise

Poisson noise was simulated according to the probability mass function, as stated earlier.

In this case, Poisson distribution functions were used to formulate an image of the Poisson noise using the toolbox in Matlab.

Several different values of λ were used to compare the differences in the effect.

Figure 5-2 shows an image of the Poisson noise with different values of λ.

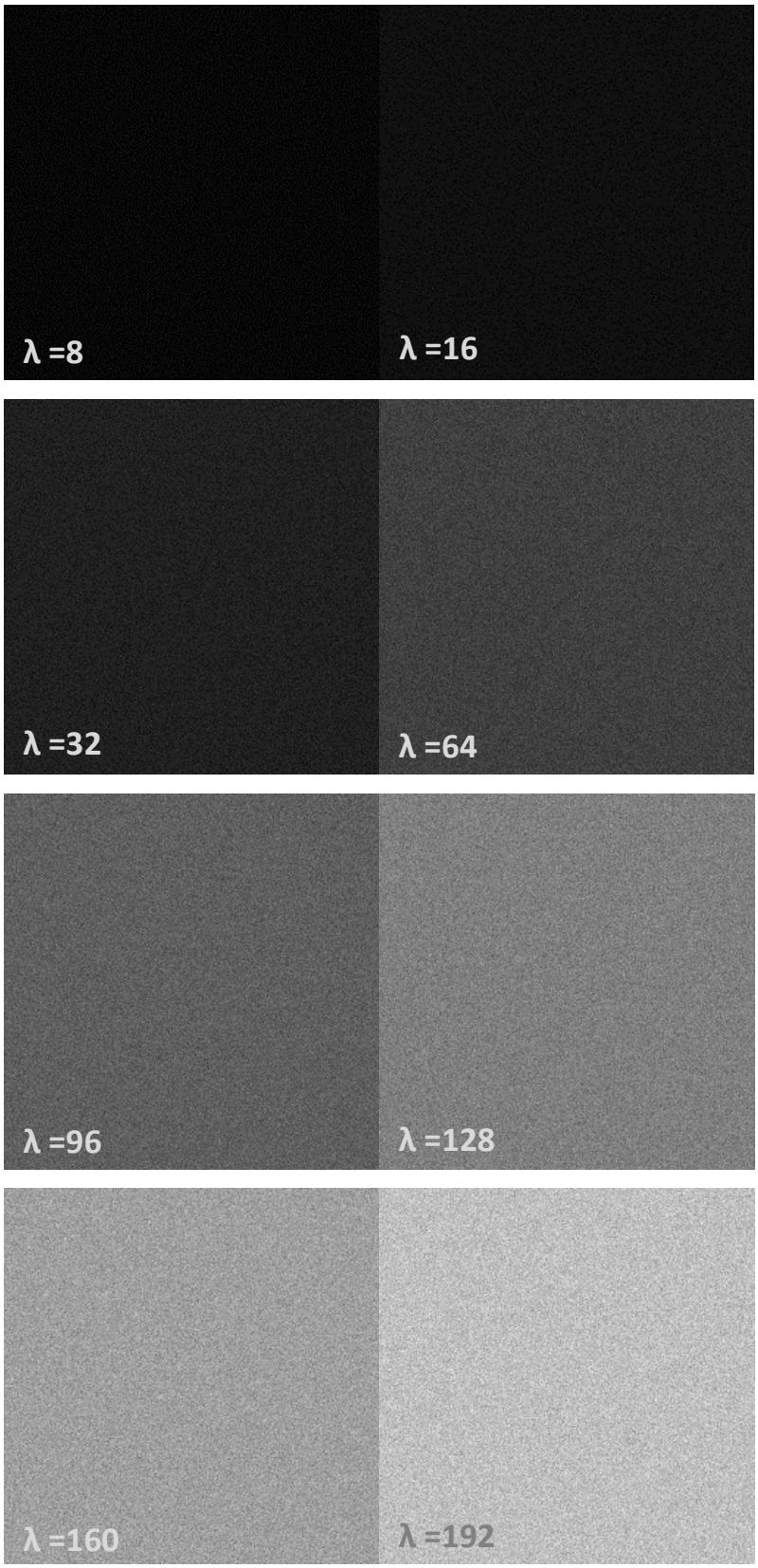

Fig. 5-2. The Poisson noise with different values of λ.

Because the value of λ is equal to the expected value of X and also equal to its variance, the value of λ is related directly to the brightness of the Poisson noise in images.

Poisson noise was added to the hologram making the pixel yield Poisson distribution in the simulation using toolbox in Matlab, which could change the brightness directly in the same manner as a weak electron-wave.

Figure 5-3 shows an image of the hologram after adding Poisson noise with different values of λ. In this case, the hologram shown in chapter four was used in the simulation.

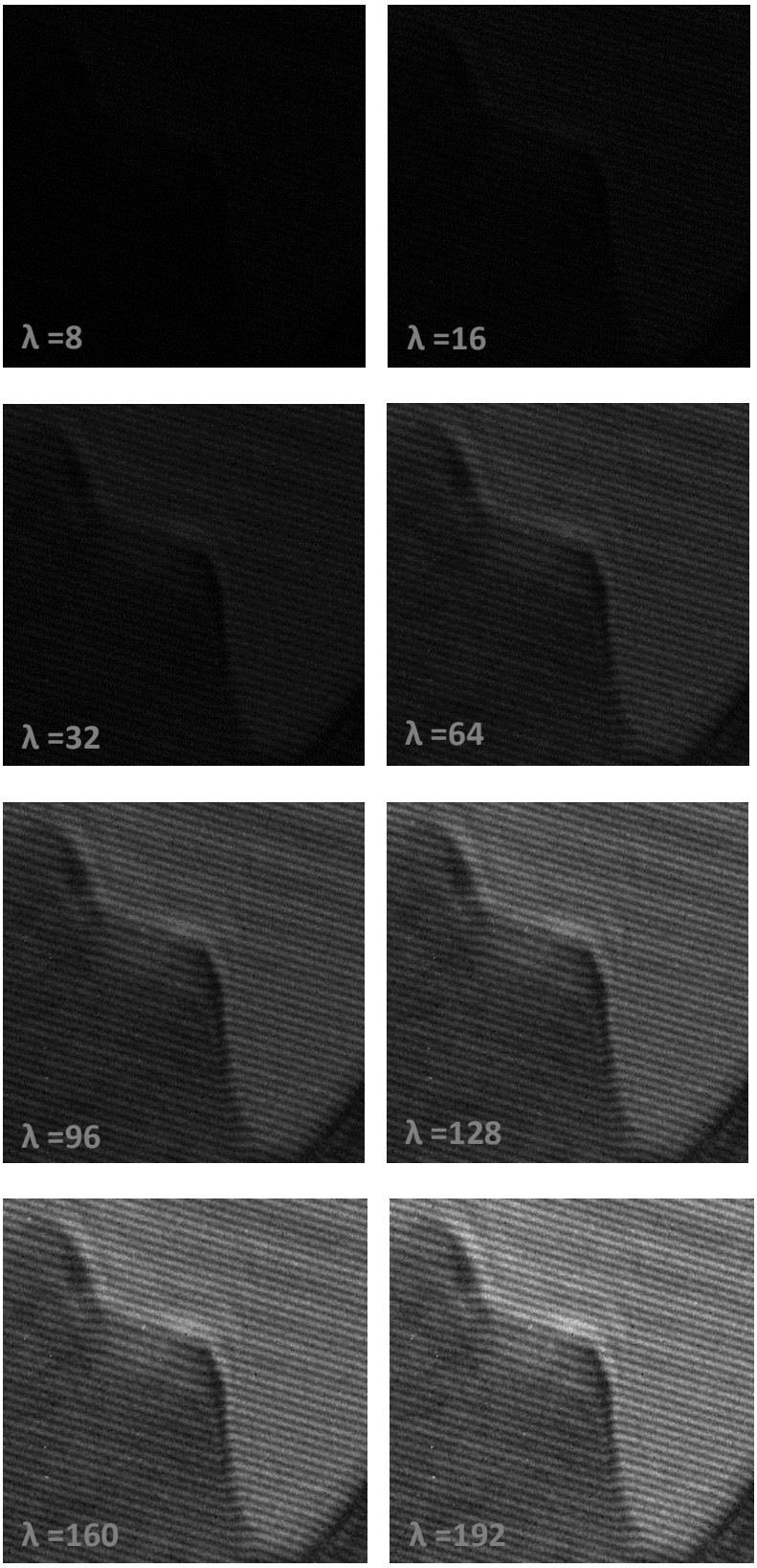

Fig. 5-3. The image of the hologram after adding Poisson noise

with different values of λ.

Because the effect of the value of λ on the brightness was fairly small, a histogram equalization processing was introduced to enhance the brightness of the hologram.

Low values of λ were more valuable in the simulation of a hologram with Poisson noise because we wanted to test the case with the weakest electron-wave with several electron emissions. Thus, a hologram with Poisson noise where the value of λ was low was selected for the next process.

Figure 5-4 shows a hologram with Poisson noise where λ has a low value after the histogram equalization process. Its distribution in Fig. 5-4(a) shows that the pixel values cover about 8 values.

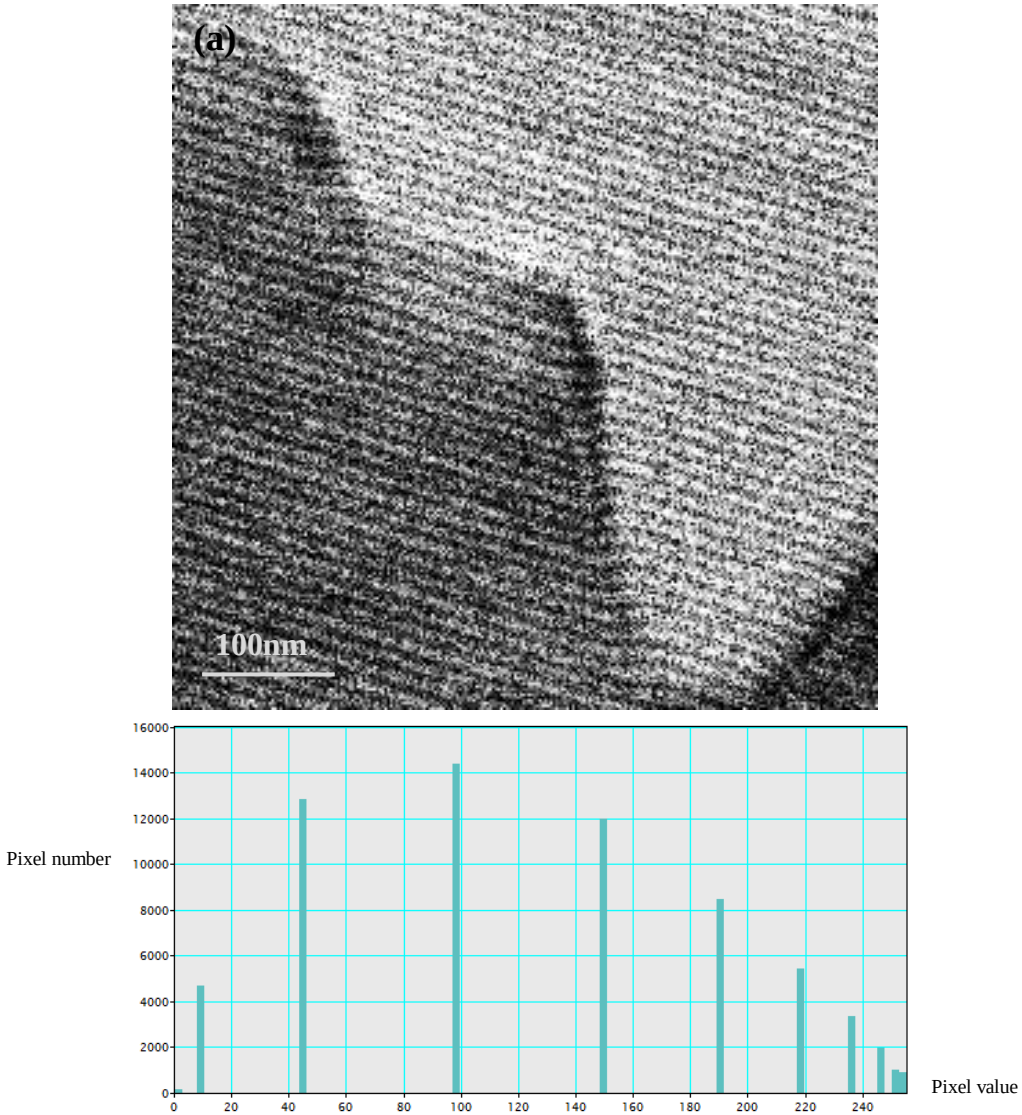

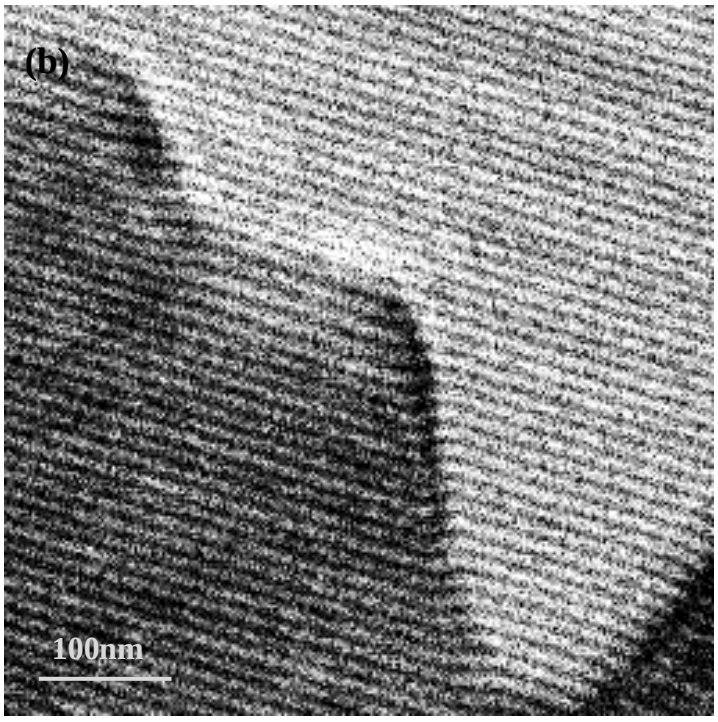

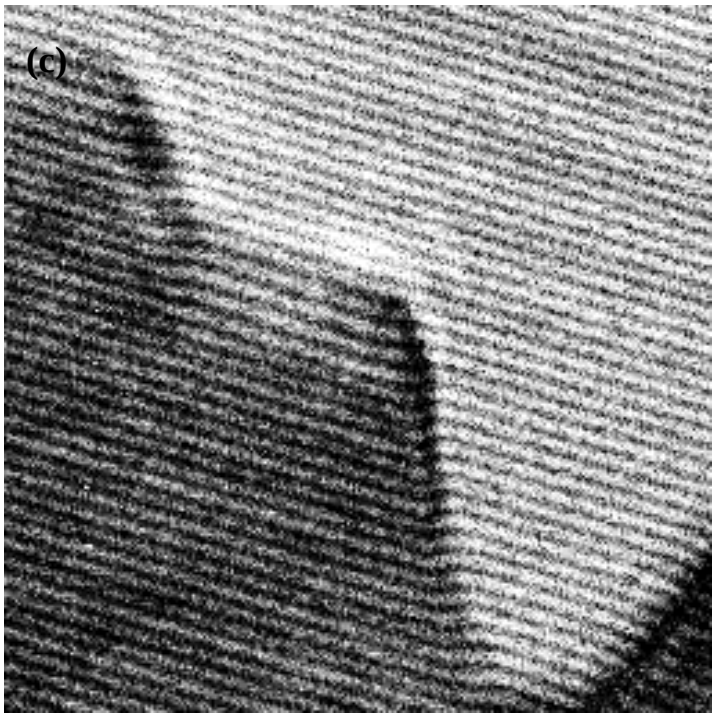

Fig. 5-4. The holograms with Poisson noise after the histogram equalization process. (a) λ=8 and its distribution; (b) λ=16;(c) λ=32.

The brightness was increased after histogram equalization processing and Poisson noise is evident in the hologram. The pixels in the histogram of the hologram intensity have various values. The distribution of the histogram agrees with the distribution of the low values of λ, which also indicates that several electrons are emitted, as indicated earlier.

The histogram of the hologram shows that a Poisson distribution was simulated successfully because the distribution of the pixel values is very similar to a Poisson distribution.

5.4 Simulation of a hologram with Gaussian noise

Gaussian noise is a type of statistical noise. The probability density function of Gaussian noise is equal to that of the normal distribution, which is also known as a Gaussian distribution.

The probability density function of a Gaussian distribution is obtained as follows:

$$f(x) = \frac{1}{\sqrt{2\pi}\sigma} exp(-\frac{(x-\mu)^2}{2\sigma^2}) \qquad (5\text{-}2)$$

where the mean value μ is equal to zero and the standard deviation is σ. This distribution is known as the standard normal distribution or the unit normal distribution.

We consider the use of a gas environment to make *in situ* observations, which obstructs clear imaging because the electrons are scattered by gas molecules.

Other sources of Gaussian noise in electron hologram images are sensor noise caused by poor illumination, high temperature, transmission noise, and electronic circuit noise [4-6]. Transmission system and electronic circuit will cause additional noise to the signal. Poor illumination and high temperature may reduce the signal noise ratio.

Figure 5-5 shows a hologram after adding Gaussian noise to Fig. 5-4(a), where the lowest value of λ was selected. Its distribution show that pixel values cover all the range of values

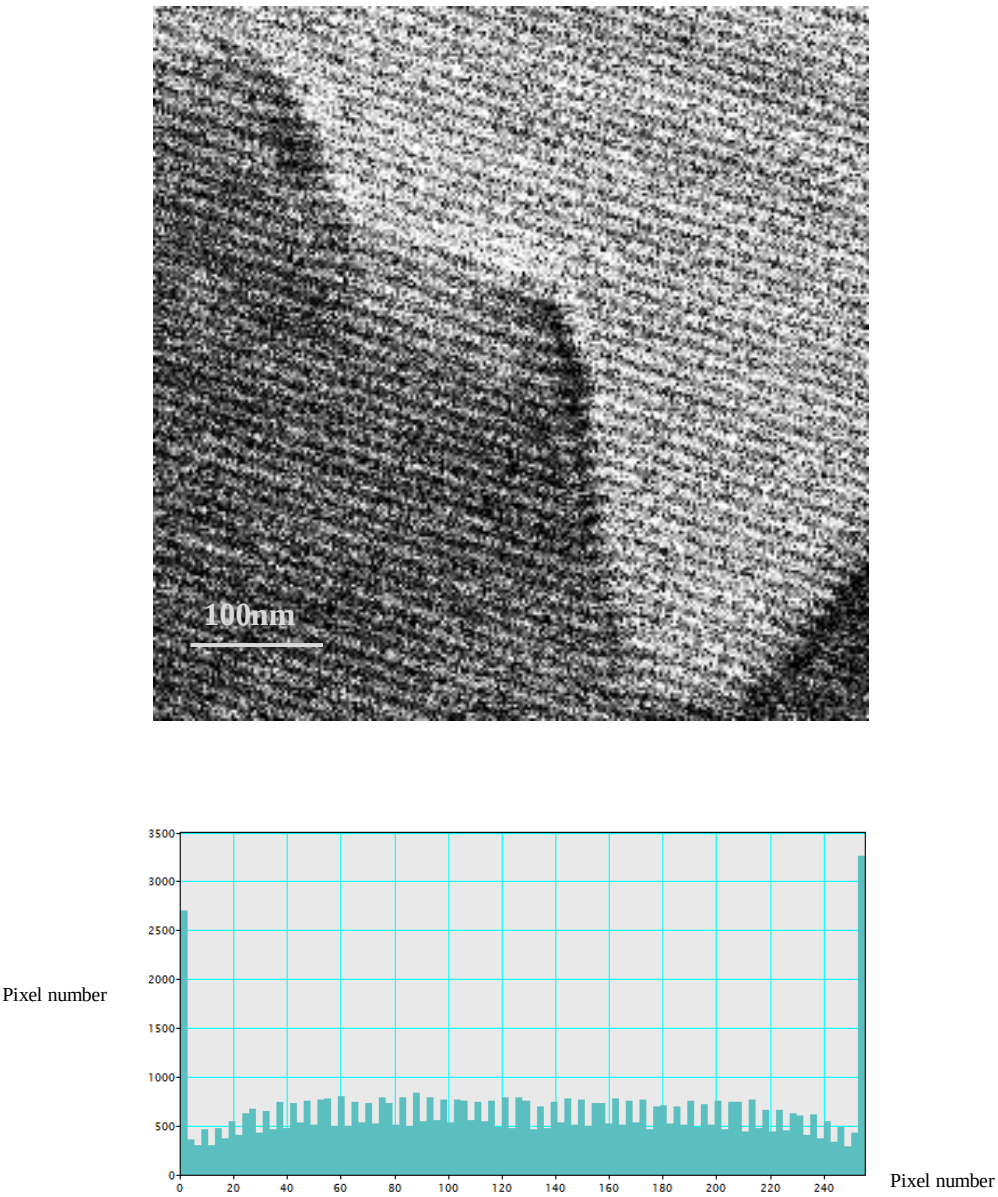

Fig. 5-5. A hologram after adding Gaussian noise to Fig. 4(a) and its distribution.

The pixels have even values in the histogram of the hologram, which means that the Gaussian noise is distributed evenly throughout the hologram.

The reconstructed phase image obtained directly from the electron hologram with Gaussian noise and Poisson noise is shown in Fig. 5-6(a), which includes many phase imperfections. This is because the interference fringes were not recognized correctly.

Figure 5-6(b) shows a phase image obtained after unwrapping processing, which cannot be used.

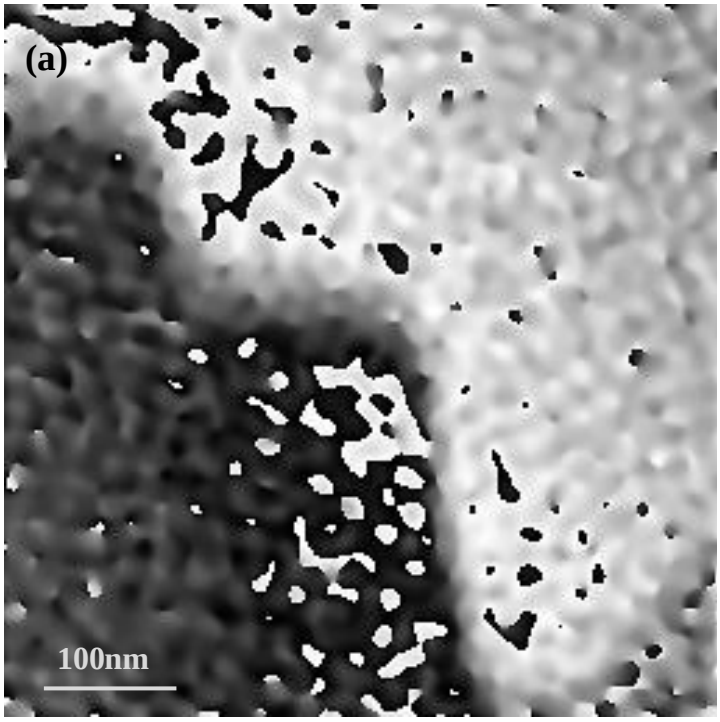

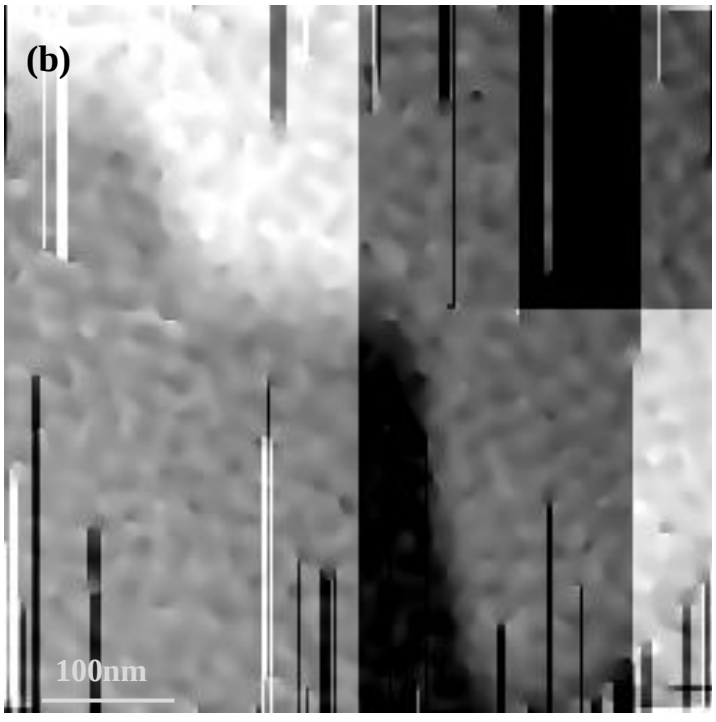

Fig. 5-6. (a) The reconstructed phase image obtained directly from the electron hologram with Gaussian noise and Poisson noise , which includes many phase imperfections; (b) shows a phase image obtained after unwrapping processing.

5.5 Restoration of singularities

A similar processing method to that described in chapter 2 is used to restore the singularities present in the reconstructed phase image.

Figure 5-7 shows the fringes of the hologram, where singularities are present in some areas.

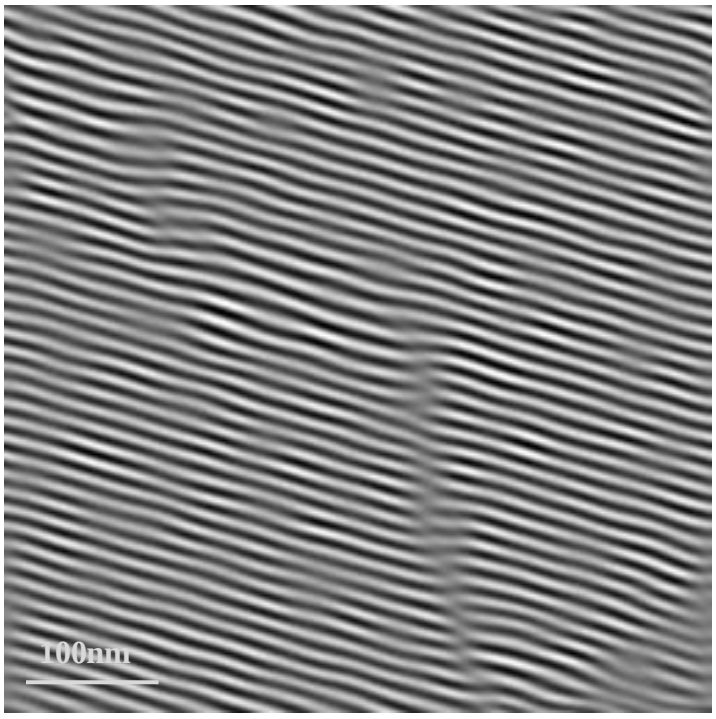

Fig. 5-7. The fringes of the hologram.

During binary conversion, the threshold value is dynamic in practice, which may have major effects on the results. In this case, a fairly low value is a good choice, e.g., 0.48 instead of 0.5.

Figure 5-8 shows the fringes of the hologram after binary conversion.

The singularities have been reduced to a great extent by binary conversion, but they

are more abundant compared with the hologram with no added noise, as described in chapter 2.

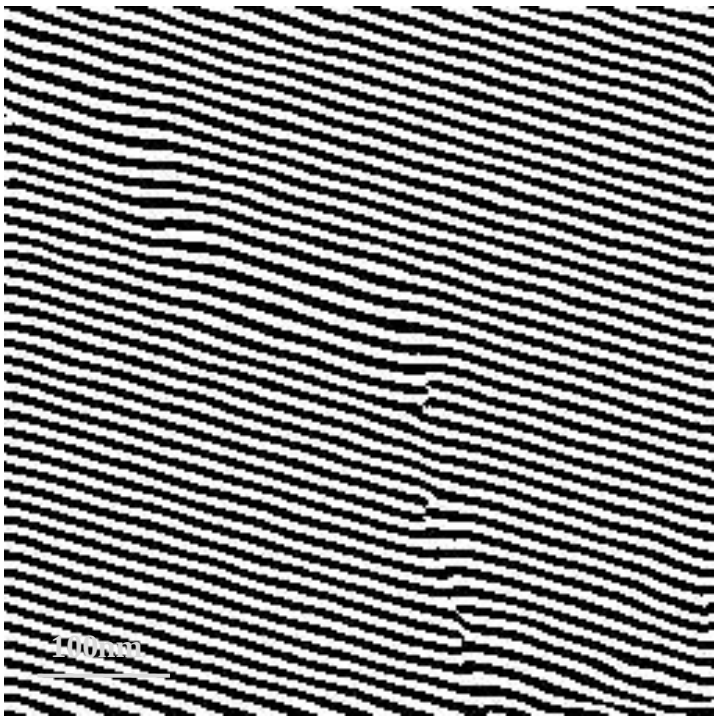

Fig. 5-8. The fringes of the hologram after binary conversion.

Next the processing method described in chapter 2 was used to restore the singularities.

Figure 5-9 shows the interference of the corrected binary fringes in the hologram.

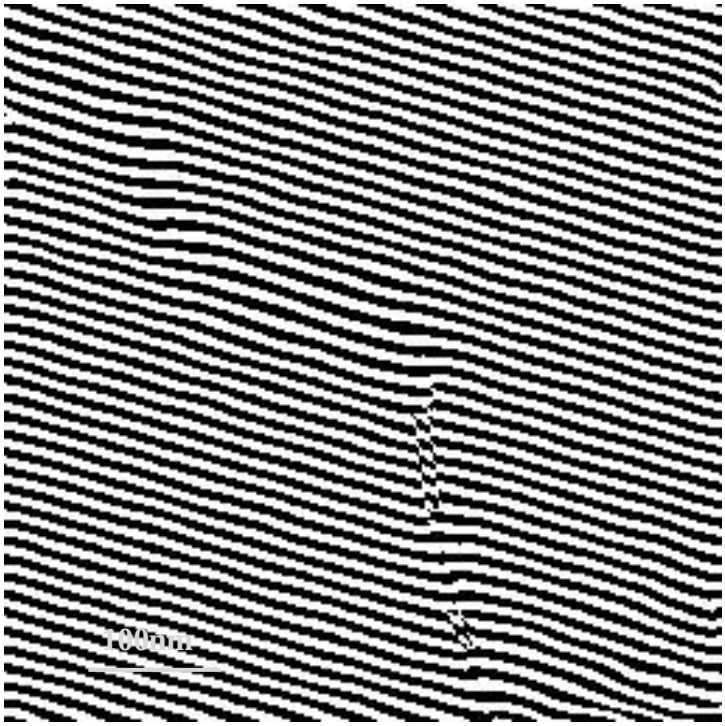

Fig. 5-9. The interference of the corrected binary fringes in the hologram.

The corrected interference fringes need to be smoothed using a median filter.

Figure 5-10 shows the corrected interference fringes after smoothing.

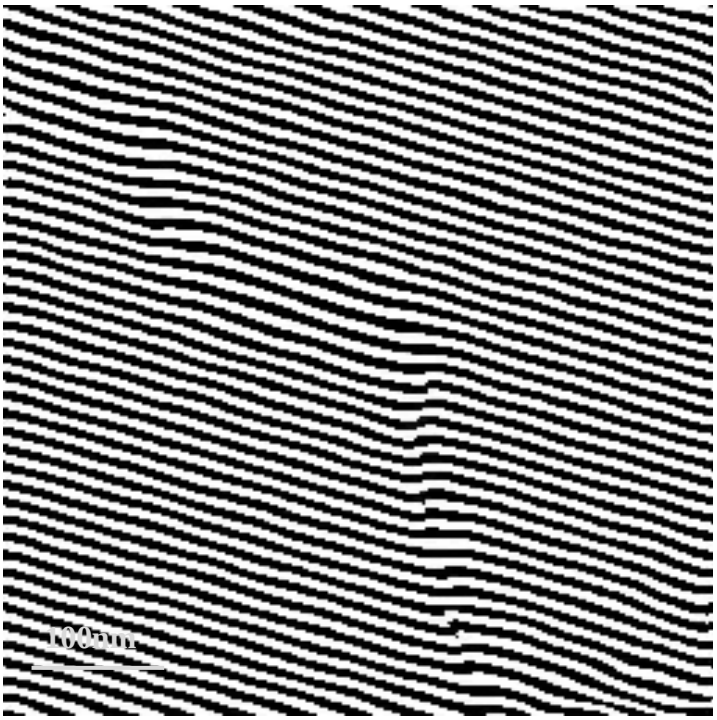

Fig. 5-10. The corrected interference fringes after smoothing.

Figure 5-11 shows the reconstructed phase image obtained from the corrected interference fringes. The phase image shows that the phase imperfections have been reduced dramatically, including the singularities. This confirms that the processing method is also effective for electron holograms with Poisson and Gaussian noise.

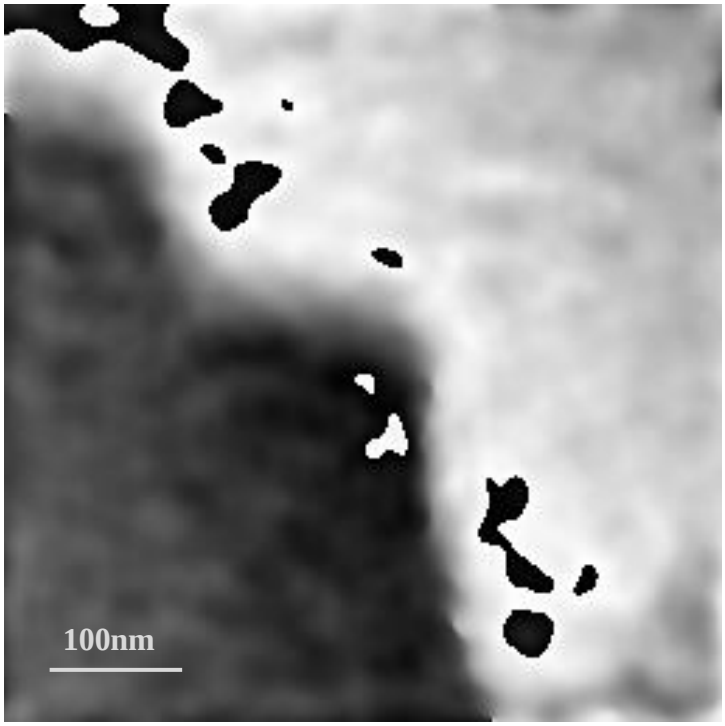

Fig. 5-11. The reconstructed phase image obtained from the corrected interference fringes.

The unwrapping process must be applied because phase jumps are produced in the reconstructed phase image by the digital reconstruction process.

Figure 5-12 shows the reconstructed phase image after the unwrapping process.

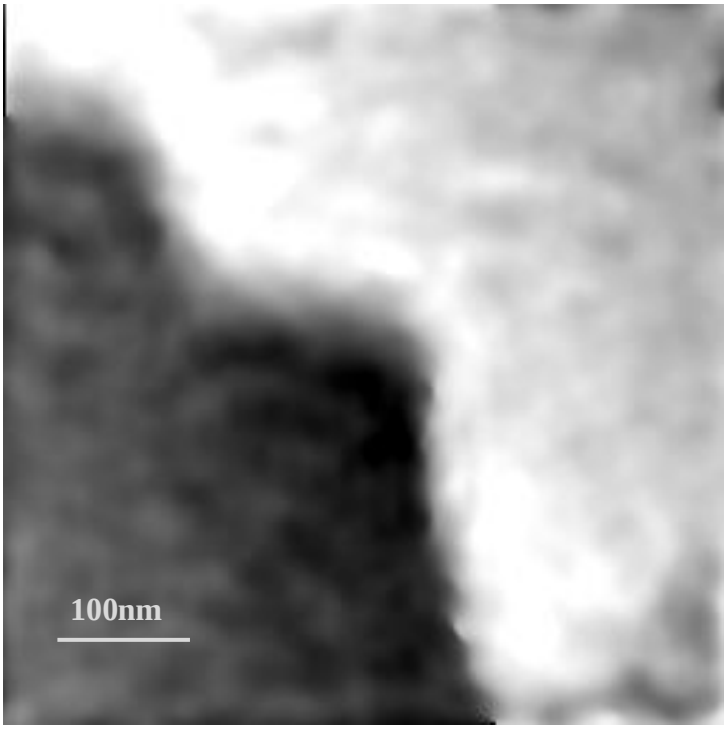

Fig.5-12. The reconstructed phase image after the unwrapping process.

5.6 Simulation of a hologram with different luminance

The interference fringes may not be distinguished for the low electron luminance, as seldom electrons hardly form the fringes.

The images of hologram after Poisson noise added with different luminance (electron numbers) are shown in Fig.5-13. Figure 5-13(a) shows the electrons of the luminance are seldom about one thousand electrons. Figure 5-13(b) shows the electrons of the luminance are just enough to distinguish the interference fringes about 25 thousands electrons. Figure 5-13(c) shows the electrons of the luminance are enough to distinguish the interference fringes clearly.

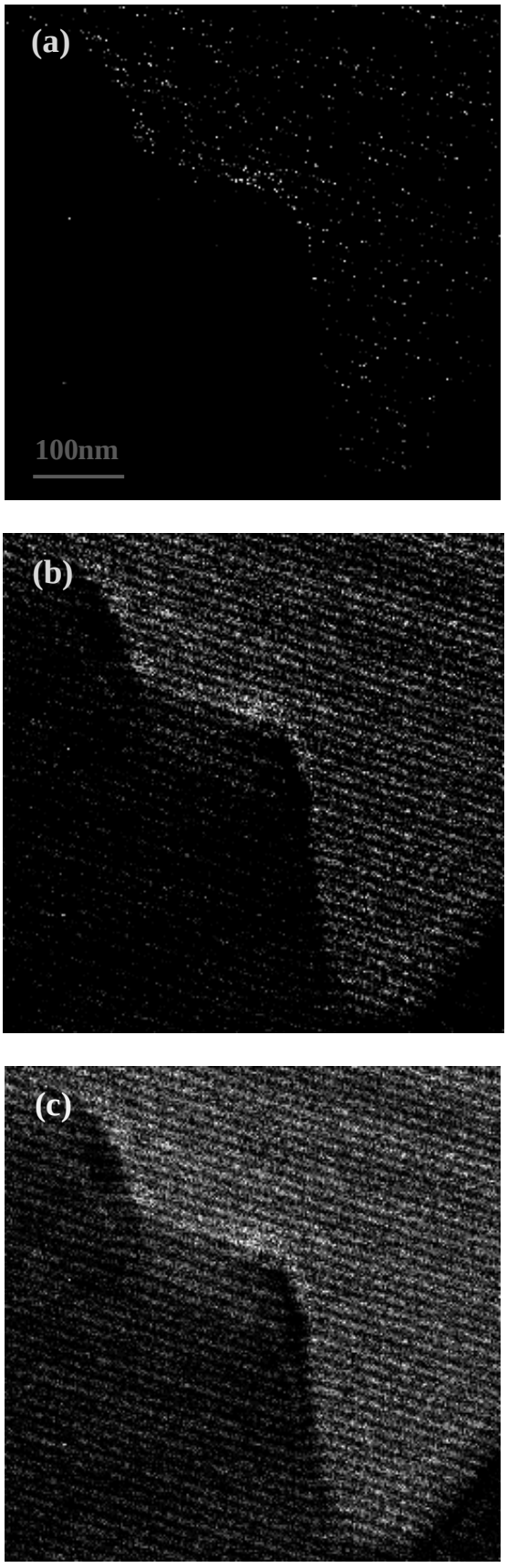

Fig.5-13. (a)Seldom electrons of the luminance about one thousand. (b) Just enough electrons of the luminance about 25 thousands. (c) Enough electrons of the luminance to form clear fringes.

Fig. 5-14(a) shows the binary fringes of the hologram in Fig. 5-13(b) after binary conversion. Fig. 5-14(b) shows the corrected interference fringes after smoothing out. Fig. 5-15(a) shows the reconstructed phase image obtained from the corrected interference fringes in Fig. 5-14(b). Fig. 5-15(b) shows the reconstructed phase image after unwrapping process.

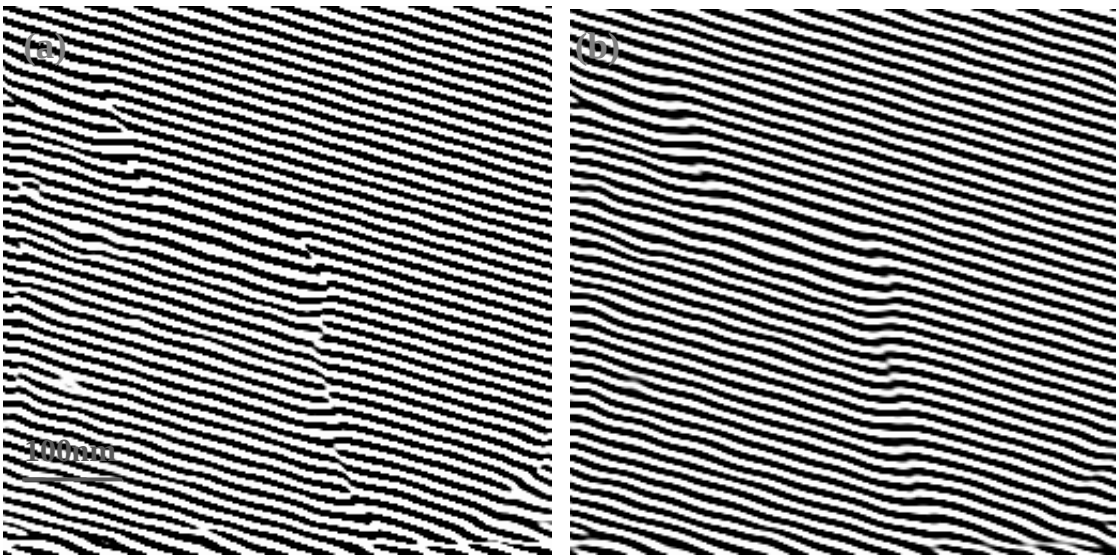

Fig.5-14. (a) The binary fringes of the hologram in Fig. 5-13(b) after binary.

(b) The corrected interference fringes after smoothing out.

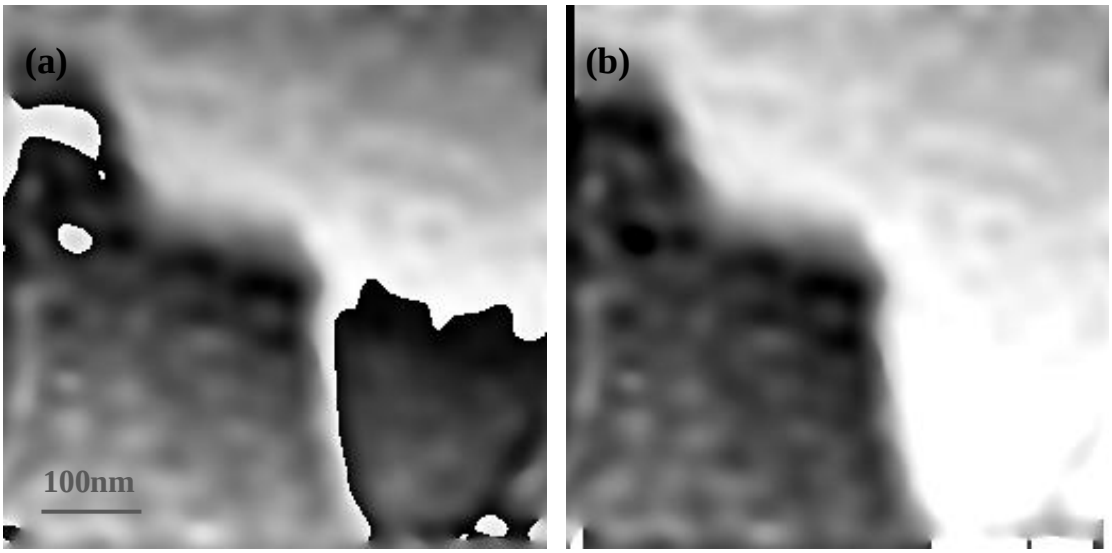

Fig. 5-15. (a) The reconstructed phase image obtained from the corrected interference fringes in Fig. 5-14(b). (b) The reconstructed phase image after unwrapping process.

From the result, the phase can be restored with phase imperfections including singularities being drastically reduced in the low electron luminance situation.

In the practice, the electrons of the luminance are about 25 thousands at least distributed in the area of 500nm × 500nm of the specimen. That means $0.016C/M^2$ though the specimen. The least value may be different according to the specimen with different thickness and properties.

5.7 Conclusion

In summary, the simulation of an electron hologram with Poisson and Gaussian noise and low electron luminance were described in this chapter.

We tested a method for restoring singularities using the digital simulation hologram with added noise and low electron luminance. The implementation demonstrated that the proposed processing method is effective and it has practical value for processing electron holograms with noise and low electron luminance situations.

References

[1] C. D. Motchenbacher, J. A. Connelly, (1993). Low-noise electronic system design. Wiley Interscience.

[2] L. B. Kish, C. G. Granqvist, (2000). "Noise in nanotechnology". Microelectronics Reliability (Elsevier) 40 (11): 1833–1837.

[3] Y. M. Blanter and M. Büttiker, (2000). Shot noise in mesoscopic conductors. Physics Reports (Dordrecht: Elsevier) 336 (1-2): 1–166

[4] P. Cattin, (2012). "Image Restoration: Introduction to Signal and Image Processing". MIAC, University of Basel.

[5] J. Ohta, (2008). Smart CMOS Image Sensors and Applications. CRC Press.

[6] J. Nakamura (2005). Image Sensors and Signal Processing for Digital Still Cameras. CRC Press.

Chapter six

6. Summary

This study was aimed to apply the digital image processing to deal with the problems that occur in the image of electron hologram.

The actual applications of electron holography overcome the limitation of absent information compared to the previous TEM. Meanwhile, the problems occur in the processing when reconstructing the hologram. Noises are primary problems to be eliminated. It makes a great effect on the quality of the reconstructed result.

In addition, the phase jumps of 2π are ought to be restored to obtain the correct phase image.

In order to obtain the correct reconstructed phase image from the hologram, digital image processing has been introduced in the processing.

Firstly, principles of the holography are of importance for digital image processing methods in the next step. The study of the procedure of hologram generation, recording and reconstruction determines which processing methods to be picked up. The morphological image processing could play a role in the description of the interference fringes of holograms. Digital image processing was introduced to the *in situ* off-axis electron holography. Many processing methods were tried to find the efficacious methods on the hologram processing for smoothing and noise removing.

Secondly, phase imperfections in the reconstructed phase image were studied. Mainly two types of phase imperfections are clarified, except the imperfection come from the external noise. One type of well-known 2π phase jump during the digital reconstruction process can be unwrapped and connected in a smooth manner using the appropriate software nowadays. However, the other type of phase jump has not been

studied and solved.

Finding out that wrong recognization of the fringes in hologram owing to low contrast of the electron wave amplitude make the other type of 2π jump, phase imperfections could be corrected by correcting the interference fringes.

Thirdly, the processing method proposed was applied to a hologram of crystal structure image. Aberration correction was introduced too. The result of the singularities restored phase image shows a good phase structures.

Fourthly, the undulation noise was studied, as it sometimes occurs. The elimination of undulation noise was accomplished after finding out the reasons of occurrence.

Finally, simulation of hologram with noise was achieved. Poisson noise and Gaussian noise were studied, and they were added to the hologram for simulating the situation of quite week electron wave. Using the simulation of hologram with much noise, the same processing methods were executed for noise elimination and singularities restoring. A comparatively clear phase image can be obtained after the processing.

Acknowledgement

First and foremost, I would like to express my sincere gratitude to my supervisor, Professor Takayoshi Tanji, Ecotopia Science Institute, Nagoya University for his instructive advice and useful suggestions on my thesis. He has walked me through all the stages of writing of this thesis. Without his consistent and illuminating instruction, this thesis could not have reached its present form. I am deeply grateful of his help in the completion of this thesis.

Second, I would like to express my heartfelt gratitude to my supervision committee, Prof. T. Fujii, Nagoya University, Prof. T. Kodama, Meijo University. Prof. S. Tanaka, Nagoya University. They have instructed and offered me many valuable comments through my thesis writing.

I greatly acknowledge Assistant Professor T. Kawasaki for his education experiments, and discussion. His kindly help conduct me in the past years.

Last my thanks would go to all the members in our lab gave me their help and time in listening to me and helping me work out my problems during the difficult course of the thesis. I also owe my sincere gratitude to Ms. A. Nemoto who offered me great help in the studying abroad life.